Ph.D. Dissertation of College of Agriculture and Life Sciences

An interdisciplinary approach to sustainable rice production

-by integrating deep learning, mechanistic model and field observations-

August 2022

Graduate School of College of Agriculture and Life Sciences

Seoul National University

Interdisciplinary Program in Agricultural and Forest Meteorology Major

Yulin Yan

An interdisciplinary approach to sustainable rice production

-by integrating deep learning, mechanistic model and field observations-

Supervisor: Prof. Dr. Youngryel Ryu

Submitting a Ph.D. Dissertation of
College of Agriculture and Life Sciences
June 2022

Graduate School of College of Agriculture and Life Sciences
Seoul National University
Interdisciplinary Program in Agricultural and Forest Meteorology Major

Yulin Yan

Confirming the Ph.D. Dissertation written by
Yulin Yan
June 2022

Chair	Kwangsoo Kim	(Seal)
Vice Chair	Youngryel Ryu	(Seal)
Examiner	Sujong Jeong	(Seal)
Examiner	Hyungsuk Kim	(Seal)
Examiner	Minseok Kang	(Seal)

1. Abstract

Rice (*Oryza sativa*) is a vital cereal crop that feeds more than 50% of the world population. However, the traditional anaerobic management leads rice production to consume ~40% of the irrigation water and emit ~10% of the global anthropogenic methane. A new paradigm for sustainable rice farming is urgently required amid challenges from increasing food demand, water scarcity, and reducing greenhouse gases emissions. Rice plants transpire considerable water overnight. Saving nighttime water loss is desirable but first need to understand the underlying mechanism of nocturnal stomatal opening. Apart from the night, optimizing daytime management is pivotal for designing an environmentally sustainable rice farming system. In a long-term strategy, detailed and reliable crop type map is compulsory to upscale new leaf level findings and site level methods to regional or global scale. Therefore, in this dissertation, we improved mechanistic understanding of nocturnal stomatal conductance in rice plants (Chapter II); provided an interdisciplinary and heuristic approach for designing an environmentally sustainable rice farming system with a case study in South Korea (Chapter III); and developed a new crop type referencing method by mining off-the-shelf Google Street View images to map crop types (Chapter IV).

In chapter II, we proposed a "coordinated leaf trait" hypothesis to explain the ecological mechanism of nocturnal stomatal conductance (g_{sn}) in rice. We conducted an open-field experiment by applying drought, nutrient deficiency, and the combined drought-nutrient deficiency stress. We found that g_{sn} was neither strongly reduced by drought nor consistently increased by nutrient deficiency. With abiotic stress as a random effect, g_{sn} was strongly positively correlated with nocturnal respiration (R_n). Notably, g_{sn} primed early morning photosynthesis, as follows: R_n (↑) → g_{sn} (↑) → g_{sd} (daytime stomatal conductance) (↑) → *A* (assimilation) (↑). This photosynthesis priming effect diminished after mid-morning. Leaves were cooled by g_{sn} as follows: g_{sn} (↑) → E (transpiration) (↑) → T_{leaf} (leaf temperature) (↓). However, our results clearly suggest that evaporative cooling did not reduce R_n cost. Our results indicate that g_{sn} is more closely related to carbon respiration and assimilation than water and nutrient availability, and that leaf trait coordination ($R_n - g_{sn} - g_{sd} - A$) is likely the primary mechanism controlling g_{sn}.

In chapter III, we aimed to increase current crop yield, reduce irrigation water consumption, and tackle the dilemma to simultaneously reducing CH_4 and N_2O emissions in a flooded rice production system. By proposing a heuristic and holistic method, we optimized farm management beyond previous most emphasized irrigation regimes while also exploring niches from other pivotal options regarding sowing window, fertilization rate, tillage depth, and their interactions. Specifically, we calibrated and validated the process-based DNDC model with five years of eddy covariance observations. The DNDC model later was integrated with the non-dominated sorting genetic algorithm (NSGA-III) to solve the multi-objective optimization problem. We found that the optimized management would maintain or even increase current crop yield to its potential (~10 t/ha) while reducing more than 50% irrigation demand and GHGs (CH_4 & N_2O) emissions. Our results indicate that earlier sowing window and improvements on irrigation practice together would be pivotal to maximizing crop yield while sustaining environmental benefits. We found that the optimal fraction of non-flooded days was around 54% of growing season length and its optimal temporal distributions were primarily in vegetative stages. Our study shows that the present farm yield (8.3-8.9 t/ha) in study site not only has not achieved its potential level but also comes at a great environmental cost to water resources (604-810 mm/yr) and GHGs emissions (CH_4: 186-220 kg C/ha/yr; N_2O: 0.3-1.6 kg C/ha/yr). Furthermore, this simple method could further be applied to evaluate the environmental sustainability of a farming system under various climate and local conditions and to guide policymakers and farming practices with comprehensive solutions.

In chapter IV, we apply a convolutional neural network (CNN) model to explore the efficacy of automatic ground truthing via Google Street View (GSV) images in two distinct farming regions: Illinois and the Central Valley in California. Ground reference data are an essential prerequisite for supervised crop mapping. The lack of a low-cost and efficient ground referencing method results in pervasively limited reference data and hinders crop classification. In this study, we demonstrate the feasibility and reliability of our new ground referencing technique by performing pixel-based crop mapping at the state level using the cloud-based Google Earth Engine platform. The mapping results are evaluated using the United States Department of Agriculture (USDA) crop data layer (CDL) products. From ~130,000 GSV images, the CNN model identified ~9,400 target crop images. These images are well classified into crop types, including alfalfa, almond,

corn, cotton, grape, rice, soybean, and pistachio. The overall GSV image classification accuracy is 92% for the Central Valley and 97% for Illinois. Subsequently, we shifted the image geographical coordinates 2–3 times in a certain direction to produce 31,829 crop reference points: 17,358 in Illinois, and 14,471 in the Central Valley. Evaluation of the mapping results with CDL products revealed satisfactory coherence. GSV-derived mapping results capture the general pattern of crop type distributions for 2011–2019. The overall agreement between CDL products and our mapping results is indicated by R^2 values of 0.44–0.99 for the Central Valley and 0.81–0.98 for Illinois. To show the applicational value of the proposed method in other countries, we further mapped rice paddy (2014–2018) in South Korea which yielded fairly well outcomes (R^2=0.91). These results indicate that GSV images used with a deep learning model offer an efficient and cost-effective alternative method for ground referencing, in many regions of the world.

Keyword: sustainable rice production, nocturnal stomata, mapping

Student Number: 2018-30098

TABLE OF CONTENTS

1. Abstract 3

LIST OF FIGURES 9

LIST OF TABLES 13

ACKNOWLEDGEMENTS 14

Chapter I. Introduction 15

1.1. Study Background 15

1.2. Purpose of Research 15

Chapter II. Nocturnal stomatal conductance in rice: a coordinating bridge between prior respiration and photosynthesis next dawn 17

Abstract 17

1. Introduction 18

2. Materials and Methods 22

2.1 Plants and growth conditions 22

2.2 Leaf physiological traits 22

2.3 Rapid A/C_i response curves 24

2.4 Stomatal anatomy measurements 24

2.5 Statistical analyses 24

3. Results 25

3.1 Effects of abiotic stress on leaf traits 25

3.2 Nighttime leaf physiological traits 26

3.3 Significant priming effects of g_{sn} on early morning photosynthesis (~5:00 – 7:00) 27

3.4 Path analyses only support the leaf trait coordination 28

3.5 Impacts of g_{sn} on g_{sd} and A_{max} under light-saturated conditions 29

3.6 Photosynthesis priming effects not detected after mid-morning (9:00) 31

4. Discussion 32

4.1 Abiotic stress results: Implications for different hypotheses 33

4.2 Enhanced carbon assimilation through coordinated regulation by g_{sn} 34
4.3 Evaporative cooling: Passive thermoregulation via leaf trait coordination 36
References 37
Chapter III. Multi-objective optimization of crop yield, water consumption, and greenhouse gases emissions for sustainable rice production 42
Abstract 42
1. Introduction 43
2. Materials and methods 46
2.1 Study site 46
2.2 DNDC model 46
2.3 In situ data 47
2.4 Multi-objective optimization (MOO) algorithm 48
2.5 DNDC-NSGA-III integration and optimization 48
3. Results 50
3.1 DNDC model validation 50
3.2 The gaps between the current farming outcomes and optimized objectives 53
3.3 Approaching Pareto fronts through the heuristic and holistic management 55
3.4 The gaps between current farming practices to potential crop yield with optimal holistic management 56
4. Discussion 58
4.1 Could heuristic and holistic management increase current rice yield with less irrigation water? 58
4.2 Could heuristic and holistic management simultaneously reduce CH_4 and N_2O emissions? 59
4.3 Limitations and uncertainties 60
Reference 61
Chapter IV. Exploring Google Street View with Deep Learning for Crop Type Mapping 70
Abstract 70
1. Introduction 71

2. Materials and Methods 74
2.1 Study area 74
2.2 General methodology 75
2.3 Google Street View image collection 76
2.4 CNN model training and validation 77
2.5 Producing ground reference data and quality control 79
2.6 Mapping crop types 80
2.7 Mapping results evaluation 81
2.8 Additional test case 82
3. Results 83
3.1 GSV image classification 83
3.2 Producing ground reference data from classified GSV images 84
3.3 Mapping using the GSV derived ground reference 86
4. Discussion 96
4.1 Can we use GSV images to efficiently produce low-cost, sufficient, and reliable crop type ground reference data covering large areas? 96
4.2 Can we use GSV-derived reference data as “ground truth” to map crop types for large areas spanning many years? 97
Appendix 99
References 105
Chapter V. Conclusions 123
Supplementary Information Chapter II 125
Supplementary Information Chapter III 131
Supplementary Information Chapter IV 135
5. Abstract in Korean 138

LIST OF FIGURES

Figure 1 Conceptual model of prior hypotheses to explain g_{sn} and the coordination hypothesis proposed in this study as its ecological mechanism. (I) Coordination of key leaf traits (R_n, g_{sn}, g_{sd}, A), simultaneous cooling (green and blue pathways), and subsequent circadian priming benefits (green and red pathways). (I-I) Circadian priming to boost photosynthesis (red pathway). (I-II) Evaporative cooling to regulate T_{leaf} and reduce respiration cost (blue pathway). (II) Nutrient uptake to alleviate abiotic stress (yellow pathway). (III) Water conservation due to DS and the unknown NDS effects (grey shaded box). 21

Figure 2 (a) Daytime non-steady-state (300 µmol m^{-2} s^{-1} PPFD) and steady-state (1,800 µmol m^{-2} s^{-1} PPFD) stomatal conductance (g_{sd}) in each treatment. (b) Nighttime steady-state stomatal conductance (g_{sn}) in each treatment, significant *p*-values indicate that samples are from different populations. (c) Grouped stomatal conductance (g_s) for daytime and nighttime. (d) Ratio between g_{sn} and the average g_{sd} at 300 and 1,800 µmol m^{-2} s^{-1} PPFD for each sample. Error bars indicate one standard deviation of uncertainty. Stomatal size (SS) on (e) adaxial (ada) and (f) abaxial (aba) leaf surfaces. The lower-case letters within each panel indicate the significance level both for the mean values and in data distribution. Nonsignificant results are unlabeled. 26

Figure 3 (a) Correlation between nocturnal respiration (R_n) and g_{sn} (n = 29). (b) Correlation between g_{sn} and T_{leaf}. (c) Correlation between nocturnal transpiration (E_n) and T_{leaf}. Solid regression line and statistics are based on all samples, colored dashed regression lines are based on each individual treatment. 27

Figure 4 (a) Correlation between nocturnal stomatal conductance (g_{sn}) and early morning (300 µmol m^{-2} s^{-1} PPFD) non-steady-state maximum stomatal conductance (g_{sd}) within a 5-min period (n = 22). (b) Maximum assimilation rate (A) within a 5-min period. (c) Correlation between g_{sn} and the time (τ_1) to reach 63% of the maximum early morning A within a 5-min period. 28

Figure 5 Path analyses of the (a) coordination-E_n cooling hypothesis (n = 29); (b) coordination-circadian priming hypothesis (early morning 300 µmol m^{-2} s^{-1} PPFD and non-steady-state conditions; n = 22, where τ_1 denotes the time to reach 63% of the maximum early morning A within a 5-min period; and (c) the R_n reduction hypothesis (n = 29). Arrows indicate speculated interactions between pairs of leaf traits. Integers in each panel denote the hypothesized sequence of interactions between leaf traits. Path coefficients were normalized from −1 to 1 and are shown in between traits; significant relationships (*P < 0.05, **P < 0.01, ***P < 0.001) are indicated by blue or green numbers. GFI, goodness of fit; AGFI, adjusted goodness of fit; CFI, comparative fit index; TLI, Tucker-Lewis index. Red text indicates poor model fit indices. Ranges of good model fit indices were defined as follows: AGFI > 0.90, CFI > 0.90, GFI > 0.95, and TLI > 0.97. 29

Figure 6 Correlation between nocturnal stomatal conductance (g_{sn}) and (a) steady-state, light-saturated (1,800 µmol m^{-2} s^{-1} PPFD) stomatal conductance, and (b) the assimilation rate (A_{max}) (n=16). (c)

Correlation between steady-state, light-saturated g_{sd} and A_{max}. (d) Path analysis of the coordination-circadian priming hypothesis (light-saturated, steady-state conditions; n=16). Path coefficients were normalized from −1 to 1 and are shown in between traits; significant relationships (***P < 0.001) are indicated in blue text. GFI, goodness of fit; AGFI, adjusted goodness of fit; CFI, comparative fit index; TLI, Tucker-Lewis index. 30
Figure 7 Light response curves of (a) A and (b) g_{sd}. Correlation between g_{sd} and (c) A and (d) g_{sn} (n = 64, 8 PPFD values × 8 light response curves). 31
Figure 8 (a) Proposed temporal (diurnal and seasonal) coordination of key leaf traits and (b) functional interpretation; g_{sn} acts as the key link. 32
Figure 9 Annual scale validation of the DNDC simulations with in situ data regarding (a) crop yield, (b) CH_4 emissions, (c) GPP, and (d) ET from 2016 to 2020. Error bars indicate 95% confidence interval. 50
Figure 10 Daily scale validation of the DNDC simulations with in situ data in terms of (a) CH_4 flux, (b) GPP flux, and (c) Reco flux from 2016 to 2020. 51
Figure 11 Daily scale validation of the DNDC simulations with in situ data in terms of (a) ET flux, (b) soil moisture, and (c) soil temperature from 2016 to 2020. 52
Figure 12 Pareto fronts and probability density distribution of the each paired two objectives, where colorized dots denote the non-dominated sets and grey dots denote the dominated sets. (a) Minimizing CH_4 emissions and maximizing crop yield, (b) minimizing CH_4 and N_2O emissions, (c) minimizing irrigation consumption and CH_4 emissions, (d) minimizing N_2O emissions and maximizing crop yield, (e) minimizing irrigation consumption and maximizing crop yield, (f) minimizing irrigation consumption and N_2O emissions. Black triangles denote the paired objectives based on the current farm management (2016-2020). 53
Figure 13 Planform of the Pareto fronts of each paired three objectives in triangular surface plot, where the color bar indicates the values of z axis; (a) minimizing N_2O, CH_4 emissions and maximizing crop yield; (b) minimizing irrigation consumption, CH_4 emissions and maximizing crop yield; (c) minimizing irrigation consumption, N_2O emissions and maximizing crop yield; (d) minimizing CH_4, N_2O emissions, and irrigation consumption. Blue triangles denote the paired objectives based on the current farm management (2016-2020). 54
Figure 14 Probability density distribution of the non-dominated farm management regarding, irrigation schedules (a) in April, (b) in May, (c) in June, (d) in July, and (e) in August; (f) sowing day and fertilization rate, (e) sowing day and tillage depth, (f) tillage depth and fertilization rate. The non-dominated sowing month only occurred in April, therefore was not presented. 56

Figure 15 Comparison between the current farming practices (n = 5) and optimized holistic managements (a-e, n = 21) with a threshold of crop yield greater than 10 t/ha (f). And the corresponding farming outcomes yielded from the current practices and the optimized managements (f-i). 57
Figure 16 Examples of the availability and spatial distribution of GSV images across the globe, indicated in light blue. Note that the red circles show the approximate location of the inset areas. Image copyright: Google Inc. 73
Figure 17 Study area I and II, the Central Valley in California and the state of Illinois, and their major crop types distribution from the CDL. 75
Figure 18 Flowchart of the convolutional neural network (CNN)-based ground referencing and pixel-based crop type classification. 76
Figure 19 GSV image samples randomly collected in this study: (a) corn, (b) soybean, (c) almond, (d) cotton, (e) alfalfa, (f) grape, (g) pistachio, (h) and (i) are classified as "other". Image copyright: Google Inc. 77
Figure 20 Architecture of the CNN model used for Google Street View (GSV) image classification. 79
Figure 21 GSV vehicle coordinates were shifted to generate ground reference points. The buffer zone indicates potential mixed pixels near the parcel edge. Red dots indicate the position of the GSV car; green dots indicate reference points; y is road width; x is Landsat pixel resolution. Image copyright: Google Inc. 80
Figure 22 Temporal and spatial distribution of crop type reference points derived from GSV images for the Central Valley (a-g) and Illinois (h-i). The doughnut plots and bar plots indicate the number and proportion of reference points for each year. 85
Figure 23 Comparison between the CDL and GSV-derived crop type maps for the Central Valley in 2017 (a, b, respectively), a year with only 190 reference points. Black squares serve as guide grids to facilitate visual comparison. 88
Figure 24 Comparison between the CDL and GSV-derived crop type maps for Illinois in 2014 (a, b, respectively), a year without reference GSV images. Black squares serve as guide grids to facilitate visual comparison. 88
Figure 25 Comparison between GSV-derived and CDL-derived crop type distribution for the Central Valley in 2017. The x and y axes show the pixel numbers of each crop type for a 5-km^2 grid resolution for the entire study area. 90
Figure 26 Comparison between GSV-derived and CDL-derived corn distribution for Illinois from 2013–-2019. The x and y axes show the pixel numbers of corn for a 5-km^2 grid resolution for the entire study area. 91

Figure 27 Comparison between GSV-derived and Dong et al., (2016) -derived rice paddy distribution for South Korea in 2014 (a). The x and y axes show the pixel numbers of rice paddy for a 5-km2 grid resolution for the entire study area. And rice paddy distribution error (%) map, expressed as the percentage difference in pixel numbers per 5km^2 (b). 92
Figure 28 Regional-scale crop type mapping comparison for the Central Valley for years with GSV as reference data. Each subplot covers approximately 2500 km^2. Black squares serve as guide grids to facilitate visual comparison. 93
Figure 29 Regional-scale crop type mapping comparison for Illinois, for the years with GSV used as reference data. Each subplot covers approximately 2500 km^2. Black squares serve as guide grids to facilitate visual comparison. 94
Figure 30 Soybean distribution error (%) map between GSV-derived and CDL-derived soybean maps for Illinois from 2013–2019, expressed as the percentage difference in pixel numbers per 5km^2. 95
Figure 31 Corn distribution error (%) map between GSV-derived and CDL-derived corn maps for Illinois from 2013–2019, expressed as the percentage difference in pixel numbers per 5km^2. 95

LIST OF TABLES

Table 1 Performance of the CNN model for GSV image classification in the Central Valley, displayed as a confusion matrix. PA: producer accuracy; UA: user accuracy; OA: overall accuracy..... 83
Table 2 Performance of the CNN model for GSV image classification in Illinois, displayed as a confusion matrix. PA: producer accuracy; UA: user accuracy; OA: overall accuracy..... 84
Table 3 Performance of the RF model for land cover classification in the Central Valley indicated as a confusion matrix. PA: producer accuracy; UA: user accuracy; OA: overall accuracy..... 86
Table 4 Performance of the RF model for land cover classification in Illinois indicated as a confusion matrix. PA: producer accuracy; UA: user accuracy; OA: overall accuracy..... 86
Table 5 Comparison of GSV-derived and CDL-derived crop type distribution maps for each crop type in the Central Valley using a 5-km^2 grid resolution. The number of references indicates data available for training and testing the random forest classifier for each year..... 89

ACKNOWLEDGEMENTS

My sincere appreciation goes to all the great person who I met on the road to PhD. First of all, I would like to thank my supervisor Prof. Dr. Youngryel Ryu for his kind guidance, generous support, positive attitude, and unconditional trust in the past four years. I have been able to enjoy and freely explore the realm of crop science by having a fertile, collaborative, and friendly environment in Ecological Sensing AI lab. I would like to thank Bolun Li, Benjamin Dechant, and all the other lab members, without whom I would not have been able to complete this research. I also would like to thank my thesis committee members: Prof. Dr. Sujong Jeong, Prof. Dr. Kwangsoo Kim, Prof. Dr. Hyungsuk Kim, and Dr. Minseok Kang. Thank you for your great efforts and constructive suggestions. My appreciation also goes to China Scholarship Council for supporting my PhD study in Seoul National University.

Chapter I. Introduction

1.1. Study Background

Rice (*Oryza sativa*) is a vital cereal crop that feeds more than 50% of the world population and over 90% is cultivated in Asia (Bouman and Tuong, 2001; Dong and Xiao, 2016). Rice has been prevalently cultivating worldwide in the flooded paddy to imitate its original subtropical growing environments, suppress weeds, and maintain yield for ~4000 years (Gutaker et al., 2020; Zong et al., 2007). However, the traditional anaerobic management leads rice production to consume ~40% of the irrigation water (Lampayan et al., 2015) and emit ~10% of the global anthropogenic methane (Saunois et al., 2020). As the largest water consumer in the agricultural sector and dominant anthropogenic methane emitter, the longstanding thousand years of flooded rice farming is no longer sustainable while challenged by water scarcity (Gosling and Arnell, 2016), carbon-neutral pledges (Flagg, 2015), and global warming (Naylor et al., 2007; Zhao et al., 2017). We urgently need new paradigms for cultivating rice sustainably.

1.2. Purpose of Research

Saving considerable transpiration water loss overnight is desirable but need to understand the underlying mechanism of nocturnal stomatal opening. Recently, Zhang et al. (2021) determined that the average transpiration ratio between night and daytime (E_n/E_d) was 16.5 ± 6.1% across 30 rice genotypes, with a maximum of ~35% (Zhang et al., 2021). Similarly, C_3 and C_4 plants transpire 5–30% of daytime water through their stomata overnight (Caird et al., 2007; Forster, 2014; Fricke, 2019; Resco de Dios et al., 2019). To elucidate the conundrum, several hypotheses have emerged regarding the potential mechanisms of nocturnal stomatal conductance (g_{sn}), including photosynthesis priming, evaporative cooling, nutrient uptake, and CO_2 removal (Caird et al., 2007; Resco de Dios et al., 2019; Wang et al., 2021). Nevertheless, little is known about the role of g_{sn} particularly in rice plants. Therefore, in chapter II, we conducted open-field experiments involving drought, nutrient deficiency, and combined nutrient and drought stress treatments to examine the primary mechanism of g_{sn} in rice. Here we propose nocturnal respiration (R_n), g_{sn}, daytime stomatal conductance (g_{sd}), and assimilation rate (*A*) would covary with the adjacent leaf traits.

Despite the considerable nocturnal water loss, improving daytime farm management would be pivotal to design an environmentally sustainable rice farming system. Considerable research efforts have been investigating to decrease water consumption, greenhouse gases (GHGs) emissions, and maintain the grain yield. In particular, altering soil redox conditions with draining management has been attracting the most attention (Bo et al., 2022; Kudo et al., 2014; LaHue et al., 2016; Li et al., 2006a; Meijide et al., 2017; Peng et al., 2006). However, solely conducting field experiments or applying the biogeochemical models with limited numerical experiments is nearly infeasible to quest all the potential optimal solutions while encountering multi competing objectives. For instance, the dilemma to reduce CH_4 and N_2O footprints simultaneously (Li et al., 2005; Liu et al., 2019). Therefore, in chapter III, we provide a new alternative to optimize irrigated rice farming systems regarding food security, GHGs emissions, and water resources. We integrated the process-based DNDC (DeNitrification DeComposition) model with the non-dominated sorting genetic algorithm (NSGA-III). Specifically, we developed a holistic and integrated approach to balance several contradictory objectives including the trade-off between conserving water resources and maximizing grain yield, reducing CH_4 and N_2O emissions.

In a long-term strategy, detailed and reliable crop type map is compulsory to assess the impacts of nocturnal stomatal opening from leaf level (chapter II) and upscale the multi-objective optimization method from site level (chapter III) to regional or global scales. However, the lack of a low-cost and efficient method for producing ground reference data results in pervasively limited cropland information and hindered supervised crop type mapping, particularly for large-scale and long periods (Phalke and Özdoğan, 2018; Wang et al., 2019; Zhong et al., 2019b). Therefore, in chapter IV, we developed a new crop type referencing method by mining off-the-shelf Google Street View (GSV) images. A successful method should be location-independent and have the ability to be upscaled efficiently to large areas where GSV images are available. Thus, we applied a convolutional neural network (CNN) model to explore the efficacy of automatic ground truthing via GSV images in three distinct large farming regions: South Korea, Illinois, and the Central Valley in California.

Chapter II. Nocturnal stomatal conductance in rice: a coordinating bridge between prior respiration and photosynthesis next dawn

Abstract

The ecological mechanism underlying nocturnal stomatal conductance (g_{sn}) in non-CAM plants remains elusive. We propose a "coordinated leaf trait" hypothesis to explain g_{sn} in rice. We conducted an open-field experiment by applying drought, nutrient deficiency, and the combined drought-nutrient deficiency stress. We found that g_{sn} was neither strongly reduced by drought nor consistently increased by nutrient deficiency. With abiotic stress as a random effect, g_{sn} was strongly positively correlated with nocturnal respiration (R_n). Notably, g_{sn} primed early morning (5:00-7:00) photosynthesis, as follows: R_n (↑) → g_{sn} (↑) → g_{sd} (daytime stomatal conductance) (↑) → *A* (assimilation) (↑). This photosynthesis priming effect diminished after mid-morning (9:00). Leaves were cooled by g_{sn} as follows: g_{sn} (↑) → E (transpiration) (↑) → T_{leaf} (leaf temperature) (↓). However, our results clearly suggest that evaporative cooling did not reduce R_n cost. Our results indicate that g_{sn} is more closely related to carbon respiration and assimilation than water and nutrient availability, and that leaf trait coordination ($R_n - g_{sn} - g_{sd} - A$) is likely the primary mechanism controlling g_{sn}. Thus, g_{sn} is driven by the prior R_n and primes next-day photosynthesis.

Key words: Abiotic stress, leaf trait coordination, nocturnal respiration, nocturnal stomatal conductance, photosynthesis, *Oryza sativa*

1. Introduction

The ecological mechanism underlying incomplete nighttime stomatal closure in C_3 and C_4 plants has remained a conundrum for more than a century. Back in circa 1886, Austrian botanist Hubert Leitgeb was the first to thoroughly examine nocturnal stomatal opening in many plant species (Leitgeb, 1886). Early related discoveries received both support (Stahl, 1897) and opposition (Schellenberg, 1896). Francis Darwin's conclusion that "*the biology of nocturnal closure is obscure*" (Darwin, 1898) remains valid today. Only fairly recently, a solid body of evidence has confirmed that C_3 and C_4 plants transpire 5–30% of daytime water through their stomata overnight (Caird et al., 2007; Forster, 2014; Fricke, 2019; Resco de Dios et al., 2019). During recent decades, several hypotheses (Fig. 1) have emerged regarding the potential mechanisms of nocturnal stomatal conductance (g_{sn}), including photosynthesis priming, evaporative cooling, nutrient uptake, and CO_2 removal (Caird et al., 2007; Resco de Dios et al., 2019; Wang et al., 2021). Nevertheless, we still cannot reconcile the aforementioned propositions into a single framework. The benefits of transpiring a non-negligible portion of water without carbon assimilation after dusk are poorly understood.

Plant functional types, intraspecific genetic diversity, leaf age, environmental conditions, stomatal anatomy, and nutrient availability all contribute to variation in g_{sn} (Caird et al., 2007; Resco de Dios et al., 2019; Zeppel et al., 2014). Several studies have demonstrated that g_{sn} is associated with the environmental origin and habitat type of species (Caird et al., 2007; Daley and Phillips, 2006; Snyder et al., 2003; Yu et al., 2019), with the highest ratio of g_{sn} to daytime stomatal conductance (g_{sd}) being reported in the tropics (Resco de Dios et al., 2019). Nocturnal stomatal opening prevents the respiratory CO_2 buildup, facilitates the cytochrome pathway (Palet et al., 1991), and reverses oxygen depletion in parenchyma cells (Gansert, 2003; Resco de Dios et al., 2019). However, a global database analysis showed that g_{sn}, a median of 0.04 mol m^{-2} s^{-1}, is unnecessarily high if the goal is to simply avoid toxic CO_2 concentration (Resco de Dios et al., 2019). Some studies have also shown that g_{sn} enhances nutrient uptake via sap flow; however, the evidence is inconsistent (Kupper et al., 2012; Lewis et al., 2011; Resco de Dios et al., 2019; Zeppel et al., 2014). Recently, Wang et al. (2021) used an optimality theory-based method to model g_{sn} under different environmental conditions. Under this approach, the key benefit of g_{sn} was assumed to be nocturnal

respiratory reduction, and the key cost was a loss of subsequent assimilation due to antecedent water use. The model well predicted the responses of g_{sn} to soil moisture and atmospheric CO_2, but not to vapor pressure deficit or temperature. Other theories proposed to explain g_{sn} include hydraulic competition (Huang et al., 2017; Resco de Dios et al., 2019) and leaky stomata (Barbour et al., 2005).

Photosynthesis/circadian priming is a promising hypothesis that may partly resolve the enigma of g_{sn}. Circadian priming proposes that plants evolved a ~24-h biological clock synchronized with the Earth's rotation to enhance photosynthesis and growth, for a competitive advantage (Dodd et al., 2005). After sunset, this clock usually regulates g_{sn} to decline continuously until midnight (Ogle et al., 2012; Resco de Dios et al., 2016) likely to conserve water. Subsequently, g_{sn} increases from predawn to facilitate photosynthesis in the early morning, particularly via a faster stomatal response and higher stomatal conductance, which result in a higher photosynthetic rate (Drake et al., 2013; Resco de Dios et al., 2016). Predawn stomatal priming has been shown to increase leaf area index and final biomass (Resco de Dios et al., 2016), but also has a marginal effect on early morning photosynthesis in the common sunflower, *Helianthus annuus* (Auchincloss et al., 2014). Recent studies have found no relation between g_{sn} and the steady-state g_{sd} or net assimilation rate (A), i.e., at a photosynthetic photon flux density (PPFD) of 1,200 μmol m^{-2} s^{-1} (McAusland et al., 2021; Resco de Dios et al., 2016; Zhang et al., 2021). Stomatal priming is likely beneficial only at low PPFD ranges, and its effects may diminish with the circadian cycle once g_{sd} has acclimated to new environmental conditions. Thus, the circadian priming hypothesis appears to be exclusive to certain plant species and constrained by environmental conditions; however, further study is required to evaluate its applicability.

Nocturnal respiration (R_n) and g_{sn} may be mechanistically related. Recent experimental and modeling studies have reported that, at the leaf scale, g_{sn} and R_n are tightly correlated (McAusland et al., 2021; Wang et al., 2021; Yu et al., 2019; Zhang et al., 2021) and that, at the cellular scale, rapid starch degradation through mitochondrial respiration promotes stomatal opening at dawn (Flütsch and Santelia, 2021; Flütsch et al., 2020; Rea, 2020). Mitochondrial respiration provides energy directly for guard cell movement before photosynthesis-derived sugars are available

(Flütsch and Santelia, 2021). Together, these new pieces of physiological evidence suggest that g_{sn} may be actively regulated by respiration both at dawn and, more importantly, overnight. As ~46% of antecedent photosynthetic products are respired for maintenance and growth (Collalti and Prentice, 2019), g_{sn} likely coordinates several photosynthetic traits continuously via R_n, such that g_{sn} responds to the trend of the previous day, from R_n to g_{sn}, and sets the trend for the following dawn, from g_{sn} to g_{sd} and *A* (Fricke, 2019). Therefore, in this study, we aimed to evaluate whether a combination of circadian priming and coordination between g_{sn} and R_n could explain nighttime and daytime leaf physiological traits as a single model (Fig. 1).

Little is known about the role of g_{sn} in rice plants. Rice is a semiaquatic crop usually grown under saturated water conditions; therefore, it can be used as a model plant for evaluating multiple hypotheses aiming to explain g_{sn}. For example, if leaf cooling and water conservation are the primary benefits of g_{sn}, rice plants might be expected to exhibit excessively stomatal opening overnight because their water supply is unlimited. Recently, Zhang et al. (2021) determined that the average g_{sn}/g_{sd} ratio was ~11% across 30 rice genotypes, with a maximum of ~50%; they reported that significant g_{sn}-induced evaporative cooling consistently, lowered leaf temperature (T_{leaf}) 0–2.2 °C below the air temperature; moreover, this was positively associated with stomatal size and related to several other leaf morphological traits. The mean g_{sn}/g_{sd} ratio (~11%) observed under saturated water conditions indicates that partial nocturnal stomatal closure in rice is a plausible strategy for conserving soil moisture; however, this hypothesis should be further tested using drought treatments. The considerable variation in g_{sn} also suggests that further study is required to determine whether other hypotheses, such as circadian priming and nutrient uptake, can explain g_{sn} dynamics in rice. Therefore, in this study, we conducted open-field experiments involving drought (DS), nutrient deficiency (NS), and combined nutrient and drought stress (NDS) treatments to examine the primary mechanism of g_{sn} in rice (Fig. 1).

The objective of this study was to improve our mechanistic understanding of g_{sn}. A conceptual model of the key hypotheses addressed in this study is provided in Fig. 1. As the main hypothesis, we expected that daytime and nighttime leaf physiological traits would tightly coordinated. Namely, g_{sn}, daytime stomatal conductance (g_{sd}), net assimilation rate (*A*), and R_n will covary with

the adjacent leaf traits. As a sub-hypothesis, we expected that g_{sn} would reduce the stomatal response time, i.e., the time taken to reach a maximum value of *A* at a certain light value (τ), and would also be positively correlated with early morning g_{sd} and *A*. Furthermore, higher R_n values were expected to increase g_{sn}, leading to higher nocturnal transpiration (E_n) and lower T_{leaf}, which would reduce R_n. Under NS, rice plants were expected to increase g_{sn} to enhance sap flow for nutrient acquisition. Finally, under DS, g_{sn} was expected to decline to reduce water loss. Thus, under NDS, rice might increase or decrease g_{sn}, depending on the dominant competing factor.

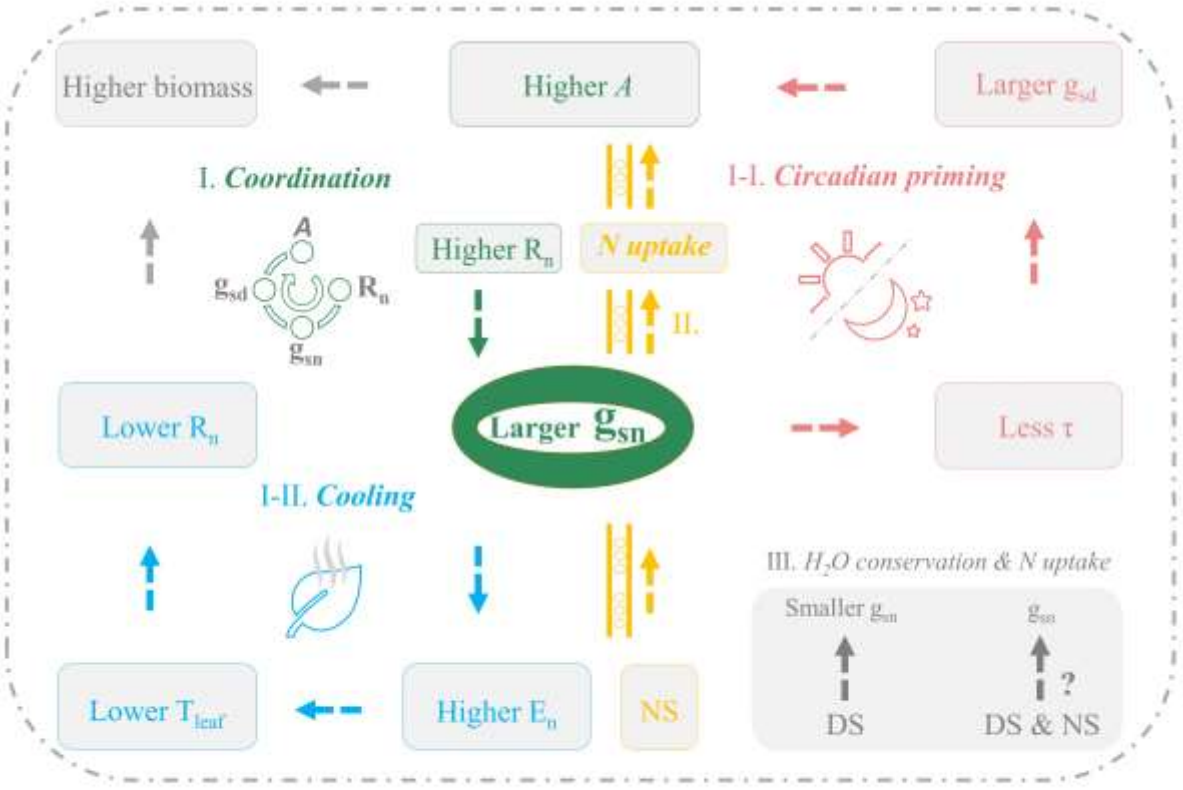

A: assimilation; $\mathbf{E_n}$: nocturnal transpiration; $\mathbf{g_{sn}}$: nocturnal stomatal conductance; $\mathbf{g_{sd}}$: daytime stomatal conductance; **DS**: drought stress; **NS**: nutrient stress; $\mathbf{R_n}$: nocturnal respiration; **τ**: stomatal responding time; $\mathbf{T_{leaf}}$: leaf temperature

Figure 1 Conceptual model of prior hypotheses to explain g_{sn} and the coordination hypothesis proposed in this study as its ecological mechanism. (I) Coordination of key leaf traits (R_n, g_{sn}, g_{sd}, *A*), simultaneous cooling (green and blue pathways), and subsequent circadian priming benefits (green and red pathways). (I-I) Circadian priming to boost photosynthesis (red pathway). (I-II) Evaporative cooling to regulate T_{leaf} and reduce respiration cost (blue pathway). (II) Nutrient uptake to alleviate abiotic stress (yellow pathway). (III) Water conservation due to DS and the unknown NDS effects (grey shaded box).

2. Materials and Methods

2.1 Plants and growth conditions

This study was conducted from May to August, 2021 on a building rooftop at the College of Agricultural and Life Sciences, Seoul National University (37.4573°N, 126.9482°E), Seoul, South Korea. We cultivated the early ripening rice cultivar "Odae" (*Oryza sativa* L. ssp. *japonica*) in silt clay loam soil (9.5 ± 0.5 kg/pot) obtained from a rice farm in Cheorwon (Huang et al., 2018; Hwang et al., 2020). On day of year (DOY) 124, we transplanted rice plants into 20 ~19-L pots (three seedlings per pot). We used a randomized block design including four treatments: control, NS, DS, and NDS. Each treatment had five replicates. Nutrient treatments started on DOY 130. In the control and DS treatments, we applied 5.1 g mineral fertilizer at a N/P/K ratio of 16:8:12 per pot. In the NS and NDS treatments, we applied 0.4 g mineral fertilizer per pot. In the control and NS treatments, we irrigated the rice plants daily to form a minimum 2-cm water table above the soil surface, to maintain a saturated volumetric water content (50 ± 1%), that was measured using a portable soil moisture sensor (HydroSense II; Campbell Scientific, Inc, Logan, UT, USA). In the DS and NDS treatments, we irrigated rice plants conservatively to sustain a volumetric water content of 25 ± 5% at a depth of 20 cm, as an ideal range for drought symptoms while avoiding excessive leaf rolling to ensure proper leaf gas exchange measurements.

2.2 Leaf physiological traits

Leaf physiological traits were measured using a portable photosynthesis system (LI-6800; LI-COR Biosciences, Lincoln, NE, USA) and cross-checked with an LI-6400XT instrument (LI-COR Biosciences). An auxiliary porometer (LI-600; LI-COR Biosciences) was used to double-check the stomatal conductance and T_{leaf} measurements obtained using the LI-6800 system. To obtain paired nighttime and daytime measurements, 3–4 healthy, fully expanded leaves of the same age were marked in each pot. We performed all measurements on the middle to upper leaf to avoid potential within-leaf heterogeneity. Measurements were performed by setting the chamber air temperature and relative humidity close to ambient conditions. A total of six measurement campaigns were scheduled, on DOY 169, 173, 197, 203, 211, and 218. Measurements planned for

DOY 169 and 211 failed due to unexpected rainfall and non-stabilized g_{sn} in the LI-6800 cuvette (3 cm × 3 cm), respectively. Nocturnal measurements were conducted from 3:30 to 5:00 am local time in full darkness (0 μmol m^{-2} s^{-1} PPFD). Marked leaves were clamped into the LI-6800 cuvette. After the target traits (g_{sn}, R_n, and T_{leaf}) had stabilized, measurements were performed for 1-min periods, with data logged at 10-s intervals. To avoid uncertainties and biases caused by dew, we only measured dry leaves. The g_{sn} presented in this study also include the cuticular conductance; we assumed the g_{sn} was equivalent to leaf diffusive conductance, as described previously (Resco de Dios et al., 2019; Zhang et al., 2021).

To test the photosynthesis priming hypothesis, we conducted early morning measurements shortly after dawn (~5:00 – 7:00) when the ambient photosynthetic active radiation (PAR) was below 300 μmol m^{-2} s^{-1}. To minimize the effects of ambient light on stomata, we first stabilized (~5 min) stomatal conductance in the cuvette without an additional light source (0 μmol m^{-2} s^{-1} PPFD), and then set the PPFD intensity to 300 μmol m^{-2} s^{-1} using a built-in red–blue light source and recorded observations for 5 min; data were logged at 10-s intervals. Due to limited time and human resources, we used a stabilization time of 5 min based on a previous study (Resco de Dios et al., 2016). We calculated the response time at which 63% [$1-e^{-1}$] to obtain the maximum assimilation values (Resco de Dios et al., 2016; Woodward, 1987), and an additional 80% response time to obtain a gradient. Although continuous measurement would be ideal for testing whether priming effects diminish throughout the diurnal cycle and change with the ambient environments, due to limited human resources, instruments, and excessively high temperatures in the field, we measured only the daily maximum assimilation rate (A_{max}) and maximum g_{sd} as boundary conditions. We measured steady-state photosynthesis between ~8:00 and 11:30 under the light-saturated conditions (1,800 μmol m^{-2} s^{-1} PPFD). Data were logged after the assimilation rate and stomatal conductance both reached steady-state (~25 min for each point). In addition, rapid light response curves were conducted on DOY 197 from ~9:00 to 13:00 (~10-20 min per curve). Each light response curve started at 1,800 μmol m^{-2} s^{-1} PPFD and dropped in steps of 300 μmol m^{-2} s^{-1}. Two extra light values, at 50 and 150 μmol m^{-2} s^{-1} PPFD, were also included (2–3 min each).

2.3 Rapid *A*/C_i response curves

To evaluate the efficacy of abiotic stress treatments, we used the rapid CO_2 response method (R*A*C_iR) (Stinziano et al., 2019; Stinziano et al., 2017) to retrieve the maximum velocity of carboxylation ($V_{c,max}$) and maximum electron transport rate (J_{max}) for marked leaves on DOY 224 and 225. For automatic control of the reference CO_2 concentration, we sued a linear ramp rate of 82 ppm/min in the range of 10–1,000 ppm. We set the light intensity to 1,800 µmol m^{-2} s^{-1} PPFD and controlled the chamber air temperature and relative humidity close to ambient conditions. Data were recorded for a 13-min period, with high–frequency data logging (2-s interval). R*A*C_iR CO_2 ramps were also conducted daily using an empty chamber to correct the raw data. Empty chamber–corrected data were later analyzed using Sharkey's method to obtain $V_{c,max}$ and J_{max} values normalized at 25°C (Sharkey, 2016).

2.4 Stomatal anatomy measurements

To determine how abiotic stress affects the stomatal size and density, and whether stomatal anatomy can explain the hypothesized stress-induced g_{sn} variation, we applied clear nail polish to both the abaxial and adaxial surfaces of marked leaves on DOY 229. The dried membrane under the polish was later peeled off using clear tape and mounted on an optical microscope (Axioskop2, Axiocam 506 Color, Zeiss, Jena, Germany) for data collection. Stomatal images were obtained at ×400 magnification. Three to five clear images were captured per microscope slide. Stomatal size and number in the field of view were later analyzed using ImageJ software (National Institutes of Health, Bethesda, MD, USA) (Schneider et al., 2012).

2.5 Statistical analyses

Statistical and linear regression analyses were performed in the Python (v3.7) environment using the SciPy (v1.4.1) library. To compare means between two groups of samples, we used the two-tailed Student's t-test ($n > 20$) and nonparametric Mann–Whitney U test ($n < 20$). To determine whether two groups of samples were from the same populations, we used the nonparametric Epps–

Singleton test (Epps and Singleton, 1986). To link multiple nocturnal leaf traits (g_{sn} and R_n) with daytime traits (g_{sd} and A) and test direct and indirect effects, we conducted path analysis using RStudio (v2021.09.0) software, with the Lavaan (v0.6-9) library. Three hypothesized paths were analyzed (Fig. 1), including the coordination–cooling path ($R_n \rightarrow g_{sn} \rightarrow E_n \rightarrow T_{leaf}$) and g_{sn} induced R_n reduction path ($g_{sn} \rightarrow E_n \rightarrow T_{leaf} \rightarrow R_n$) for nocturnal (0 μmol m^{-2} s^{-1} PPFD) steady-state conditions, and the coordination–circadian priming path ($R_n \rightarrow g_{sn} \rightarrow g_{sd}/\tau \rightarrow A$) for early morning (300 μmol m^{-2} s^{-1} PPFD) non-steady-state and light-saturated (1,800 μmol m^{-2} s^{-1} PPFD) steady-state conditions.

3. Results

3.1 Effects of abiotic stress on leaf traits

We detected a clear drought-induced reduction in g_{sd} across treatments, which was unresponsive to nutrient deficiency (Fig. 2a). By contrast, we found non-significant differences in the group mean g_{sn} (~0.05 mol m^{-2} s^{-1}) among all treatments (Fig. 2b). Both NS and DS significantly altered the distribution of g_{sn} (Fig. 2b). Compared to the control, NS increased g_{sn} from the lower to middle quartiles, whereas DS tended to decrease g_{sn} in the upper quartile to the maximum range (Fig. 2b). In addition, g_{sn} accounted for a large proportion (~30–60%) of g_{sd} regardless of the DS (Fig. 2c, d). An effect of abiotic stress was also reflected in the clear reduction of both $V_{c,max}$ and J_{max} (Fig. S1). Abiotic stress significantly reduced stomatal size on both adaxial and abaxial leaf surfaces (Fig. 2e, f), as well as the adaxial/abaxial stomatal size ratio (Fig. S2). The distribution of stomatal size (Fig. 2e, f) displayed a similar pattern to that of g_{sn} among all treatments (Fig. 2b). The abiotic effect on stomatal size was considerably larger on the adaxial leaf surface, and we detected no significant effects on stomatal density (Fig. S2).

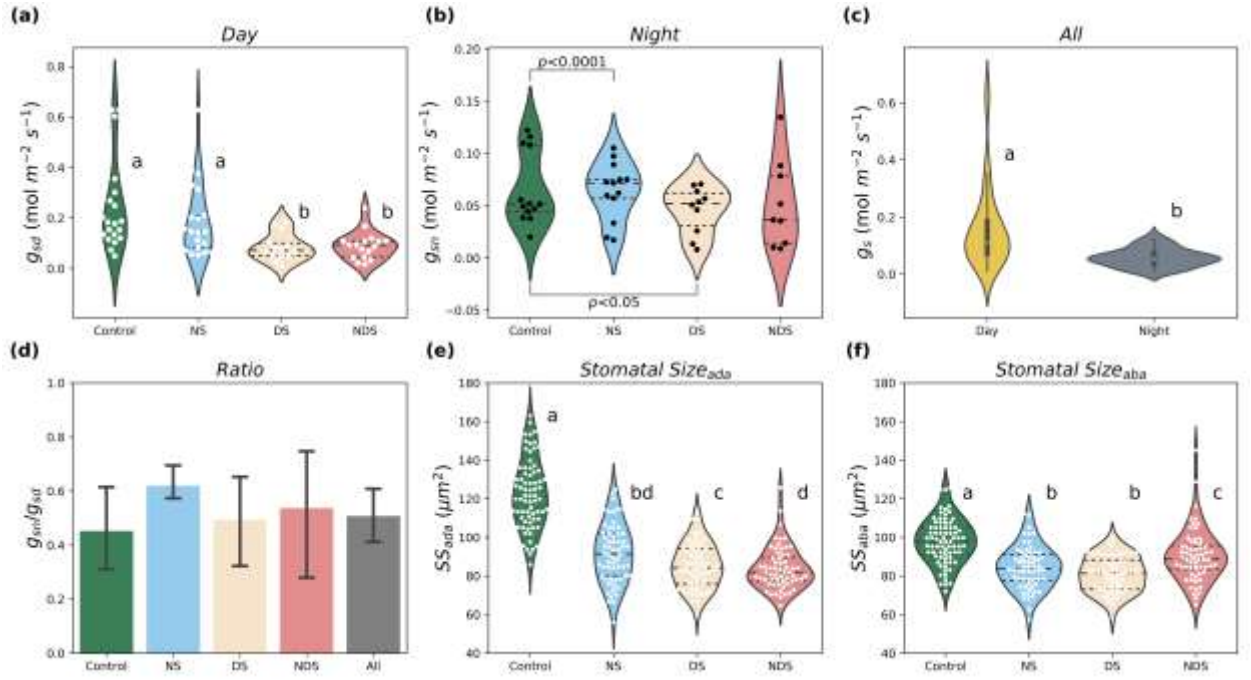

Figure 2 (a) Daytime non-steady-state (300 µmol m^{-2} s^{-1} PPFD) and steady-state (1,800 µmol m^{-2} s^{-1} PPFD) stomatal conductance (g_{sd}) in each treatment. (b) Nighttime steady-state stomatal conductance (g_{sn}) in each treatment, significant *p*-values indicate that samples are from different populations. (c) Grouped stomatal conductance (g_s) for daytime and nighttime. (d) Ratio between g_{sn} and the average g_{sd} at 300 and 1,800 µmol m^{-2} s^{-1} PPFD for each sample. Error bars indicate one standard deviation of uncertainty. Stomatal size (SS) on (e) adaxial (ada) and (f) abaxial (aba) leaf surfaces. The lower-case letters within each panel indicate the significance level both for the mean values and in data distribution. Nonsignificant results are unlabeled.

3.2 Nighttime leaf physiological traits

Next, we pooled observations collected on different dates, (n = 29), and found that leaf R_n was significantly correlated with g_{sn}, regardless of abiotic stress (R^2 = 0.35, P < 0.001) (Fig. 3a). T_{leaf} was reduced at higher g_{sn} values (Fig. 3b), and was negatively correlated with nocturnal E_n (R^2 = 0.42, P < 0.001) (Fig. 3c and Fig. S3a). R_n and E_n were positively correlated (R^2 = 0.28, P < 0.01) (Fig. S3c).

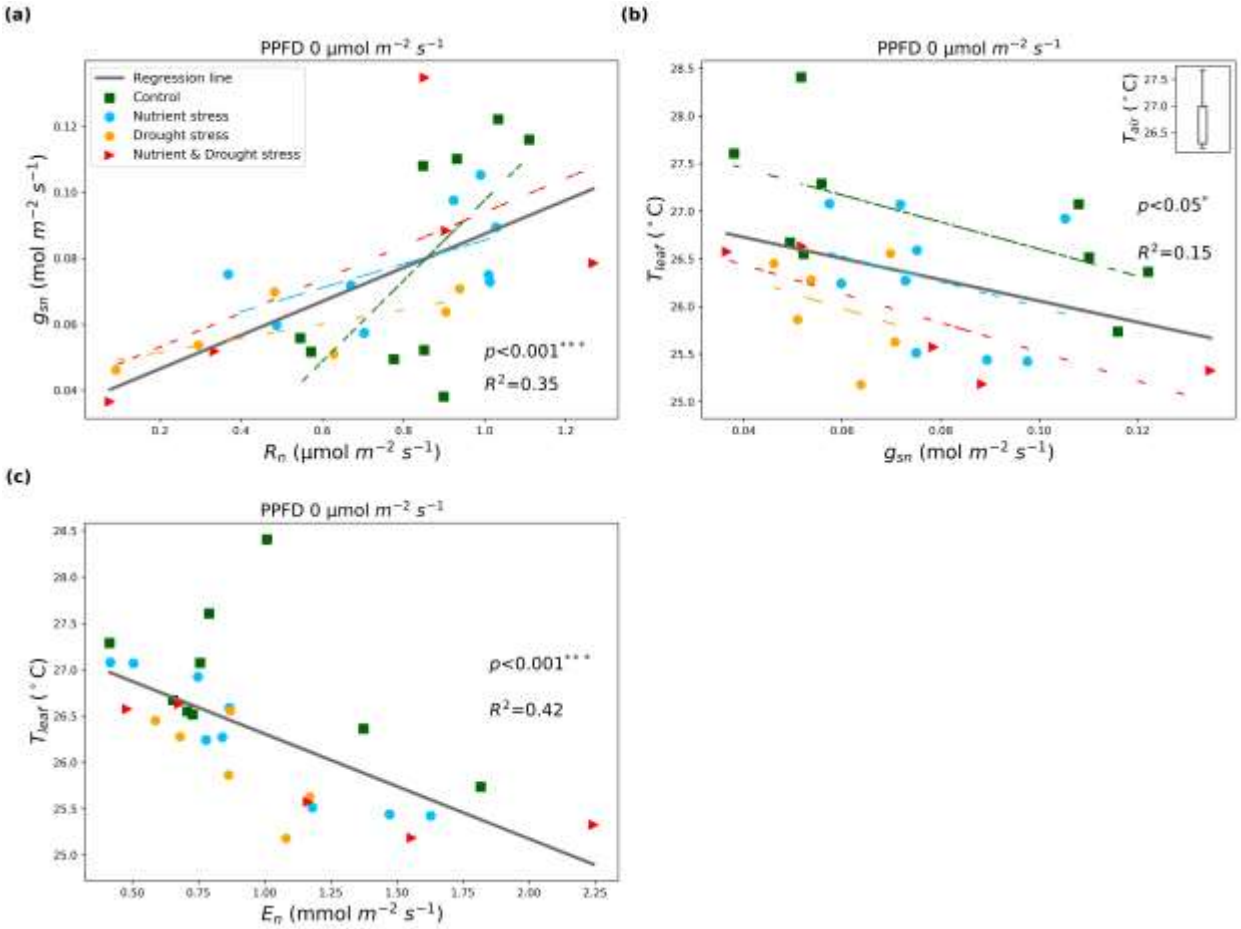

Figure 3 (a) Correlation between nocturnal respiration (R_n) and g_{sn} (n = 29). (b) Correlation between g_{sn} and T_{leaf}. (c) Correlation between nocturnal transpiration (E_n) and T_{leaf}. Solid regression line and statistics are based on all samples, colored dashed regression lines are based on each individual treatment.

3.3 Significant priming effects of g_{sn} on early morning photosynthesis (~5:00 – 7:00)

We found that g_{sn} was positively correlated with non-steady-state g_{sd}, with a PAR of 300 µmol m^{-2} s^{-1} PPFD, which includes abiotic stress disturbance (R^2 = 0.38, P < 0.01, Fig. 4a). We also found that g_{sn} was positively correlated with early morning A (R^2 = 0.18, P < 0.05, Fig. 4b) and significantly reduced the time required to reach maximum early morning A (R^2 = 0.27, P < 0.05, Fig. 4c; R^2 = 0.29, P < 0.01, Fig. S4a). Larger g_{sd} values (R^2 = 0.63, P < 0.001) and shorter response times were both tightly coupled with higher A values (Fig. S3b, c).

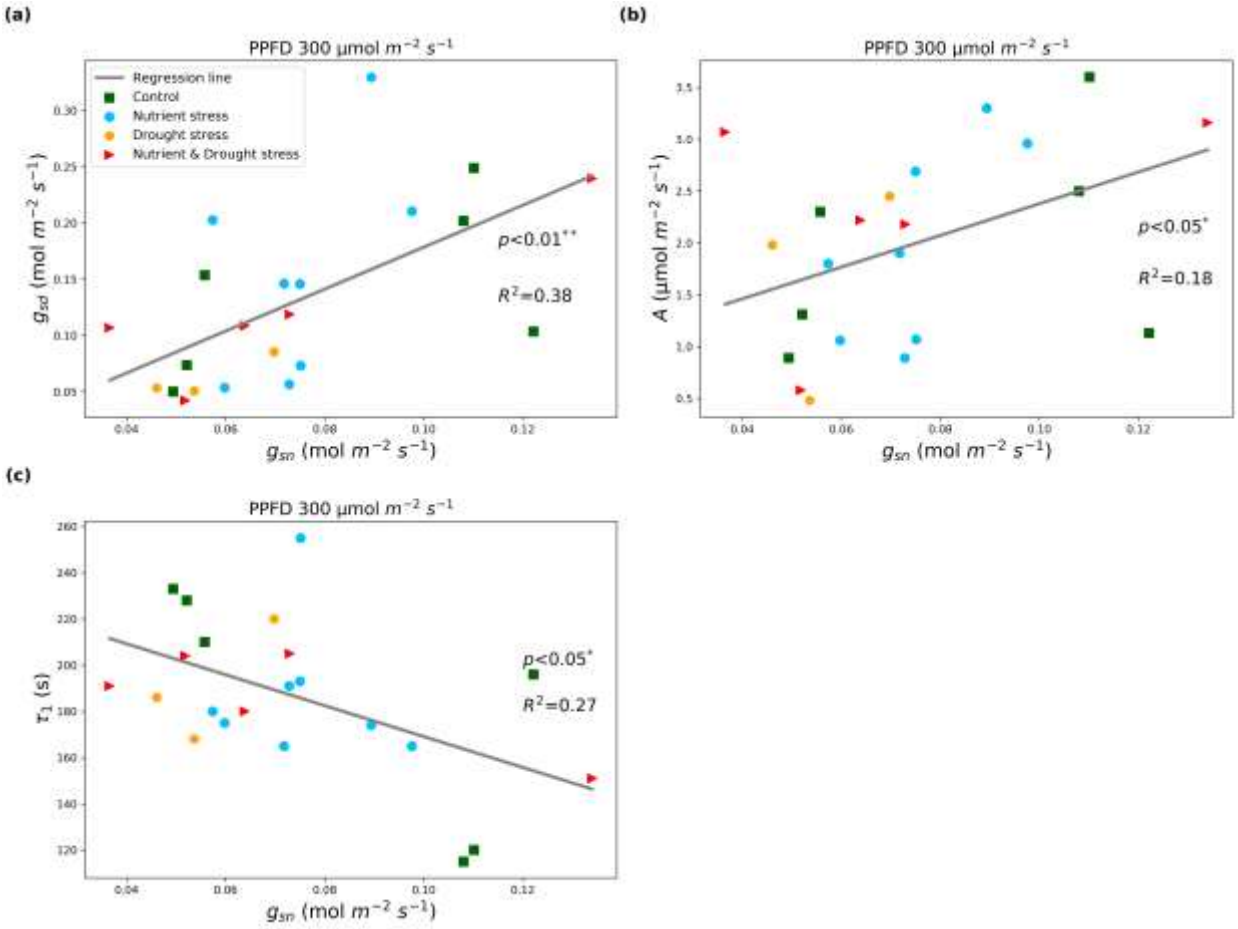

Figure 4 (a) Correlation between nocturnal stomatal conductance (g_{sn}) and early morning (300 µmol m^{-2} s^{-1} PPFD) non-steady-state maximum stomatal conductance (g_{sd}) within a 5-min period (n = 22). (b) Maximum assimilation rate (A) within a 5-min period. (c) Correlation between g_{sn} and the time (τ_1) to reach 63% of the maximum early morning A within a 5-min period.

3.4 Path analyses only support the leaf trait coordination

To determine how different leaf traits influence each other and ultimately act on T_{leaf}, A, or Rn, we conducted path analyses based on the proposed hypotheses, including abiotic stress as a random effect (Fig. 1). We detected no significant direct effects of g_{sn} on T_{leaf} or A (Fig. 5a, b). The observed coordination-E_n cooling result was achieved through the pathway $R_n \rightarrow g_{sn} \rightarrow E_n \rightarrow T_{leaf}$ (Fig. 5a), while the coordination-circadian priming effect was associated with the pathway $R_n \rightarrow g_{sn} \rightarrow \tau_1 \rightarrow g_{sd} \rightarrow A$ (Fig. 5b). Notably, R_n was tightly coupled with g_{sn} in both pathways (Fig. 5a,

b), and in our linear regression analysis (Fig. 3a). We also found that lower T_{leaf} significantly increased R_n, however, the overall path model had poor fit indices (Fig. 5c). Based on these results, we conducted additional path analyses by increasing the degrees of freedom (Fig. S5). We found that the key pathways to lower T_{leaf} and higher A were identical.

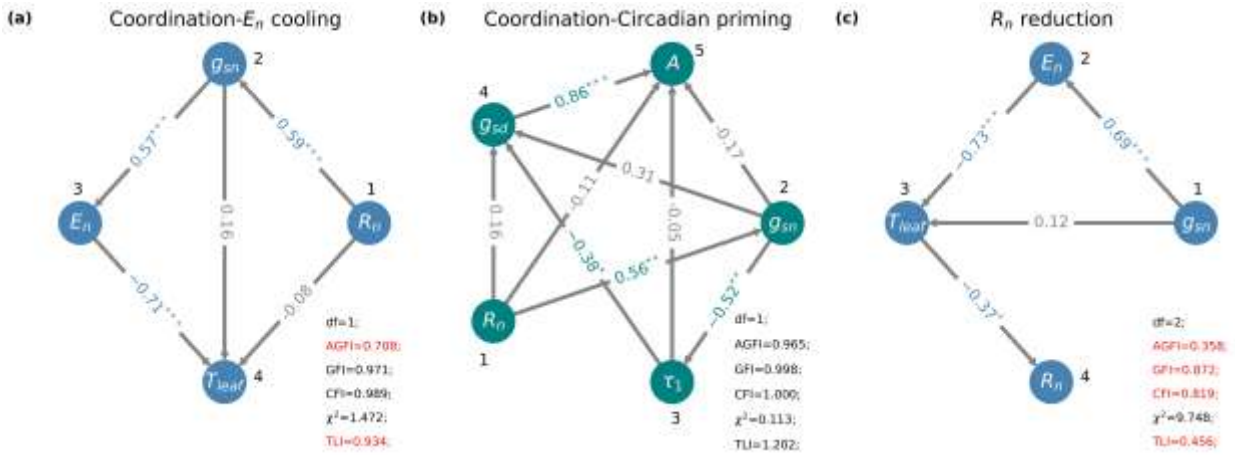

Figure 5 Path analyses of the (a) coordination-E_n cooling hypothesis (n = 29); (b) coordination-circadian priming hypothesis (early morning 300 μmol m^{-2} s^{-1} PPFD and non-steady-state conditions; n = 22, where τ_1 denotes the time to reach 63% of the maximum early morning A within a 5-min period; and (c) the R_n reduction hypothesis (n = 29). Arrows indicate speculated interactions between pairs of leaf traits. Integers in each panel denote the hypothesized sequence of interactions between leaf traits. Path coefficients were normalized from −1 to 1 and are shown in between traits; significant relationships (*P < 0.05, **P < 0.01, ***P < 0.001) are indicated by blue or green numbers. GFI, goodness of fit; AGFI, adjusted goodness of fit; CFI, comparative fit index; TLI, Tucker-Lewis index. Red text indicates poor model fit indices. Ranges of good model fit indices were defined as follows: AGFI > 0.90, CFI > 0.90, GFI > 0.95, and TLI > 0.97.

3.5 Impacts of g_{sn} on g_{sd} and A_{max} under light-saturated conditions

We found that g_{sn} was not significantly correlated with g_{sd} or A_{max} under light-saturated and steady-state conditions (Fig. 6a, b). By contrast, we detected a significant positive correlation between R_n and g_{sd}, and between R_n and A_{max} (Fig. S6c, d). However, we did not detect significant direct or indirect effects of nocturnal leaf traits g_{sn} and R_n on either A_{max} or maximum g_{sd} (Fig. 6d). Also,

we did not detect g_{sn}-induced priming effects on g_{sd}. Finally, A_{max} was strongly positively correlated with g_{sd} (R^2 = 0.80, Fig. 6c).

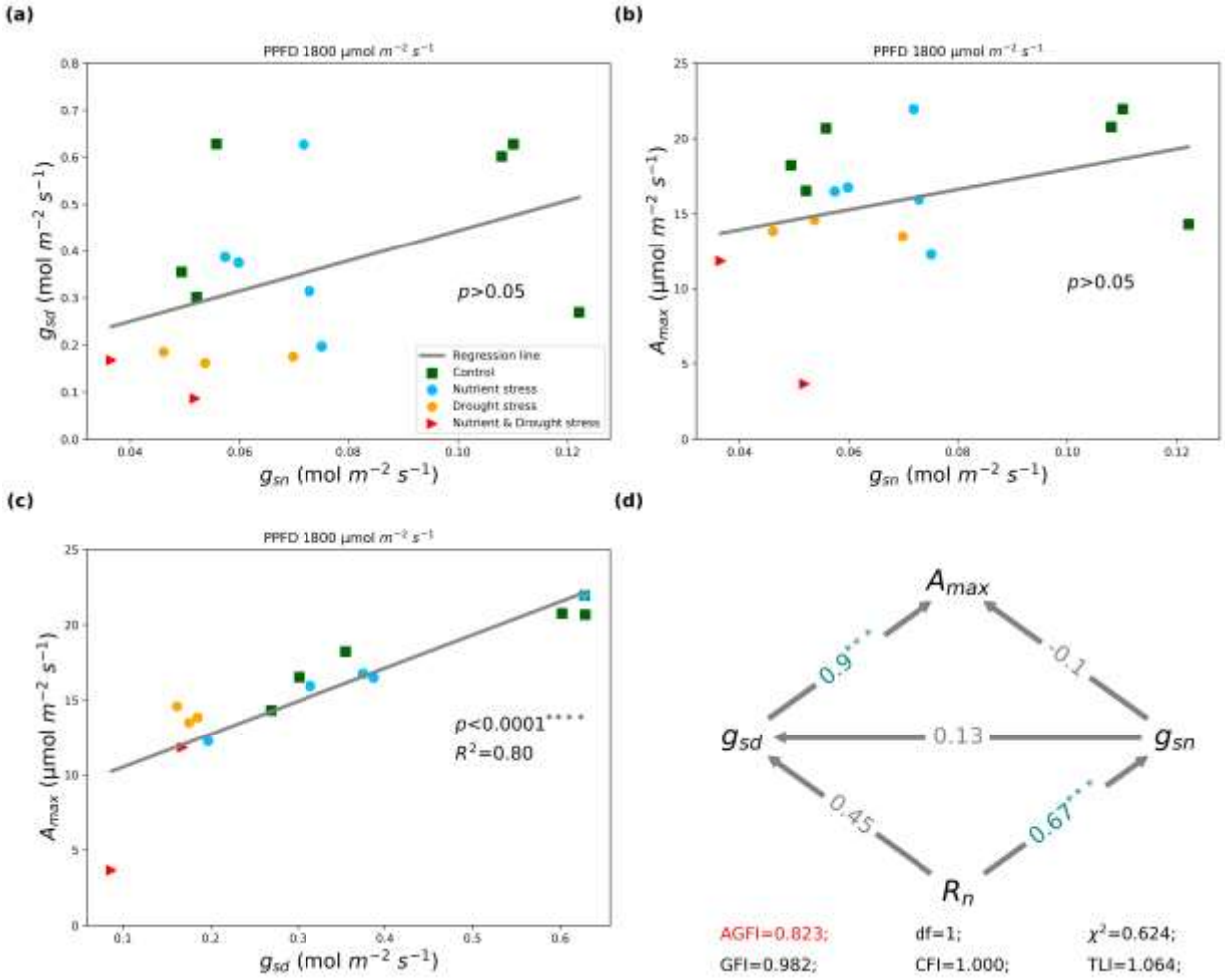

Figure 6 Correlation between nocturnal stomatal conductance (g_{sn}) and (a) steady-state, light-saturated (1,800 µmol m^{-2} s^{-1} PPFD) stomatal conductance, and (b) the assimilation rate (A_{max}) (n=16). (c) Correlation between steady-state, light-saturated g_{sd} and A_{max}. (d) Path analysis of the coordination-circadian priming hypothesis (light-saturated, steady-state conditions; n=16). Path coefficients were normalized from −1 to 1 and are shown in between traits; significant relationships (***P < 0.001) are indicated in blue text. GFI, goodness of fit; AGFI, adjusted goodness of fit; CFI, comparative fit index; TLI, Tucker-Lewis index.

3.6 Photosynthesis priming effects not detected after mid-morning (9:00)

Based on light response curve measurements obtained on DOY 197, we found that neither *A* nor g_{sd} was clearly associated with g_{sn} (Fig. 7a, b). At all light values, *A* was significantly correlated with g_{sd} in all treatments (Fig. 7c). We also detected a non-significant positive correlation between g_{sn} and g_{sd} after mid-morning (9:00), even at low PAR values (50–300 µmol m^{-2} s^{-1} PPFD; Fig. 7d).

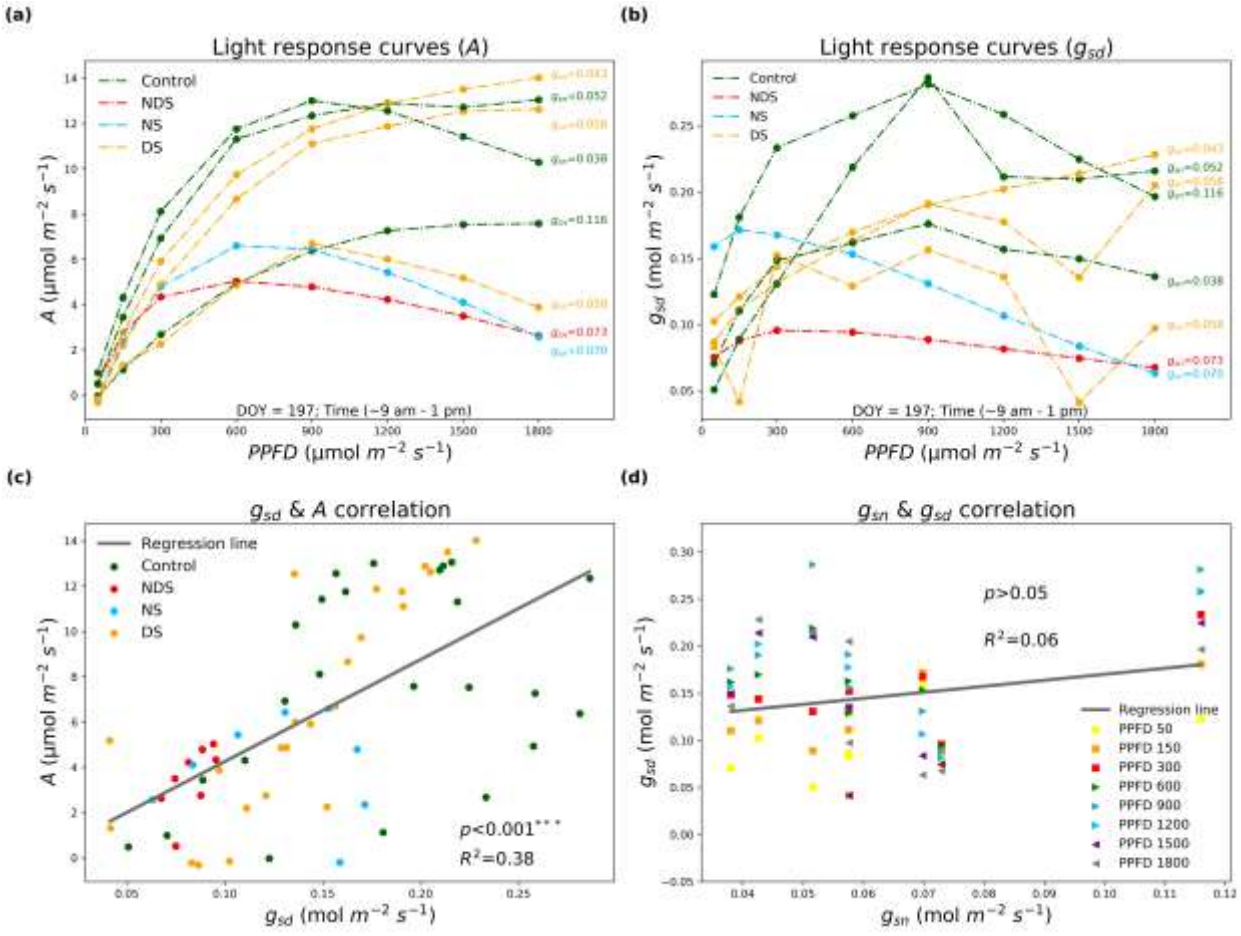

Figure 7 Light response curves of (a) *A* and (b) g_{sd}. Correlation between g_{sd} and (c) *A* and (d) g_{sn} (*n* = 64, 8 PPFD values × 8 light response curves).

4. Discussion

In this study, we proposed that daytime and nighttime leaf traits would covary with each other in the circadian cycle in rice (Fig. 1). Based on our new results (Fig. 5) and previous findings (Collalti and Prentice, 2019; Flütsch and Santelia, 2021; Van Oijen et al., 2010; Yu et al., 2019), we propose a new coordination framework for g_{sn} (Fig. 8), in which the prior daily accumulated assimilate is the prerequisite nocturnal substrate, and is proportional to R_n (Collalti and Prentice, 2019; Van Oijen et al., 2010); mitochondrial respiration within guard cells provides energy to regulate g_{sn} and light-induced stomatal opening (Flütsch and Santelia, 2021; Flütsch et al., 2020); g_{sn} priming facilitates *A* through a shorter stomatal response time (Resco de Dios et al., 2016); nocturnal leaf traits (g_{sn} and Rn) act to coordinate individual diurnal cycles to form a seasonal continuum (Fig. 8).

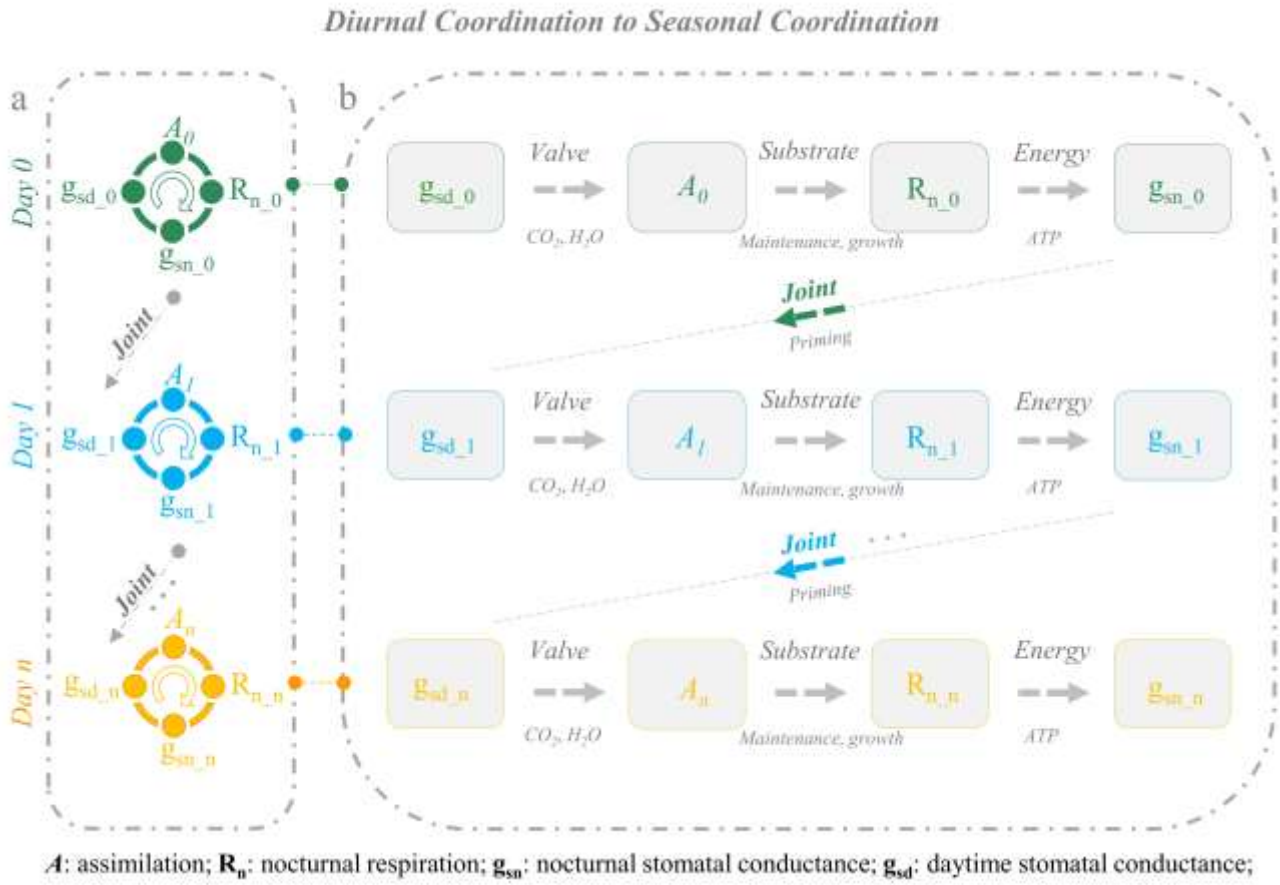

Figure 8 (a) Proposed temporal (diurnal and seasonal) coordination of key leaf traits and (b) functional interpretation; g_{sn} acts as the key link.

4.1 Abiotic stress results: Implications for different hypotheses

Our findings partly support the nutrient uptake hypothesis. We found that NS altered the distribution of g_{sn} and stomatal size (Fig. 2). Unexpectedly, however, NS had no significant effects on mean g_{sn} (Fig. 2b). Nutrient uptake hypothesis still lacks convincing evidence (Kupper et al., 2012; Lewis et al., 2011; Resco de Dios et al., 2019; Zeppel et al., 2014). In this study, nutrient stress selectively increased g_{sn}, for example, we obtained the highest median g_{sn} in the NS treatment and highest g_{sn} in the NDS treatment (Fig. 2b). Larger stomata maintained higher g_{sn} in rice plants (Zhang et al., 2021), which is consistent with the findings that high g_{sn} values and large stomata were both more frequent in the control and NDS treatments (Fig. 2b, e, f). We also found that stomatal size distribution pattern (Fig. 2e, f) was similar to that of g_{sn} among all treatments (Fig. 2b). Thus, the proposed g_{sn}-induced nutrient acquisition is likely achieved by increasing stomatal size. In addition, g_{sn} tended to increase and decrease g_{sn} in the upper and lower observation ranges, respectively, in the NDS treatment. Limited soil moisture partly offset nutrient acquisition demand via g_{sn} regulation of sap flow, leading to competition in the combined NDS treatment between water conservation and N uptake. However, given our limited sample sizes and measurement uncertainty, we encourage further investigations across the growing season using larger sample sizes.

The lack of a strong g_{sn} response to drought (Fig. 2b) indicates that water conservation is not the key factor limiting g_{sn}**.** In general, g_{sn} decreases with lower soil water potential (Chowdhury et al., 2021), but also exhibits high heterogeneity, even within the same species and treatment, see Fig. 3a in Wang et al. (2021); this is consistent with the findings of this study (Fig. 2b). To date, g_{sn} responses to drought stress were divergent (Chowdhury et al., 2021; Wang et al., 2021; Yu et al., 2019; Zeppel et al., 2014). A recent meta-analysis also reported that g_{sn} exhibits variable responses to environmental drivers such as drought, see Fig. 2 in Chowdhury et al. (2021). Notably, we observed high g_{sn}/g_{sd} ratios even under DS (Fig. 2d), which were identical to those of the control treatment. Drought only decreased g_{sn} from the upper quartile (Fig. 2b). Furthermore, if the key benefit of stomatal closure is the conservation of water overnight (e.g., drought), why do stomata close under ample water supply (e.g., during water saturation)? The counterintuitive results

obtained in this study clearly indicate that g_{sn} in rice plants is not closely related to water availability.

This study found no clear evidence to reject the CO_2 flushing hypothesis, however, g_{sn} is excessively high for the sole reason of avoiding toxic CO_2 concentrations. Excessive CO_2 flushing is thought to prevent toxic CO_2 concentrations in leaves, and therefore to assist the cytochrome respiration pathway. Following Resco de Dios et al. (2019), we applied Fick's law of diffusion ($g_n = \frac{R_n}{C_i - C_a}$), using the lowest g_{sn} value (0.01 mol m^{-2} s^{-1}) and highest R_n value (1.27 μmol m^{-2} s^{-1}) as an extreme case, and obtained an intercellular CO_2 concentration (C_i) of 603 ppm ($400 + \frac{1.27 \times 1.6}{0.01}$); this is unlikely to be sufficient to inhibit cytochrome respiration. We then computed C_i based on median values (g_{sn} = 0.054 mol m^{-2} s^{-1}; R_n = 0.85 μmol m^{-2} s^{-1}), and obtained C_i = 425 ppm, which was close to the ambient level. These findings are consistent with the results of the previous global g_{sn} based study, in that g_{sn} is favorable for CO_2 removal but excessive relative to the requirement for cytochrome respiratory benefit (Resco de Dios et al., 2019). Importantly, we found that stomata did not close completely overnight, under which circumstances intercellular CO_2 would accumulate over time, resulting in toxic CO_2 levels. Therefore, we conclude that excessive CO_2 flushing is only a secondary mechanism in the nocturnal stomatal opening seen in rice plants.

4.2 Enhanced carbon assimilation through coordinated regulation by g_{sn}

We proposed that g_{sn} acts as a "bridge" between antecedent R_n and photosynthesis occurring during the following dawn through the pathway $R_n \rightarrow g_{sn} \rightarrow \tau \rightarrow g_{sd} \rightarrow A$ (Fig. 5b). Importantly, we found that g_{sn} was tightly coupled with R_n (Fig. 3a), which has also been reported previously (McAusland et al., 2021; Wang et al., 2021; Yu et al., 2019; Zhang et al., 2021). Interpreting g_{sn} through R_n appears promising, but a main mechanism (i.e., beyond the secondary CO_2 flushing mechanism) is required. The current literature suggests that starch metabolism is involved in guard cell osmoregulation (Caird et al., 2007; Chowdhury et al., 2021), which affects predawn g_{sn}. Recent studies have applied isotope labeling techniques to obtain new cellular-level evidence that starch

degradation has distinct functions in dawn stomatal opening (Flütsch and Santelia, 2021). Specifically, sucrose metabolism (glycolysis and mitochondrial respiration) within guard cells provides energy for faster stomatal responses (Daloso et al., 2016; Flütsch et al., 2020; Lima et al., 2018). Therefore, we suggest that R_n is not simply correlated with g_{sn}, but is likely the causal factor and energy driver of nocturnal stomatal opening. Future studies should further investigate this hypothesis at the leaf level by collecting time-series R_n and g_{sn} data under ambient conditions, as well as by conducting causality analyses.

In this study, we found that g_{sn} induced photosynthesis priming remained effective for at least 2 h after dawn (~5:00; Fig. 4) and diminished after mid-morning (9:00; Fig. 7). Circadian clock resonating g_{sn} enhances growth (McAusland et al., 2021; Resco de Dios et al., 2016), although priming benefits likely also depend on plant species (Auchincloss et al., 2014), stomatal size and density (Drake et al., 2013) and, in particular, PPFD (Chieppa et al., 2021; Resco de Dios et al., 2016; Zhang et al., 2021). In this study, we observed that circadian priming facilitated *A* in the early morning (~5:00 – 7:00, 300 µmol m^{-2} s^{-1} PPFD) (Figs. 4 and 5b), independent of the abiotic stress and stomatal anatomy (Fig. 2e, f). We found that g_{sn} did not influence steady-state A_{max} (1,800 µmol m^{-2} s^{-1} PPFD) or the corresponding g_{sd} (Fig. 6). More importantly, no photosynthesis priming effects were detected after mid-morning (9:00) at any PPFD values (Fig. 7d). Thus, based on the new evidence discussed above, these coordinated priming effects diminished over time and with changing environmental conditions. This phenomenon is likely influenced by a contribution of several confounding variables, particularly during circadian regulation and acclimation of g_{sd} to new PPFD and temperature conditions (Matthews et al., 2018). To date, g_{sn} has shown no effects on steady-state *A* at a PPFD of 1,200 µmol m^{-2} s^{-1} in rice plants, see Fig. S4c in Zhang et al. (2021). A similar result was reported for C_4 switchgrass under light-saturated PPFD (Chieppa et al., 2021). To our knowledge, the upper limit of PPFD at which g_{sn} influences *A* and g_{sd} is 1,000 µmol m^{-2} s^{-1}, based on measurements in wheat (McAusland et al., 2021). Therefore, we suggest that future studies should quantify the role of coordinated priming on daily carbon budgets using continuous time-series observations.

The proposed "coordinated leaf physiological trait" hypothesis is consistent with current literature findings. In this study, we used R_n as a proxy of prior assimilation, based on evidence showing that the magnitude of nocturnal respiration is proportional to and constrained by antecedent photosynthesis (through the law of mass conservation), with a homeostatic R_n-to-photosynthesis ratio of 0.4–0.5 (Collalti and Prentice, 2019; Van Oijen et al., 2010). A recent meta-analysis also reported that changes in g_{sn} are positively related to photosynthesis, see Fig. 2 in Chowdhury et al. (2021). These findings are consistent with the proposed coordination hypothesis (Fig. 8), in which R_n is first coordinated with *A*, subsequently provides energy for g_{sn}, and eventually primes early morning g_{sd} and photosynthesis. In this study, we tested the hypothesis that g_{sn} responses to the previous-day R_n trend and sets the trend for the following dawn through the pathway R_n (day 1) $\rightarrow g_{sn} \rightarrow \tau \rightarrow g_{sd} \rightarrow A$ (day 2) (Fig. 5b). However, the full coordinated circle, starting with *A*, has yet to be completely elucidated (Fig. 8), for example, it may proceed through the pathway A_1 (day 1) $\rightarrow R_n \rightarrow g_{sn} \rightarrow g_{sd} \rightarrow A_2$ (day 2). The quantitative impact of g_{sn} on carbon assimilation is an important question that remains to be addressed.

4.3 Evaporative cooling: Passive thermoregulation via leaf trait coordination

We propose that leaf cooling is byproduct of coordinated leaf physiological traits. As potential benefit of g_{sn}, evaporative cooling has been suggested to lower T_{leaf}, thereby also reducing respiratory cost**.** Wang et al. (2021) assumed that E_n loss was the key cost of g_{sn}. However, this assumption may not be applicable in a flooded rice cultivation system, as semiaquatic plants can experience the full cooling benefits of large g_{sn}, without any clear costs. In this study, we found that significant cooling effects were obtained through by g_{sn}-induced transpiration (Fig. 3b, c), consistent with previous findings (Wang et al., 2021; Zhang et al., 2021). More importantly, we found clear evidence that lower T_{leaf} did not reduce the R_n cost under ambient conditions (Fig. 5c and Fig. S3b). Both linear regression and path analysis results contradicted the hypothesis of g_{sn}-derived R_n reduction through evaporative cooling. Nevertheless, our experiments were conducted under ambient conditions, with relatively low air temperature variation (27.0 ± 0.65 °C) during the sampling periods (Fig. 3b); this may explain why we were unable to detect respiratory reduction effects. Our findings, particularly the clear positive relationship between R_n and g_{sn} over a large

range (Fig. 3a), conclusively demonstrate that cooling is byproduct of leaf trait coordination, rather than active thermoregulation, and reduces R_n cost. However, this finding does not fully exclude the possibility that leaf cooling is a driver in other situations, such as active at high temperatures. For example, Wang et al. (2021) detected a positive leaf-level response of g_{sn}, ranging from 0.02 to 0.05 mol m^{-2} s^{-1}, to a temperature increase from 19°C to 35°C in red birch without DS. Thus, to determine whether evaporative cooling is an important component of g_{sn} behavior, or rather a passive byproduct of leaf trait coordination at higher temperature, future studies should conduct measurements over a wider range of temperatures, and possibly also conduct warming treatments, ideally at the canopy scale (Resco de Dios et al., 2018; Stuerz and Asch, 2021).

References

Auchincloss, L., Easlon, H.M., Levine, D., Donovan, L., Richards, J.H. (2014) Pre-dawn stomatal opening does not substantially enhance early-morning photosynthesis in Helianthus annuus. Plant, Cell & Environment 37, 1364-1370.

Barbour, M.M., Cernusak, L.A., Whitehead, D., Griffin, K.L., Turnbull, M.H., Tissue, D.T., Farquhar, G.D. (2005) Nocturnal stomatal conductance and implications for modelling 18O of leaf-respired CO2 in temperate tree species. Functional Plant Biology 32, 1107-1121.

Caird, M.A., Richards, J.H., Donovan, L.A. (2007) Nighttime Stomatal Conductance and Transpiration in C3 and C4 Plants. Plant Physiology 143, 4-10.

Chieppa, J., Brown, T., Giresi, P., Juenger, T.E., Resco de Dios, V., Tissue, D.T., Aspinwall, M.J. (2021) Climate and stomatal traits drive covariation in nighttime stomatal conductance and daytime gas exchange rates in a widespread C4 grass. New Phytologist 229, 2020-2034.

Chowdhury, F.I., Arteaga, C., Alam, M.S., Alam, I., Resco de Dios, V. (2021) Drivers of nocturnal stomatal conductance in C3 and C4 plants. Science of The Total Environment, 151952.

Collalti, A., Prentice, I.C. (2019) Is NPP proportional to GPP? Waring's hypothesis 20 years on. Tree Physiology 39, 1473-1483.

Daley, M.J., Phillips, N.G. (2006) Interspecific variation in nighttime transpiration and stomatal conductance in a mixed New England deciduous forest. Tree Physiology 26, 411-419.

Daloso, D.M., dos Anjos, L., Fernie, A.R. (2016) Roles of sucrose in guard cell regulation. New Phytologist 211, 809-818.

Darwin, F. (1898) IX. Observations on stomata. Philosophical Transactions of the Royal Society of London. Series B, Containing Papers of a Biological Character 190, 531-621.

Dodd, A., N., Salathia, N., Hall, A., Kévei, E., Tóth, R., Nagy, F., Hibberd Julian, M., Millar Andrew, J., Webb Alex, A.R. (2005) Plant Circadian Clocks Increase Photosynthesis, Growth, Survival, and Competitive Advantage. Science 309, 630-633.

Drake, P.L., Froend, R.H., Franks, P.J. (2013) Smaller, faster stomata: scaling of stomatal size, rate of response, and stomatal conductance. Journal of Experimental Botany 64, 495-505.

Epps, T.W., Singleton, K.J. (1986) An omnibus test for the two-sample problem using the empirical characteristic function. Journal of Statistical Computation and Simulation 26, 177-203.

Flütsch, S., Santelia, D. (2021) Mesophyll-derived sugars are positive regulators of light-driven stomatal opening. New Phytologist 230, 1754-1760.

Flütsch, S., Wang, Y., Takemiya, A., Vialet-Chabrand, S.R.M., Klejchová, M., Nigro, A., Hills, A., Lawson, T., Blatt, M.R., Santelia, D. (2020) Guard Cell Starch Degradation Yields Glucose for Rapid Stomatal Opening in Arabidopsis[CC-BY]. The Plant Cell 32, 2325-2344.

Forster, M.A. (2014) How significant is nocturnal sap flow? Tree Physiology 34, 757-765.

Fricke, W. (2019) Night-Time Transpiration – Favouring Growth? Trends in Plant Science 24, 311-317.

Gansert, D. (2003) Xylem sap flow as a major pathway for oxygen supply to the sapwood of birch (Betula pubescens Ehr.). Plant, Cell & Environment 26, 1803-1814.

Huang, C.-W., Domec, J.-C., Ward, E.J., Duman, T., Manoli, G., Parolari, A.J., Katul, G.G. (2017) The effect of plant water storage on water fluxes within the coupled soil–plant system. New Phytologist 213, 1093-1106.

Huang, Y., Ryu, Y., Jiang, C., Kimm, H., Kim, S., Kang, M., Shim, K. (2018) BESS-Rice: A remote sensing derived and biophysical process-based rice productivity simulation model. Agricultural and Forest Meteorology 256-257, 253-269.

Hwang, Y., Ryu, Y., Huang, Y., Kim, J., Iwata, H., Kang, M. (2020) Comprehensive assessments of carbon dynamics in an intermittently-irrigated rice paddy. Agricultural and Forest Meteorology 285-286, 107933.

Kupper, P., Rohula, G., Saksing, L., Sellin, A., Lõhmus, K., Ostonen, I., Helmisaari, H.-S., Sõber, A. (2012) Does soil nutrient availability influence night-time water flux of aspen saplings? Environmental and Experimental Botany 82, 37-42.

Leitgeb, H. (1886) Beiträge zur Physiologie der Spaltöffnungsapparate. Mittheilungen aus dem Botanischen Institute zu Graz, 123-184.

Lewis, J.D., Phillips, N.G., Logan, B.A., Hricko, C.R., Tissue, D.T. (2011) Leaf photosynthesis, respiration and stomatal conductance in six Eucalyptus species native to mesic and xeric environments growing in a common garden. Tree Physiology 31, 997-1006.

Lima, V.F., Medeiros, D.B., Dos Anjos, L., Gago, J., Fernie, A.R., Daloso, D.M. (2018) Toward multifaceted roles of sucrose in the regulation of stomatal movement. Plant Signaling & Behavior 13, e1494468.

McAusland, L., Smith, K.E., Williams, A., Molero, G., Murchie, E.H. (2021) Nocturnal stomatal conductance in wheat is growth-stage specific and shows genotypic variation. New Phytologist 232, 162-175.

Ogle, K., Lucas, R.W., Bentley, L.P., Cable, J.M., Barron-Gafford, G.A., Griffith, A., Ignace, D., Jenerette, G.D., Tyler, A., Huxman, T.E., Loik, M.E., Smith, S.D., Tissue, D.T. (2012) Differential daytime and night-time stomatal behavior in plants from North American deserts. New Phytologist 194, 464-476.

Palet, A., Ribas-Carbó, M., Argilés, J.M., Azcón-Bieto, J. (1991) Short-Term Effects of Carbon Dioxide on Carnation Callus Cell Respiration 1. Plant Physiology 96, 467-472.

Rea, A.C. (2020) Sugar Is Sweeter: Plants Open Their “Mouths” for Glucose, Not Malate, in the Morning[OPEN]. The Plant Cell 32, 2071-2072.

Resco de Dios, V., Chowdhury, F.I., Granda, E., Yao, Y., Tissue, D.T. (2019) Assessing the potential functions of nocturnal stomatal conductance in C3 and C4 plants. 223, 1696-1706.

Resco de Dios, V., Loik, M.E., Smith, R., Aspinwall, M.J., Tissue, D.T. (2016) Genetic variation in circadian regulation of nocturnal stomatal conductance enhances carbon assimilation and growth. Plant, Cell & Environment 39, 3-11.

Resco de Dios, V., Loik, M.E., Smith, R.A., Tissue, D.T. (2018) Effects of a Heat Wave on Nocturnal Stomatal Conductance in Eucalyptus camaldulensis. Forests 9.

Schellenberg, H.C. (1896) Beiträge zur Kenntnis von Bau und Funktion der Spaltöffnungen. Botanische Zeitung 1, 169.

Schneider, C.A., Rasband, W.S., Eliceiri, K.W. (2012) NIH Image to ImageJ: 25 years of image analysis. Nature Methods 9, 671-675.

Sharkey, T.D. (2016) What gas exchange data can tell us about photosynthesis. Plant, Cell & Environment 39, 1161-1163.

Snyder, K.A., Richards, J.H., Donovan, L.A. (2003) Night-time conductance in C3 and C4 species: do plants lose water at night? Journal of Experimental Botany 54, 861-865.

Stahl, E., (1897) Über den Pflanzenschlaf und verwandte Erscheinungen. A. Förstner.

Stinziano, J.R., McDermitt, D.K., Lynch, D.J., Saathoff, A.J., Morgan, P.B., Hanson, D.T. (2019) The rapid A/Ci response: a guide to best practices. New Phytologist 221, 625-627.

Stinziano, J.R., Morgan, P.B., Lynch, D.J., Saathoff, A.J., McDermitt, D.K., Hanson, D.T. (2017) The rapid A–Ci response: photosynthesis in the phenomic era. Plant, Cell & Environment 40, 1256-1262.

Stuerz, S., Asch, F. (2021) Responses of Rice Growth to Day and Night Temperature and Relative Air Humidity—Leaf Elongation and Assimilation. Plants 10.

Van Oijen, M., Schapendonk, A., Höglind, M. (2010) On the relative magnitudes of photosynthesis, respiration, growth and carbon storage in vegetation. Annals of Botany 105, 793-797.

Wang, Y., Anderegg, W.R.L., Venturas, M.D., Trugman, A.T., Yu, K., Frankenberg, C. (2021) Optimization theory explains nighttime stomatal responses. New Phytologist 230, 1550-1561.

Woodward, F.I. (1987) Climate and plant distribution. Cambridge University Press.

Yu, K., Goldsmith, G.R., Wang, Y., Anderegg, W.R.L. (2019) Phylogenetic and biogeographic controls of plant nighttime stomatal conductance. New Phytologist 222, 1778-1788.

Zeppel, M.J.B., Lewis, J.D., Phillips, N.G., Tissue, D.T. (2014) Consequences of nocturnal water loss: a synthesis of regulating factors and implications for capacitance, embolism and use in models. Tree Physiology 34, 1047-1055.

Zhang, Q., Yang, Y., Peng, S., Li, Y. (2021) Nighttime transpirational cooling enabled by circadian regulation of stomatal conductance is related to stomatal anatomy and leaf morphology in rice. Planta 254, 12.

Chapter III. Multi-objective optimization of crop yield, water consumption, and greenhouse gases emissions for sustainable rice production

Abstract

A new paradigm for sustainable rice farming is urgently required amid challenges from increasing food demand, water scarcity, and carbon-neutral pledges. This study aimed to increase current crop yield, reduce irrigation water consumption, and tackle the dilemma to simultaneously reducing CH_4 and N_2O emissions in a flooded rice production system. By proposing a heuristic and holistic method, we optimized farm management beyond previous most emphasized irrigation regimes while also exploring niches from other pivotal options regarding sowing window, fertilization rate, tillage depth, and their interactions. Specifically, we calibrated and validated the process-based DNDC model with five years of eddy covariance observations. The DNDC model later was integrated with the non-dominated sorting genetic algorithm (NSGA-III) to solve the multi-objective optimization problem. We found that the optimized management would maintain or even increase current crop yield to its potential (~10 t/ha) while reducing more than 50% irrigation demand and GHGs (CH_4 & N_2O) emissions. Our results indicate that earlier sowing window and improvements on irrigation practice together would be pivotal to maximizing crop yield while sustaining environmental benefits. We found that the optimal fraction of non-flooded days was around 54% of growing season length and its optimal temporal distributions were primarily in vegetative stages. Our study shows that the present farm yield (8.3-8.9 t/ha) in study site not only has not achieved its potential level but also comes at a great environmental cost to water resources (604-810 mm/yr) and GHGs emissions (CH_4: 186-220 kg C/ha/yr; N_2O: 0.3-1.6 kg C/ha/yr). Furthermore, this simple method could further be applied to evaluate the environmental sustainability of a farming system under various climate and local conditions and to guide policymakers and farming practices with comprehensive solutions.

1. Introduction

By around 2050, one of the most urgent global missions is to feed 10 billion people by doubling food production (Ray et al., 2013; Tilman et al., 2011) while achieving carbon neutrality (Flagg, 2015). Rice (*Oryza sativa*) is a vital cereal crop that feeds more than 50% of the world population and over 90% is cultivated in Asia (Bouman and Tuong, 2001; Dong and Xiao, 2016). Rice, domesticated from wild grass as the semiaquatic crop in Yangtze valley China (Fuller et al., 2009; Gross and Zhao, 2014; Li et al., 2006b), has been prevalently cultivating worldwide in the flooded paddy to imitate its original subtropical growing environments, suppress weeds, and maintain yield for ~4000 years (Gutaker et al., 2020; Zong et al., 2007). However, the traditional anaerobic management leads rice production to consume ~40% of the irrigation water (Lampayan et al., 2015) and emit ~10% of the global anthropogenic methane (Saunois et al., 2020). Unfortunately, 4.0 billion people and many Asian countries comprised are already facing severe water scarcity (Mekonnen and Hoekstra, 2016). To slow climate warming, numerous countries have committed to achieving carbon neutrality in the next few decades. As the largest water consumer in the agricultural sector and dominant anthropogenic methane emitter, the longstanding thousand years of flooded rice farming is no longer sustainable while challenged by water scarcity (Gosling and Arnell, 2016), carbon-neutral pledges (Flagg, 2015), and global warming (Naylor et al., 2007; Zhao et al., 2017). We urgently need new paradigms for cultivating rice sustainably.

Considerable research efforts have been investigating to decrease water consumption, greenhouse gases (GHGs) emissions, and maintain the grain yield. In particular, altering soil redox conditions with draining management has been attracting the most attention (Bo et al., 2022; Kudo et al., 2014; LaHue et al., 2016; Li et al., 2006a; Meijide et al., 2017; Peng et al., 2006). Overall, a global meta-analysis finds non-continuous flooding mitigating CH_4 budgets (53%) but substantially spiking N_2O emissions (105%) and decreasing crop yield to some extent (3.6%) (Jiang et al., 2019a). Specifically, by periodically draining the paddy, Alternate Wetting and Drying (AWD) technology shows up to 38% reduced irrigation water requirement without yield compromise (Lampayan et al., 2015). Similarly, the midseason drainage significantly reduces CH_4 emissions (50–53%) and global warming potential (GWP) (46–50%) but increases N_2O emissions (20–37%) (Haque et al., 2016). Early-season drainage also demonstrates effective GWP reduction while

maintaining the crop yield and constraining N_2O footprints based on a growth chamber experiment (Islam et al., 2018). Thus, delicate planning of the duration and timing of the draining events is crucial to achieving the overall picture of sustainability. Mechanistic models and field experiments are therefore predominately applied to investigate the effects of various water-saving regimes (Chen et al., 2016; Fumoto et al., 2010; Liang et al., 2016; Linquist et al., 2015; Minamikawa et al., 2016; Tian et al., 2021). Among them, AWD has been recognized as the most promising water management approach and has been adopted in many regions (Ishfaq et al., 2020). Nevertheless, the emissions of long-lived N_2O could also surge (30–45 times) from the non-continuous flooding management (Kritee et al., 2018). The anaerobic decomposition (Neue, 1993) and aerobic nitrification processes (Bouwman, 1998) conspire towards the dilemma to reduce CH_4 and N_2O footprints simultaneously (Li et al., 2005; Liu et al., 2019).

In the context of rice production systems, while the bi-objective optimization problems have been well investigated, three or even more objectives remain less explored. Many key farming regimes affect the sustainability performance (Shang et al., 2021), therefore a new paradigm shall manage several key factors holistically such as the irrigation events (Jiang et al., 2019a), type and rate of the fertilization (Pandey et al., 2021; Zhong et al., 2016), straw addition (Jiang et al., 2019b), and tillage depth (Zhao et al., 2020). A holistic and integrated approach shall also balance several contradictory objectives including the trade-off between conserving water resources and maximizing grain yield, reducing CH_4 and N_2O emissions. With the extensive focus on improving water regimes, current solutions (e.g. AWD) are valuable to mitigate negative environmental impacts and sustain the social-economic benefits (Chen et al., 2016; Fumoto et al., 2010; Liang et al., 2016; Linquist et al., 2015; Minamikawa et al., 2016; Tian et al., 2021) but are unlikely to reach carbon neutrality in the mid of 21st century. To date, only a few studies consider the interaction of water regimes with fertilization and other farm management options by field experiments or scenario modeling (Kim et al., 2014; Towprayoon et al., 2005; Zhao et al., 2020). Furthermore, it remains unclear what the upper bound limit of irrigated rice farming system could achieve by optimizing rice production, GHGs emissions, and water consumption if integrated management is fully explored. Nevertheless, solely applying the biophysical models or conducting

field experiments is challenging to approach the optimal scenarios and nearly infeasible to quest all the potential integrated solutions while encountering multi competing objectives.

To resolve a conflicting multi-objective problem efficiently, coupling a process-based model with a Pareto-dominance-based optimization algorithm has been demonstrated as a promising solution (Coleman et al., 2017; Groot et al., 2012; Kropp et al., 2019). Back in the 19th century, economists Francis Edgeworth and Vilfredo Pareto were the pioneers to initiate multi-objective optimization (MOO) problems (de Weck, 2004). Among the available MOO methods, the evolutionary algorithms are one of the state-of-the-art options to approximate the Pareto efficiency/front, which is inspired by the natural evolution (selection, recombination, and mutation) (Emmerich and Deutz, 2018). In general, by executing the process model with vast different combinations of inputs (e.g. farm management), the optimization algorithm evaluates the model outputs to approach a set of solutions that possess the optimal values of the targeting objectives (e.g. crop yield) (Prina et al., 2018). More specifically, the optimal solutions jointly formulate the Pareto front, where none of the objectives can be further improved without deterioration of any others. Therefore, it forms an efficient and powerful method to balance the trade-offs and synergy farm decision planning without developing sophisticated mathematical equations.

This study aims to provide an interdisciplinary and heuristic approach for designing an environmentally sustainable rice farming system with a case study in South Korea. Specifically, we estimated Pareto fronts regarding the combination of the following key objectives: CH_4 budgets, N_2O emissions, irrigation water consumption, and crop yield. In this study, we integrated the process-based DNDC (DeNitrification DeComposition) model with the non-dominated sorting genetic algorithm (NSGA-III). Before coupling, we extensively validated a wide range of DNDC outputs to examine the robustness of the model. Subsequently, by comanaging the flooding events, fertilization dosage, and other pivotal farm regimes, this study provides a new alternative to optimize irrigated rice farming systems regarding food security, GHGs emissions, and water resources. Finally, we attempt to deploy the new method to address the following questions:

I. Could heuristic and holistic management increase current rice yield with less irrigation water?

II. Could heuristic and holistic management simultaneously reduce CH_4 and N_2O emissions?

2. Materials and methods

2.1 Study site

This study was conducted based on the data collected at a rice paddy site (38.2013°N, 127.2505°E), Cheorwon, South Korea, included in both the Korean Flux network (KoFlux) and AsiaFlux. During the study period (2016-2020), the farmer adopted a single cropping system and midseason drainage practice with the early ripening japonica variety "Odae". The site has a temperate monsoon climate. In the last three decades, the annual mean air temperature and precipitation were 10.2 ℃ and 1390 mm (Supplementary Fig. 1), respectively (Huang et al., 2018). The typical growing season starts in late April and ends in early September.

2.2 DNDC model

To assess the impacts of farm management on crop yield, GHGs emissions, and irrigation requirements, this study applied the process-based DeNitrification-DeComposition model (DNDC, version 9.5). DNDC is a carbon and nitrogen biogeochemistry model particularly developed for agroecosystems and comprises the following core interacting sub-modules: thermal-hydraulic, decomposition, denitrification, fermentation, and plant growth (Gilhespy et al., 2014; Giltrap et al., 2010; Li et al., 1992). DNDC has been shown to have considerable performance to predict the emissions of multiple GHGs (CO_2, CH_4, and N_2O), crop growth, and soil climate under a wide range of climate conditions and farming practices (Chen et al., 2016; Jiang et al., 2021; Zhang et al., 2019; Zhao et al., 2020). To run DNDC properly, we first calibrated soil physicochemical properties and crop parameters including soil texture (silt clay loam), soil organic carbon, bulk density, growing degree days, maximum biomass production, biomass fraction, etc., by using the data from our previous studies (Huang et al., 2018; Hwang et al., 2020). After thoroughly validating simulations from DNDC with field daily and annual observations (CH_4, GPP, Reco, ET,

Soil moisture, Soil temperature), the model was later integrated with a multi-objective optimization algorithm (section 2.5). For a detailed explanation of the DNDC model structure, see Gilhespy et al. (2014).

2.3 In situ data

Daily GHGs (CO_2 and CH_4) fluxes, latent heat flux, and meteorological data including air temperature, precipitation, wind speed, net radiation, and humidity were recorded half-hourly with an eddy covariance system mounted at a 10-meter high tower. The eddy covariance system comprises the following key instruments: a three-dimensional sonic anemometer (CSAT3, Campbell Scientific, Inc.); a closed path infrared gas analyzer (LI-7200, LI-COR Inc.); an open path CH_4 analyzer based on wavelength modulation spectroscopy (LI-7700, LI-COR, Inc.) (Hwang et al., 2020). A nighttime method was used to partition CO_2 fluxes into gross primary production (GPP) and ecosystem respiration (Reco). For detailed descriptions of the flux measurement and data processing, see Hwang et al. (2020). Soil volumetric water content and soil temperature were measured half-hourly at the depth of 0-0.1m and 0.1-0.2m, respectively with four soil moisture and temperature sensors (CS655, Campbell Scientific, Inc.). Other data including crop yield, rice phenology, irrigation schedule, and fertilization were obtained from the farming records and field measurements. The in-situ records were later used to validate simulation results from DNDC at both the daily and annual scale. To validate the annual simulation results from DNDC, we used the processed data (quality controlled & gap-filled) following the KoFlux protocol (Hong, 2009; Kang, 2018). To validate the daily simulation results from DNDC regarding GPP, Reco, CH_4 emissions and evapotranspiration (ET), we used the gap-filled data but with a threshold of the observed percentile greater than 50-55%. Due to the common unclosed energy balance issue of eddy covariance measurements, we corrected measured ET with the following method: $ET_{corrected} = (Rn - G) / (H_{uncorrected} + ET_{uncorrected}) \times ET_{uncorrected}$. Where Rn is the net radiation, H is the sensible heat flux, and G is the soil heat flux (Jung et al., 2010).

2.4 Multi-objective optimization (MOO) algorithm

To date, scalarization approaches and the Edgeworth-Pareto principle have become the key to solving a MOO problem efficiently. Scalarization methods, in essence, are deductive reasoning which decomposes a multi-objective problem into a single-objective by assembling objective functions or reconstructing them as constraints, such as linear weighting, Chebyshev distance, ε-constraint method. Therefore, applying scalarization methods requires prior knowledge to design the constraints and parameters of the scalarization function carefully. In contrast, the Edgeworth-Pareto principle by using inductive reasoning to find the Pareto front/set which contains a series of optimal solutions or so-called Pareto-nondominated solutions. In this study, to allow the algorithm enumerating potential optimal solutions on the Pareto front, we adopted the bioinspired non-dominated sorting genetic algorithm (NSGA-III) to solve the many (>3) objective optimization problems (Deb and Jain, 2014). In this study, we implemented the NSGA-III algorithm with the DEAP (Distributed Evolutionary Algorithms in Python) library (Rainville et al., 2012).

2.5 DNDC-NSGA-III integration and optimization

DNDC was coupled with the NSGA-III optimization framework. Particularly, we addressed the following four objective functions derived from DNDC:

$$f_{objectives} = [f_{max}\{DNDC(yield)\}, f_{min}\{DNDC(CH_4\ emissions, N_2O\ emissions, Irrigatrion)\}] \quad (1)$$

DNDC does not directly compute irrigation water consumption, here we used the water balance method to retrieve annual irrigation demand as:

$$f_{Irrigation} = \left(DNDC_{ET} + DNDC_{run\ off} + DNDC_{leaching} + DNDC_{soil\ water\ change} - precipitaion\right) \quad (2)$$

Where the objective functions were subject to:

$$\begin{bmatrix} Sowing: April.1st \leq date \leq May.31th; \\ Fertilization: 0 \leq rate \leq 140\ kg/ha; \\ Tillage: depth = [10, 20, 30]\ cm; \end{bmatrix} \quad (3)$$

In addition, the objective functions were also subject to the following irrigation schedules. To maintain its simplicity and therefore practical relevance, we scheduled ten flooding events with a ~15 days moving interval, which randomly started half-monthly and ended in the middle and end of each month respectively.

The optimization framework was partly based on previous work (Prina et al., 2018) and comprised the following processes: i) Setting up NSGA-III algorithm, constraints, and objective functions. Specifically, we initialized a parental population with random solutions, 4500 individuals generated, namely 4500 random holistic farm managements (sowing, fertilization, tillage, and irrigation). ii) Computing the values of the objective functions by executing DNDC model with each solution, here we used the averaged climate data (2016-2020) and assumed the soil properties remained stable during the study period. As the source code of DNDC is not available, we used Python library 'pyautogui' to automate interactions between the DNDC model and NSGA-III algorithm. iii) Evaluating the performance of each individual by ranking the fitness of its objective functions. iv) Generating a new generation through selection, crossover, and mutation, based on the performance of fitness. v) Approaching Pareto fronts after all pre-defined generations, 10 generations in this study, of individuals generated and evaluated. By testing the NSGA-III with varied population sizes and generations, we found that the configuration of 4,500 individuals and 10 generations can obtain stable Pareto fronts with a relatively time-efficient (around 60 hours) optimization process. Considering the possibility of different farming management combinations, a smaller size of population or fewer generations would either omit potential non-dominated solutions or result in a biased Pareto front. By contrast, we found a larger population or more generations were notably time-consuming but did not further improve the Pareto fronts in the context of this study.

3. Results

3.1 DNDC model validation

The performance of DNDC was evaluated with in situ observations both at annual (Fig. 9) and daily (Fig. 10 and 11) scales. At the annual scale, we found that DNDC reasonably captured interannual variations of the four key objectives, including crop yield, CH_4 emissions, GPP dynamics, and ET budgets (Fig. 8a-d).

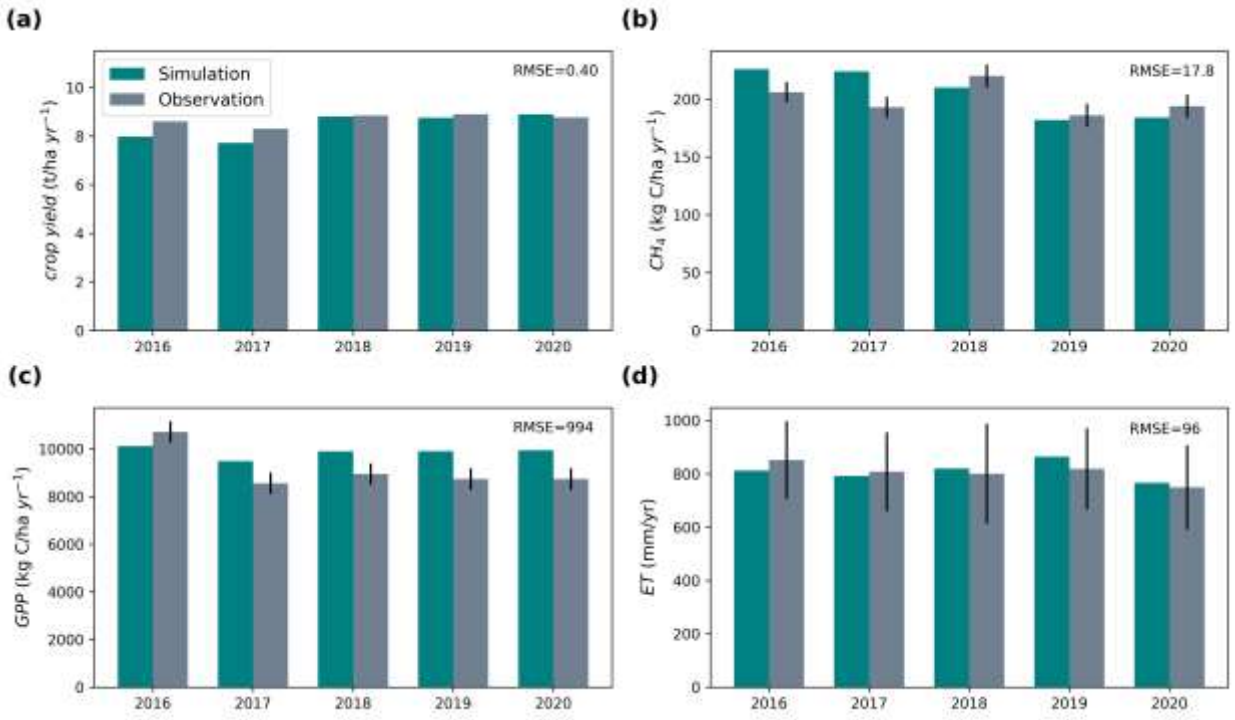

Figure 9 Annual scale validation of the DNDC simulations with in situ data regarding (a) crop yield, (b) CH_4 emissions, (c) GPP, and (d) ET from 2016 to 2020. Error bars indicate 95% confidence interval.

At the daily scale, we found that DNDC simulated well of CH4 flux under the current mid-season drainage practice and through the study periods (Fig. 10a). However, DNDC greatly overestimated GPP during the early growing season, particularly a biased spiking jumping from 0 to ~80 kg C/ha

following the sowing (Fig. 10b). By contrast, GPP simulations matched with observations from around middle growing seasons to the rest of investigated periods. DNDC also captured Reco fairly reasonably during the growing seasons, but also underestimated the flux at ~1-2 (g C m-2 d-1) during the non-growing seasons. Importantly, we detected marginal effects of the early season GPP mismatch on crop yield estimations depicted in Fig. 9a.

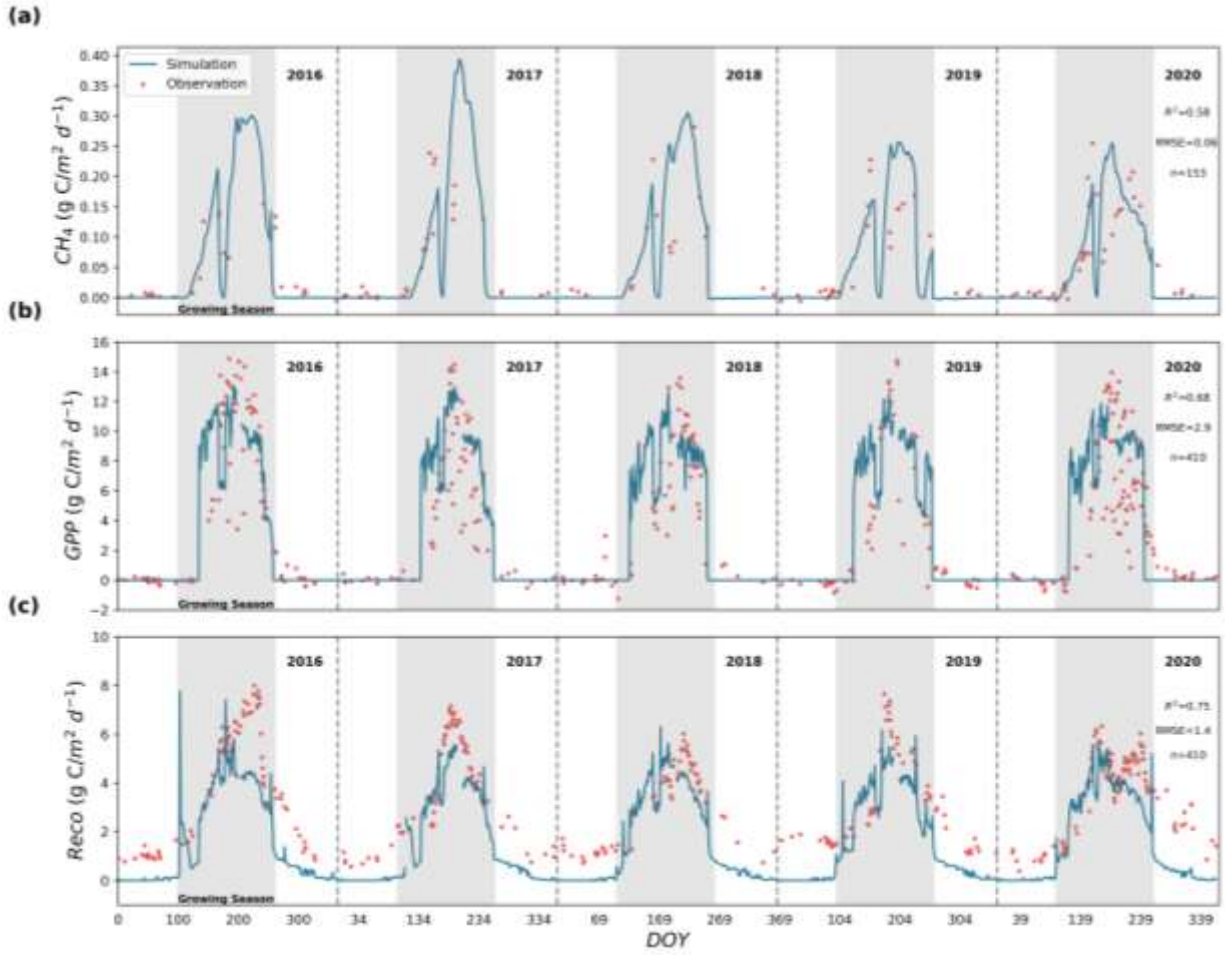

Figure 10 Daily scale validation of the DNDC simulations with in situ data in terms of (a) CH_4 flux, (b) GPP flux, and (c) Reco flux from 2016 to 2020.

Daily scale ET and soil environment simulations also showed reasonable agreements with the observations (Fig. 11). During growing seasons, we found that DNDC well tracked the dynamics of water-related fluxes under the current mid-season drainage practice.

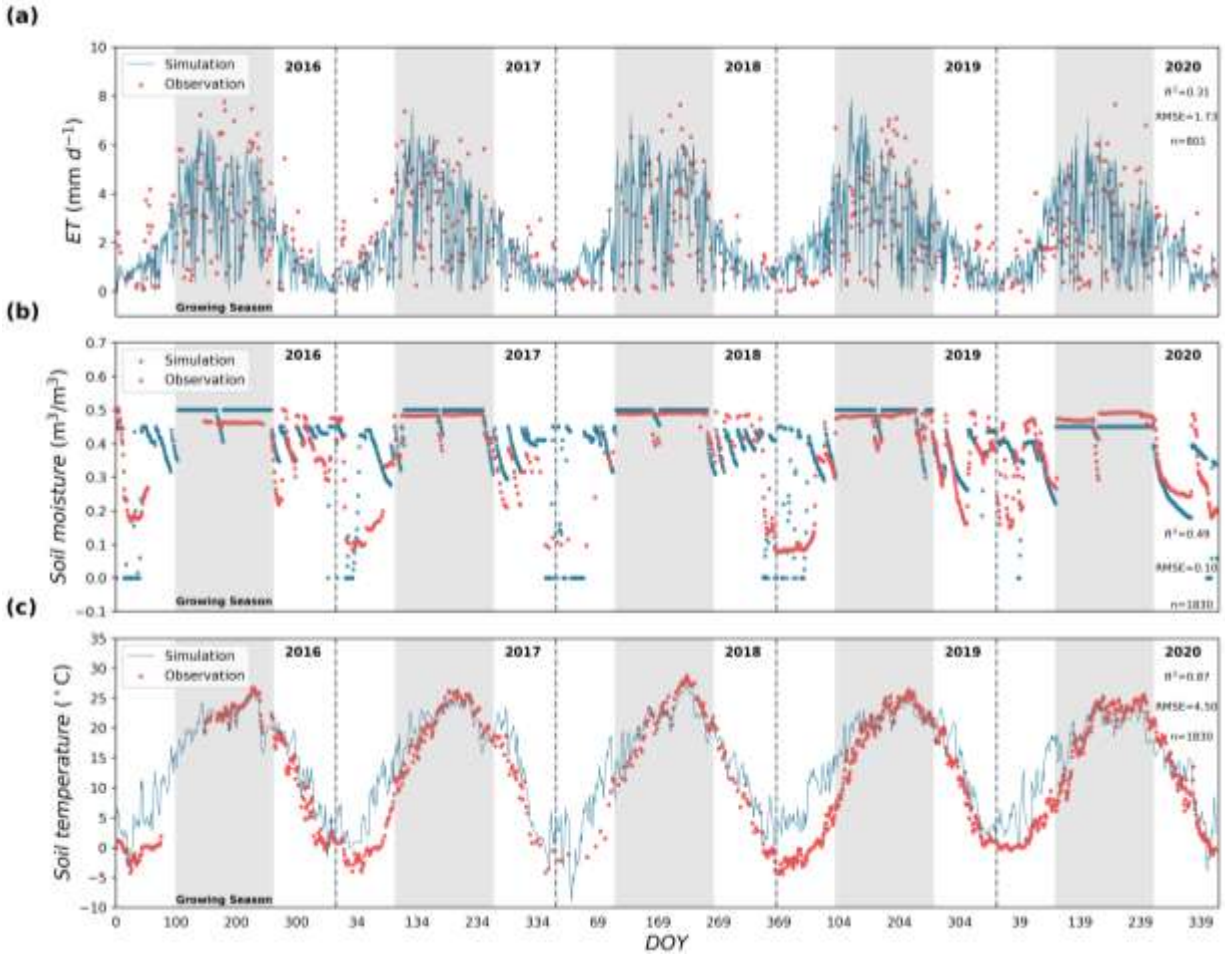

Figure 11 Daily scale validation of the DNDC simulations with in situ data in terms of (a) ET flux, (b) soil moisture, and (c) soil temperature from 2016 to 2020.

3.2 The gaps between the current farming outcomes and optimized objectives

By DNDC-NSGA-III integration and optimization, we approached Pareto fronts and obtained the probability density distribution of each paired dual objective (Fig. 12). Crop yields were maintained at a relatively high level, but at a great environmental cost in both CH_4 emissions (Fig. 12a) and water consumption (Fig. 12b). We found that current farming practices resulted in considerable gaps to reach Pareto fronts for all the objectives (Fig. 12a-f), particularly for reducing CH_4 emissions and irrigation water consumption (Fig. 12c). By contrast, the majority paired objectives between crop yield and N_2O emissions located in the non-dominated sets, however, they were neither close to the Pareto front (Fig. 12d).

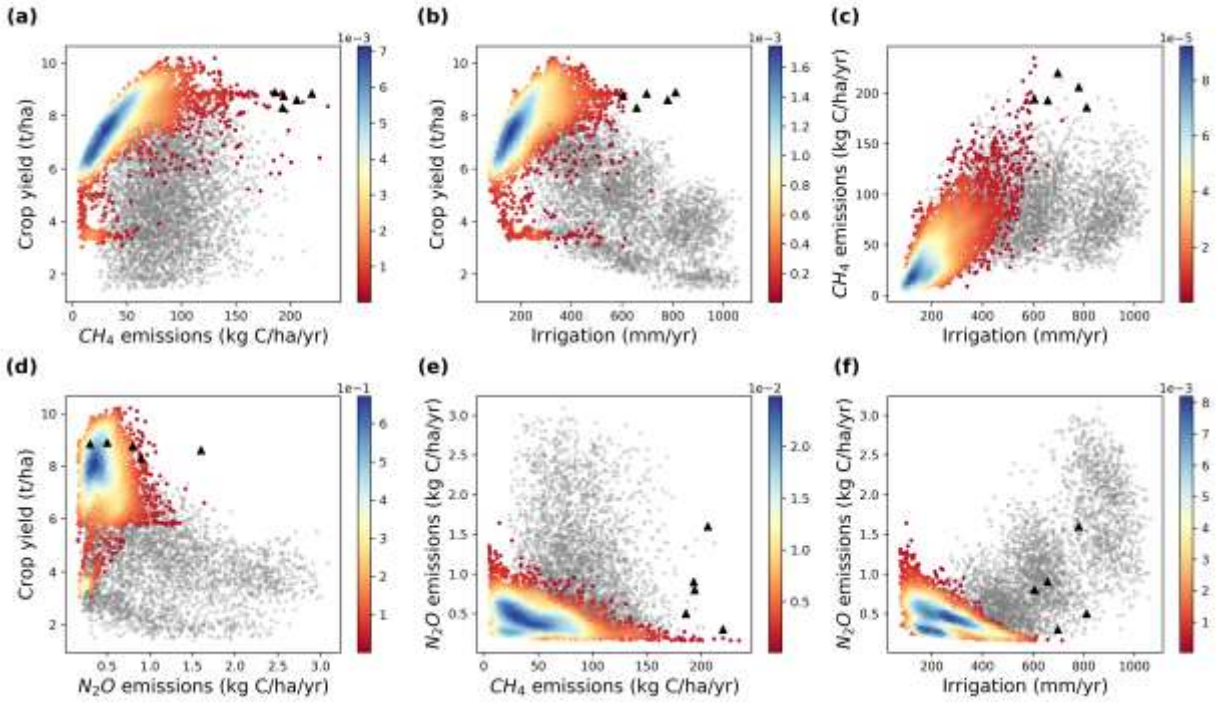

Figure 12 Pareto fronts and probability density distribution of the each paired two objectives, where colorized dots denote the non-dominated sets and grey dots denote the dominated sets. (a) Minimizing CH_4 emissions and maximizing crop yield, (b) minimizing CH_4 and N_2O emissions, (c) minimizing irrigation consumption and CH_4 emissions, (d) minimizing N_2O emissions and maximizing crop yield, (e) minimizing irrigation consumption and maximizing crop yield, (f) minimizing irrigation consumption and N_2O emissions. Black triangles denote the paired objectives based on the current farm management (2016-2020).

By plotting 3-D Pareto fronts in planform, we simultaneously showed the present farming efficiency for each paired triplet state (Fig. 13). We found that the mean crop yield has reached 87% of the potential level (~10 t/ha). Nevertheless, most of the paired objectives (blue triangles) have fallen out of the optimal sets (colorized planform, Fig. 13). Compared to the current farming systems, the optimized holistic management would achieve nearly potential rice yield while reducing more than half of the CH_4 emissions (Fig. 12a & Fig. 13b), water consumption (Fig. 12e and Fig. 13b), and maintaining similar N_2O emissions (Fig. 12d & Fig. 13a).

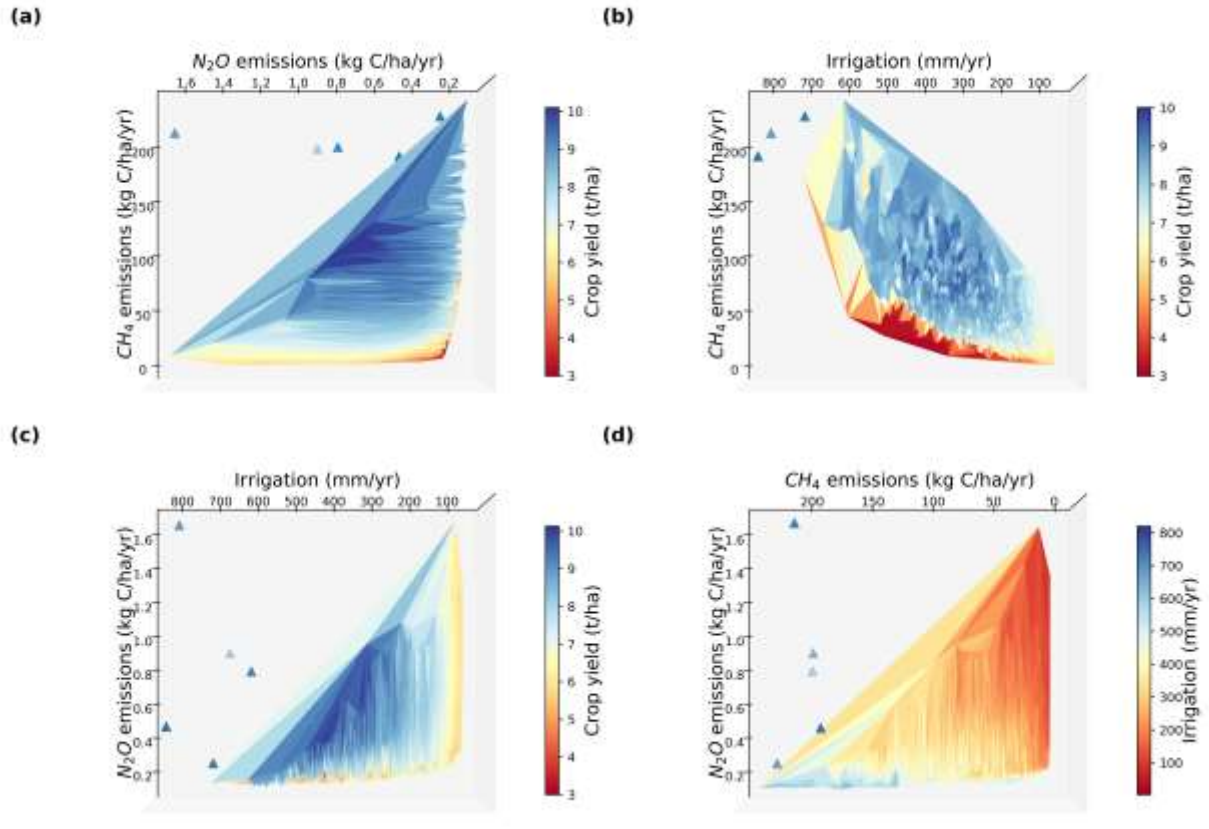

Figure 13 Planform of the Pareto fronts of each paired three objectives in triangular surface plot, where the color bar indicates the values of z axis; (a) minimizing N_2O, CH_4 emissions and maximizing crop yield; (b) minimizing irrigation consumption, CH_4 emissions and maximizing crop yield; (c) minimizing irrigation consumption, N_2O emissions and maximizing crop yield; (d) minimizing CH_4, N_2O emissions, and irrigation consumption. Blue triangles denote the paired objectives based on the current farm management (2016-2020).

3.3 Approaching Pareto fronts through the heuristic and holistic management

To demonstrate how the Pareto fronts were achieved (Fig. 12), we show the corresponding density distributions of the heuristic management (Fig. 14). Here we emphasized that the distributions (Fig. 14) only indicate the optimization process (non-dominated population) to approach Pareto fronts (Fig. 12 & Fig. 13) rather than the set of optimal management *per se*. We found that irrigation schedules converged evidently to several narrow time windows in each month (Fig. 14a-e). The convergence, particularly depicted in the upper right corner (Fig. 14b & c), showed a higher likelihood of late initiation for the early to middle growing season. By contrast, an early irrigation schedule appeared higher probability for the peak to late growing season (Fig. 14d & e).

In addition, we detected that the sowing window congregated in early April (Fig. 14f & g). We found that the fertilization rate at ~60-120 kg/ha occurred more frequently together with the early sowing day and shallow tillage depth (Fig. 14f & h). Finally, we found a considerably higher probability density between early sowing day and shallow tillage depth (Fig. 14g). The distribution of the holistic farm management depicted in Fig. 14 was also presented in form of different combinations (Supplementary Fig. 2 & 3) and three dimensions (Supplementary Fig. 4). Overall, we found identical interactions in the paired triple managements as well.

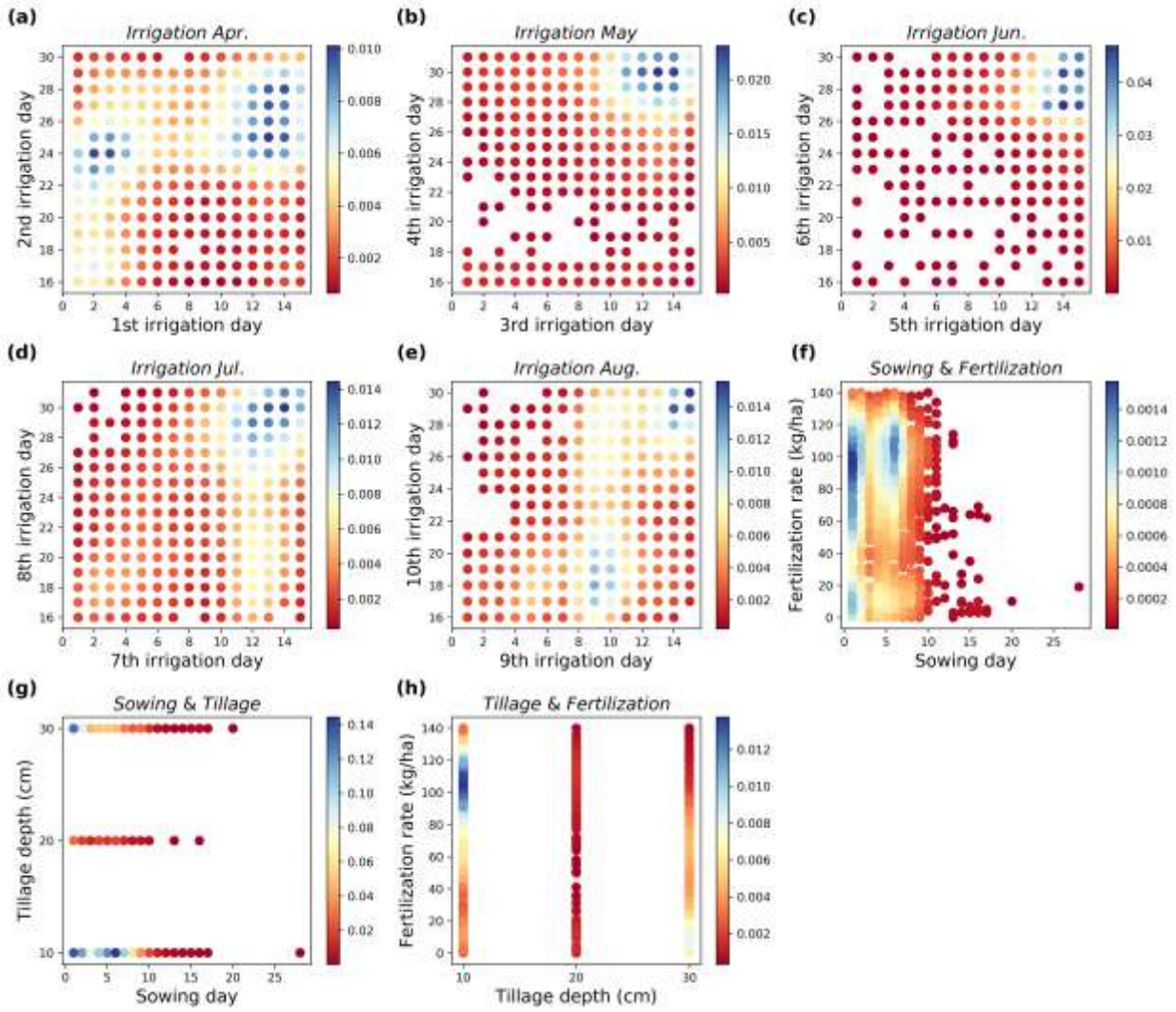

Figure 14 Probability density distribution of the non-dominated farm management regarding, irrigation schedules (a) in April, (b) in May, (c) in June, (d) in July, and (e) in August; (f) sowing day and fertilization rate, (e) sowing day and tillage depth, (f) tillage depth and fertilization rate. The non-dominated sowing month only occurred in April, therefore was not presented.

3.4 The gaps between current farming practices to potential crop yield with optimal holistic management

Numerous optimal holistic managements exist alongside the Pareto fronts. By applying a threshold of crop yield greater than 10 t/ha, here we showed the differences between the current farm

managements to the subset of optimized ones nearby the potential yield (Fig. 15). The optimal management all suggested advanced sowing dates, around 10-30 days earlier compared to current practices (Fig. 15a). However, the impacts of tillage depth on crop yields were marginal (Fig. 15b). We found that the current static fertilization rate matched the optimal range (Fig. 15c). Additionally, we also presented the optimized irrigation schedules as the dynamics of the water table (Fig. 15d) and soil moisture (Fig. 15e). We found that optimized irrigation schedules all showed the transitory duration of the flooding events from early to middle growing seasons. By contrast, current management only suspends irrigation in the mid of the growing season.

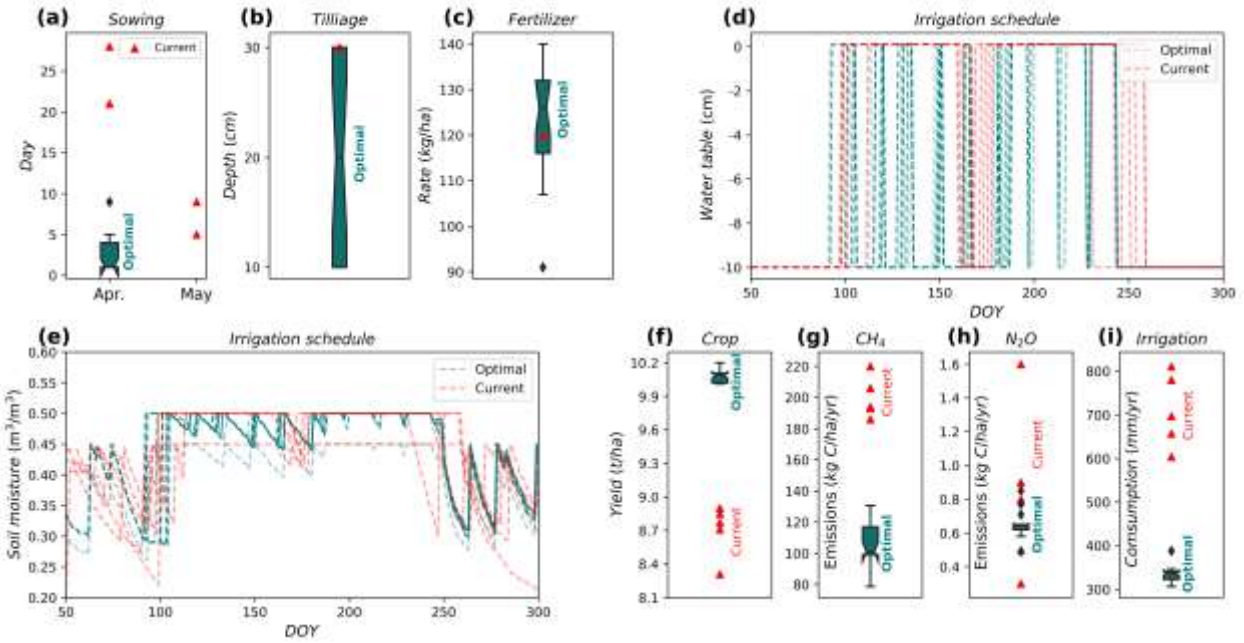

Figure 15 Comparison between the current farming practices (n = 5) and optimized holistic managements (a-e, n = 21) with a threshold of crop yield greater than 10 t/ha (f). And the corresponding farming outcomes yielded from the current practices and the optimized managements (f-i).

4. Discussion

By proposing a simple heuristic and holistic method, this study optimized rice farming beyond previous most emphasized irrigation regimes (Bo et al., 2022; Lampayan et al., 2015; Tian et al., 2021), while also exploring niches from other pivotal farm managements regarding sowing window, fertilization rate, tillage depth, and their interactions. Specifically, we validated and coupled the DNDC model with the NSGA-III algorithm to maximize crop yield, minimize water consumption, and minimize N_2O, CH_4 emissions. By approaching four objectives on its paired Pareto fronts, we quantified the gaps in current farming practices in South Korea to achieve optimal solutions. Our results indicate that the optimized holistic farm management would maintain or even increase current crop yield while reducing more than 50% irrigation demand and GHGs emissions (Fig. 12). Furthermore, this new method also tackled the dilemma of simultaneously reducing CH_4 and N_2O emissions. Our study clearly shows that the present rice farming system in the study site not only has not achieved its potential yield level but also comes at a great environmental cost to water resources and GHGs emissions. More importantly, this simple method could further be applied to evaluate the environmental sustainability of a rice farming system under various climate and local conditions and to guide policymakers and farming practices with detailed solutions.

4.1 Could heuristic and holistic management increase current rice yield with less irrigation water?

Our results indicate that improvements on sowing window and flooding events together would be pivotal to approaching potential/maximum crop yield (~10 t/ha), as other present farming practices are already well-matched with the optimal solutions (Fig. 12). Early sowing date has been reported to increase crop biomass and grain yield particularly due to higher leaf area index and assimilation rate at vegetative stages and owing to the benefits of lower temperature on starch accumulation at the late grain filling stage (Huang et al., 2020; Li et al., 2021; Wenting et al., 2021). These physiological mechanisms support our findings that all non-dominated sowing dates converged in early April (Fig. 14f & g), roughly 10-40 days advanced compared to the present (Fig. 12). In addition, early planting also reduced the risk of extreme heat events and has been shown as a cost-

effective strategy for adapting to climate warming (Acharjee et al., 2019; Ding et al., 2020). Nevertheless, the early sowing suggested in this study does not imply it is a "silver bullet" in other regions, as the optimal sowing window is highly dependent on both the local climate conditions and cultivar characteristics (Deng et al., 2022; Tu et al., 2020). Furthermore, the risk of cold or frost damage should also be considered while advancing the sowing date.

Regarding the irrigation schedule, the optimized solutions all indicate that the current japonica variety ('Odae') in the study site requires nearly saturated water content during the grain filling stage (~DOY 190–240) to avoid yield penalty (Fig. 12e), which is a well-known drought-sensitive growth period (Lilley and Fukai, 1994; Saini and Westgate, 1999; Zhang et al., 2018). By contrast, multi-transitory flooding events at the vegetative stage conserve considerable water resources (> 50%) while showing marginal negative effects on crop yield (Fig. 12e & f). To note that the optimized heuristic irrigation practice initiated new flooding events to maintain the soil moisture in rootzone mostly above ~0.45 m^3/m^3, which is identical to the threshold of soil water potential should be greater than −10 kPa to avoid drought stress, following the safe alternate wetting and drying guideline (Lampayan et al., 2015). Therefore, the heuristic-derived optimized managements, particularly adjusting sowing date and irrigation schedule, are not only consistent with the current literature findings but also highlight the essential role of a holistic approach to systematically manage rice farming.

4.2 Could heuristic and holistic management simultaneously reduce CH_4 and N_2O emissions?

This study demonstrated the feasibility to reduce CH_4 emissions substantially while containing N_2O footprints at similar or lower than current levels (Fig. 15g & h), although a trade-off between CH_4 and N_2O emissions is well expected (Fig. 12e) due to the anaerobic decomposition (Neue, 1993) and aerobic nitrification processes (Bouwman, 1998). Lately, a global meta-analysis identified that non-flooded days ratio, bulk density, and nitrogen application rate primarily explained the benefits of non-continuous flooding on global warming potential (Bo et al., 2022), as fertilization is the source of nitrification-denitrification and moisture content affects relative gas diffusivity of N_2O through the soil column (Klefoth et al., 2014). In this study, by giving the

priority to reaching the potential yield, the heuristic optimization process resulted in nearly all identical water table dynamics (Fig. 15d) to sustain the balance between anaerobic and aerobic soil environments. Importantly, we detected a fraction (~54%) of non-flooding days to growing season length (Fig. 15d & e), which is comparable to the optimal results (>50%) reported in the aforementioned meta-analysis for South Korea (Bo et al., 2022). Additionally, this study further indicates the optimal temporal distributions of the non-flooded days, which should primarily schedule in vegetative stages, shortly after sowing and before the grain filling stage.

4.3 Limitations and uncertainties

Several limitations should be noted in the present study. We did not validate N_2O simulation results from DNDC due to a lack of observations. Although a well-calibrated DNDC model is capable to track the daily N_2O fluxes reliability (Katayanagi et al., 2012; Li et al., 2005; Zhao et al., 2020). In this study, we have demonstrated the robustness of the calibrated DNDC model through multifaceted validation (Figs. 8-11), but the uncertainties about the N_2O remain to be addressed. Additionally, to maintain the simplicity and practical relevance of the holistic method, this study narrowed down farming management to several pivotal options (Fig. 14) rather than including all possible practices. Future studies could also consider and explore other measures including but not limited to, new rice cultivars (drought-resistant & high-yielding), nitrification inhibitor (Sun et al., 2016), straw addition (Jiang et al., 2019b), fertilizer selection, and fertilizer application method (Hussain et al., 2015). Furthermore, this study accounted for the very limited spatial heterogeneity of the rice farming system which only comprised one farming site although with 5 years of observations. Nevertheless, we have provided a new simple method that could be promptly adopted in other regions if sufficient data are available.

Reference

Acharjee, T.K., van Halsema, G., Ludwig, F., Hellegers, P., Supit, I. (2019) Shifting planting date of Boro rice as a climate change adaptation strategy to reduce water use. Agricultural Systems 168, 131-143.

Bo, Y., Jägermeyr, J., Yin, Z., Jiang, Y., Xu, J., Liang, H., Zhou, F. (2022) Global benefits of non-continuous flooding to reduce greenhouse gases and irrigation water use without rice yield penalty. Global change biology n/a.

Bouman, B.A.M., Tuong, T.P. (2001) Field water management to save water and increase its productivity in irrigated lowland rice. Agricultural Water Management 49, 11-30.

Bouwman, A.F. (1998) Nitrogen oxides and tropical agriculture. Nature 392, 866-867.

Chen, H., Yu, C., Li, C., Xin, Q., Huang, X., Zhang, J., Yue, Y., Huang, G., Li, X., Wang, W. (2016) Modeling the impacts of water and fertilizer management on the ecosystem service of rice rotated cropping systems in China. Agriculture, Ecosystems & Environment 219, 49-57.

Coleman, K., Muhammed, S.E., Milne, A.E., Todman, L.C., Dailey, A.G., Glendining, M.J., Whitmore, A.P. (2017) The landscape model: A model for exploring trade-offs between agricultural production and the environment. Science of The Total Environment 609, 1483-1499.

de Weck, O. (2004) Multiobjective Optimization: History and Promise. Invited Keynote Paper, GL2-2, the Third China-Japan-Korea Joint Symposium on Optimization of Structural and Mechanical Systems 2.

Deb, K., Jain, H. (2014) An Evolutionary Many-Objective Optimization Algorithm Using Reference-Point-Based Nondominated Sorting Approach, Part I: Solving Problems With Box Constraints. IEEE Transactions on Evolutionary Computation 18, 577-601.

Deng, F., Zhang, C., He, L., Liao, S., Li, Q., Li, B., Zhu, S., Gao, Y., Tao, Y., Zhou, W., Lei, X., Wang, L., Hu, J., Chen, Y., Ren, W. (2022) Delayed sowing date improves the quality of mechanically transplanted rice by optimizing temperature conditions during growth season. Field Crops Research 281, 108493.

Ding, Y., Wang, W., Zhuang, Q., Luo, Y. (2020) Adaptation of paddy rice in China to climate change: The effects of shifting sowing date on yield and irrigation water requirement. Agricultural Water Management 228, 105890.

Dong, J., Xiao, X. (2016) Evolution of regional to global paddy rice mapping methods: A review. ISPRS Journal of Photogrammetry and Remote Sensing 119, 214-227.

Emmerich, M.T.M., Deutz, A.H. (2018) A tutorial on multiobjective optimization: fundamentals and evolutionary methods. Natural Computing 17, 585-609.

Flagg, J.A. (2015) Aiming for zero: what makes nations adopt carbon neutral pledges? Environmental Sociology 1, 202-212.

Fuller, D.Q., Qin, L., Zheng, Y., Zhao, Z., Chen, X., Hosoya, L.A., Sun, G.-P. (2009) The Domestication Process and Domestication Rate in Rice: Spikelet Bases from the Lower Yangtze. Science 323, 1607.

Fumoto, T., Yanagihara, T., Saito, T., Yagi, K. (2010) Assessment of the methane mitigation potentials of alternative water regimes in rice fields using a process-based biogeochemistry model. Global change biology 16, 1847-1859.

Gilhespy, S.L., Anthony, S., Cardenas, L., Chadwick, D., del Prado, A., Li, C., Misselbrook, T., Rees, R.M., Salas, W., Sanz-Cobena, A., Smith, P., Tilston, E.L., Topp, C.F.E., Vetter, S., Yeluripati, J.B. (2014) First 20 years of DNDC (DeNitrification DeComposition): Model evolution. Ecological Modelling 292, 51-62.

Giltrap, D.L., Li, C., Saggar, S. (2010) DNDC: A process-based model of greenhouse gas fluxes from agricultural soils. Agriculture, Ecosystems & Environment 136, 292-300.

Gosling, S.N., Arnell, N.W. (2016) A global assessment of the impact of climate change on water scarcity. Climatic Change 134, 371-385.

Groot, J.C.J., Oomen, G.J.M., Rossing, W.A.H. (2012) Multi-objective optimization and design of farming systems. Agricultural Systems 110, 63-77.

Gross, B.L., Zhao, Z. (2014) Archaeological and genetic insights into the origins of domesticated rice. Proceedings of the National Academy of Sciences 111, 6190.

Gutaker, R.M., Groen, S.C., Bellis, E.S., Choi, J.Y., Pires, I.S., Bocinsky, R.K., Slayton, E.R., Wilkins, O., Castillo, C.C., Negrão, S., Oliveira, M.M., Fuller, D.Q., Guedes, J.A.d.A., Lasky, J.R.,

Purugganan, M.D. (2020) Genomic history and ecology of the geographic spread of rice. Nature Plants 6, 492-502.

Haque, M.M., Kim, G.W., Kim, P.J., Kim, S.Y. (2016) Comparison of net global warming potential between continuous flooding and midseason drainage in monsoon region paddy during rice cropping. Field Crops Research 193, 133-142.

Hong, J.-K., et al. (2009) Standardization of KoFlux Eddy-Covariance Data Processing. Korean Journal of Agricultural and Forest Meteorology 11, 19-26.

Huang, M., Fang, S., Cao, F., Chen, J., Shan, S., Liu, Y., Lei, T., Tian, A., Tao, Z., Zou, Y. (2020) Early sowing increases grain yield of machine-transplanted late-season rice under single-seed sowing. Field Crops Research 253, 107832.

Huang, Y., Ryu, Y., Jiang, C., Kimm, H., Kim, S., Kang, M., Shim, K. (2018) BESS-Rice: A remote sensing derived and biophysical process-based rice productivity simulation model. Agricultural and Forest Meteorology 256-257, 253-269.

Hussain, S., Peng, S., Fahad, S., Khaliq, A., Huang, J., Cui, K., Nie, L. (2015) Rice management interventions to mitigate greenhouse gas emissions: a review. Environmental Science and Pollution Research 22, 3342-3360.

Hwang, Y., Ryu, Y., Huang, Y., Kim, J., Iwata, H., Kang, M. (2020) Comprehensive assessments of carbon dynamics in an intermittently-irrigated rice paddy. Agricultural and Forest Meteorology 285-286, 107933.

Ishfaq, M., Farooq, M., Zulfiqar, U., Hussain, S., Akbar, N., Nawaz, A., Anjum, S.A. (2020) Alternate wetting and drying: A water-saving and ecofriendly rice production system. Agricultural Water Management 241, 106363.

Islam, S.F.-u., van Groenigen, J.W., Jensen, L.S., Sander, B.O., de Neergaard, A. (2018) The effective mitigation of greenhouse gas emissions from rice paddies without compromising yield by early-season drainage. Science of The Total Environment 612, 1329-1339.

Jiang, R., Yang, J.Y., Drury, C.F., He, W., Smith, W.N., Grant, B.B., He, P., Zhou, W. (2021) Assessing the impacts of diversified crop rotation systems on yields and nitrous oxide emissions in Canada using the DNDC model. Science of The Total Environment 759, 143433.

Jiang, Y., Carrijo, D., Huang, S., Chen, J., Balaine, N., Zhang, W., van Groenigen, K.J., Linquist, B. (2019a) Water management to mitigate the global warming potential of rice systems: A global meta-analysis. Field Crops Research 234, 47-54.

Jiang, Y., Qian, H., Huang, S., Zhang, X., Wang, L., Zhang, L., Shen, M., Xiao, X., Chen, F., Zhang, H., Lu, C., Li, C., Zhang, J., Deng, A., van Groenigen, K.J., Zhang, W. (2019b) Acclimation of methane emissions from rice paddy fields to straw addition. Science Advances 5, eaau9038.

Jung, M., Reichstein, M., Ciais, P., Seneviratne, S.I., Sheffield, J., Goulden, M.L., Bonan, G., Cescatti, A., Chen, J., de Jeu, R., Dolman, A.J., Eugster, W., Gerten, D., Gianelle, D., Gobron, N., Heinke, J., Kimball, J., Law, B.E., Montagnani, L., Mu, Q., Mueller, B., Oleson, K., Papale, D., Richardson, A.D., Roupsard, O., Running, S., Tomelleri, E., Viovy, N., Weber, U., Williams, C., Wood, E., Zaehle, S., Zhang, K. (2010) Recent decline in the global land evapotranspiration trend due to limited moisture supply. Nature 467, 951-954.

Kang, M., et al. (2018) Changes and Improvements of the Standardized Eddy Covariance Data Processing in KoFlux. Korean Journal of Agricultural and Forest Meteorology 20, 5-17.

Katayanagi, N., Furukawa, Y., Fumoto, T., Hosen, Y. (2012) Validation of the DNDC-Rice model by using CH4 and N2O flux data from rice cultivated in pots under alternate wetting and drying irrigation management. Soil Science and Plant Nutrition 58, 360-372.

Kim, G.-Y., Gutierrez, J., Jeong, H.-C., Lee, J.-S., Haque, M.D.M., Kim, P.J. (2014) Effect of intermittent drainage on methane and nitrous oxide emissions under different fertilization in a temperate paddy soil during rice cultivation. Journal of the Korean Society for Applied Biological Chemistry 57, 229-236.

Klefoth, R.R., Clough, T.J., Oenema, O., Van Groenigen, J.-W. (2014) Soil Bulk Density and Moisture Content Influence Relative Gas Diffusivity and the Reduction of Nitrogen-15 Nitrous Oxide. Vadose Zone Journal 13, vzj2014.2007.0089.

Kritee, K., Nair, D., Zavala-Araiza, D., Proville, J., Rudek, J., Adhya, T.K., Loecke, T., Esteves, T., Balireddygari, S., Dava, O., Ram, K., S. R, A., Madasamy, M., Dokka, R.V., Anandaraj, D., Athiyaman, D., Reddy, M., Ahuja, R., Hamburg, S.P. (2018) High nitrous oxide fluxes from

rice indicate the need to manage water for both long- and short-term climate impacts. Proceedings of the National Academy of Sciences 115, 9720.

Kropp, I., Nejadhashemi, A.P., Deb, K., Abouali, M., Roy, P.C., Adhikari, U., Hoogenboom, G. (2019) A multi-objective approach to water and nutrient efficiency for sustainable agricultural intensification. Agricultural Systems 173, 289-302.

Kudo, Y., Noborio, K., Shimoozono, N., Kurihara, R. (2014) The effective water management practice for mitigating greenhouse gas emissions and maintaining rice yield in central Japan. Agriculture, Ecosystems & Environment 186, 77-85.

LaHue, G.T., Chaney, R.L., Adviento-Borbe, M.A., Linquist, B.A. (2016) Alternate wetting and drying in high yielding direct-seeded rice systems accomplishes multiple environmental and agronomic objectives. Agriculture, Ecosystems & Environment 229, 30-39.

Lampayan, R.M., Rejesus, R.M., Singleton, G.R., Bouman, B.A.M. (2015) Adoption and economics of alternate wetting and drying water management for irrigated lowland rice. Field Crops Research 170, 95-108.

Li, C., Frolking, S., Frolking, T.A. (1992) A model of nitrous oxide evolution from soil driven by rainfall events: 1. Model structure and sensitivity. Journal of Geophysical Research: Atmospheres 97, 9759-9776.

Li, C., Frolking, S., Xiao, X., Moore Iii, B., Boles, S., Qiu, J., Huang, Y., Salas, W., Sass, R. (2005) Modeling impacts of farming management alternatives on CO2, CH4, and N2O emissions: A case study for water management of rice agriculture of China. Global Biogeochemical Cycles 19.

Li, C., Salas, W., DeAngelo, B., Rose, S. (2006a) Assessing Alternatives for Mitigating Net Greenhouse Gas Emissions and Increasing Yields from Rice Production in China Over the Next Twenty Years. Journal of Environmental Quality 35, 1554-1565.

Li, C., Zhou, A., Sang, T. (2006b) Rice Domestication by Reducing Shattering. Science 311, 1936.

Li, G., Chen, T., Xu, K., Liu, Y., Dai, Q., Huo, Z., Wei, H. (2021) Early sowing increases grain yield and cooking and eating quality of machine-transplanted rice in eastern China. Crop Science 61, 4383-4401.

Liang, K., Zhong, X., Huang, N., Lampayan, R.M., Pan, J., Tian, K., Liu, Y. (2016) Grain yield, water productivity and CH4 emission of irrigated rice in response to water management in south China. Agricultural Water Management 163, 319-331.

Lilley, J.M., Fukai, S. (1994) Effect of timing and severity of water deficit on four diverse rice cultivars III. Phenological development, crop growth and grain yield. Field Crops Research 37, 225-234.

Linquist, B.A., Anders, M.M., Adviento-Borbe, M.A.A., Chaney, R.L., Nalley, L.L., da Rosa, E.F.F., van Kessel, C. (2015) Reducing greenhouse gas emissions, water use, and grain arsenic levels in rice systems. Global change biology 21, 407-417.

Liu, X., Zhou, T., Liu, Y., Zhang, X., Li, L., Pan, G. (2019) Effect of mid-season drainage on CH4 and N2O emission and grain yield in rice ecosystem: A meta-analysis. Agricultural Water Management 213, 1028-1035.

Meijide, A., Gruening, C., Goded, I., Seufert, G., Cescatti, A. (2017) Water management reduces greenhouse gas emissions in a Mediterranean rice paddy field. Agriculture, Ecosystems & Environment 238, 168-178.

Mekonnen, M.M., Hoekstra, A.Y. (2016) Four billion people facing severe water scarcity. Science Advances 2, e1500323.

Minamikawa, K., Fumoto, T., Iizumi, T., Cha-un, N., Pimple, U., Nishimori, M., Ishigooka, Y., Kuwagata, T. (2016) Prediction of future methane emission from irrigated rice paddies in central Thailand under different water management practices. Science of The Total Environment 566-567, 641-651.

Naylor, R.L., Battisti, D.S., Vimont, D.J., Falcon, W.P., Burke, M.B. (2007) Assessing risks of climate variability and climate change for Indonesian rice agriculture. Proceedings of the National Academy of Sciences 104, 7752.

Neue, H.-U. (1993) Methane Emission from Rice Fields. BioScience 43, 466-474.

Pandey, A., Dou, F., Morgan, C.L.S., Guo, J., Deng, J., Schwab, P. (2021) Modeling organically fertilized flooded rice systems and its long-term effects on grain yield and methane emissions. Science of The Total Environment 755, 142578.

Peng, S., Bouman, B., Visperas, R.M., Castañeda, A., Nie, L., Park, H.-K. (2006) Comparison between aerobic and flooded rice in the tropics: Agronomic performance in an eight-season experiment. Field Crops Research 96, 252-259.

Prina, M.G., Cozzini, M., Garegnani, G., Manzolini, G., Moser, D., Filippi Oberegger, U., Pernetti, R., Vaccaro, R., Sparber, W. (2018) Multi-objective optimization algorithm coupled to EnergyPLAN software: The EPLANopt model. Energy 149, 213-221.

Rainville, F.-M.D., Fortin, F.-A., Gardner, M.-A., Parizeau, M., Gagné, C., (2012) DEAP: a python framework for evolutionary algorithms, Proceedings of the 14th annual conference companion on Genetic and evolutionary computation. Association for Computing Machinery, Philadelphia, Pennsylvania, USA, pp. 85–92.

Ray, D.K., Mueller, N.D., West, P.C., Foley, J.A. (2013) Yield Trends Are Insufficient to Double Global Crop Production by 2050. PLOS ONE 8, e66428.

Saini, H.S., Westgate, M.E., (1999) Reproductive Development in Grain Crops during Drought, in: Sparks, D.L. (Ed.), Advances in Agronomy. Academic Press, pp. 59-96.

Saunois, M., Stavert, A.R., Poulter, B., Bousquet, P., Canadell, J.G., Jackson, R.B., Raymond, P.A., Dlugokencky, E.J., Houweling, S., Patra, P.K., Ciais, P., Arora, V.K., Bastviken, D., Bergamaschi, P., Blake, D.R., Brailsford, G., Bruhwiler, L., Carlson, K.M., Carrol, M., Castaldi, S., Chandra, N., Crevoisier, C., Crill, P.M., Covey, K., Curry, C.L., Etiope, G., Frankenberg, C., Gedney, N., Hegglin, M.I., Höglund-Isaksson, L., Hugelius, G., Ishizawa, M., Ito, A., Janssens-Maenhout, G., Jensen, K.M., Joos, F., Kleinen, T., Krummel, P.B., Langenfelds, R.L., Laruelle, G.G., Liu, L., Machida, T., Maksyutov, S., McDonald, K.C., McNorton, J., Miller, P.A., Melton, J.R., Morino, I., Müller, J., Murguia-Flores, F., Naik, V., Niwa, Y., Noce, S., O'Doherty, S., Parker, R.J., Peng, C., Peng, S., Peters, G.P., Prigent, C., Prinn, R., Ramonet, M., Regnier, P., Riley, W.J., Rosentreter, J.A., Segers, A., Simpson, I.J., Shi, H., Smith, S.J., Steele, L.P., Thornton, B.F., Tian, H., Tohjima, Y., Tubiello, F.N., Tsuruta, A., Viovy, N., Voulgarakis, A., Weber, T.S., van Weele, M., van der Werf, G.R., Weiss, R.F., Worthy, D., Wunch, D., Yin, Y., Yoshida, Y., Zhang, W., Zhang, Z., Zhao, Y., Zheng, B., Zhu, Q., Zhu, Q., Zhuang, Q. (2020) The Global Methane Budget 2000–2017. Earth Syst. Sci. Data 12, 1561-1623.

Shang, Z., Abdalla, M., Xia, L., Zhou, F., Sun, W., Smith, P. (2021) Can cropland management practices lower net greenhouse emissions without compromising yield? Global change biology 27, 4657-4670.

Sun, L., Lu, Y., Yu, F., Kronzucker, H.J., Shi, W. (2016) Biological nitrification inhibition by rice root exudates and its relationship with nitrogen-use efficiency. New Phytologist 212, 646-656.

Tian, Z., Fan, Y., Wang, K., Zhong, H., Sun, L., Fan, D., Tubiello, F.N., Liu, J. (2021) Searching for "Win-Win" solutions for food-water-GHG emissions tradeoffs across irrigation regimes of paddy rice in China. Resources, Conservation and Recycling 166, 105360.

Tilman, D., Balzer, C., Hill, J., Befort, B.L. (2011) Global food demand and the sustainable intensification of agriculture. Proceedings of the National Academy of Sciences 108, 20260.

Towprayoon, S., Smakgahn, K., Poonkaew, S. (2005) Mitigation of methane and nitrous oxide emissions from drained irrigated rice fields. Chemosphere 59, 1547-1556.

Tu, D., Jiang, Y., Liu, M., Zhang, L., Chen, L., Cai, M., Ling, X., Zhan, M., Li, C., Wang, J., Cao, C. (2020) Improvement and stabilization of rice production by delaying sowing date in irrigated rice system in central China. Journal of the Science of Food and Agriculture 100, 595-606.

Wenting, W., Wenpei, C., Ke, X., Hui, G., Haiyan, W., Hongcheng, Z. (2021) Effects of Early- and Late-Sowing on Starch Accumulation and Associated Enzyme Activities During Grain Filling Stage in Rice. Rice Science 28, 191-199.

Zhang, J., Zhang, S., Cheng, M., Jiang, H., Zhang, X., Peng, C., Lu, X., Zhang, M., Jin, J. (2018) Effect of Drought on Agronomic Traits of Rice and Wheat: A Meta-Analysis. International Journal of Environmental Research and Public Health 15.

Zhang, W., Liu, C., Zheng, X., Wang, K., Cui, F., Wang, R., Li, S., Yao, Z., Zhu, J. (2019) Using a modified DNDC biogeochemical model to optimize field management of a multi-crop (cotton, wheat, and maize) system: a site-scale case study in northern China. Biogeosciences 16, 2905-2922.

Zhao, C., Liu, B., Piao, S., Wang, X., Lobell, D.B., Huang, Y., Huang, M., Yao, Y., Bassu, S., Ciais, P., Durand, J.-L., Elliott, J., Ewert, F., Janssens, I.A., Li, T., Lin, E., Liu, Q., Martre, P., Müller, C.,

Peng, S., Peñuelas, J., Ruane, A.C., Wallach, D., Wang, T., Wu, D., Liu, Z., Zhu, Y., Zhu, Z., Asseng, S. (2017) Temperature increase reduces global yields of major crops in four independent estimates. Proceedings of the National Academy of Sciences 114, 9326.

Zhao, Z., Cao, L., Deng, J., Sha, Z., Chu, C., Zhou, D., Wu, S., Lv, W. (2020) Modeling CH4 and N2O emission patterns and mitigation potential from paddy fields in Shanghai, China with the DNDC model. Agricultural Systems 178, 102743.

Zhong, Y., Wang, X., Yang, J., Zhao, X., Ye, X. (2016) Exploring a suitable nitrogen fertilizer rate to reduce greenhouse gas emissions and ensure rice yields in paddy fields. Science of The Total Environment 565, 420-426.

Zong, Y., Chen, Z., Innes, J.B., Chen, C., Wang, Z., Wang, H. (2007) Fire and flood management of coastal swamp enabled first rice paddy cultivation in east China. Nature 449, 459-462.

Chapter IV. Exploring Google Street View with Deep Learning for Crop Type Mapping

Abstract

Ground reference data are an essential prerequisite for supervised crop mapping. The lack of a low-cost and efficient ground referencing method results in pervasively limited reference data and hinders crop classification. In this study, we apply a convolutional neural network (CNN) model to explore the efficacy of automatic ground truthing via Google Street View (GSV) images in two distinct farming regions: Illinois and the Central Valley in California. We demonstrate the feasibility and reliability of our new ground referencing technique by performing pixel-based crop mapping at the state level using the cloud-based Google Earth Engine platform. The mapping results are evaluated using the United States Department of Agriculture (USDA) crop data layer (CDL) products. From ~130,000 GSV images, the CNN model identified ~9,400 target crop images. These images are well classified into crop types, including alfalfa, almond, corn, cotton, grape, rice, soybean, and pistachio. The overall GSV image classification accuracy is 92% for the Central Valley and 97% for Illinois. Subsequently, we shifted the image geographical coordinates 2–3 times in a certain direction to produce 31,829 crop reference points: 17,358 in Illinois, and 14,471 in the Central Valley. Evaluation of the mapping results with CDL products revealed satisfactory coherence. GSV-derived mapping results capture the general pattern of crop type distributions for 2011–2019. The overall agreement between CDL products and our mapping results is indicated by R^2 values of 0.44–0.99 for the Central Valley and 0.81–0.98 for Illinois. To show the applicational value of the proposed method in other countries, we further mapped rice paddy (2014–2018) in South Korea which yielded fairly well outcomes (R^2=0.91). These results indicate that GSV images used with a deep learning model offer an efficient and cost-effective alternative method for ground referencing, in many regions of the world.

Keywords: crop type mapping, deep learning, Google Earth Engine, Google Street View, ground referencing

1. Introduction

Supervised crop type classification requires extensive ground reference data for model training and validation (Foody and Mathur, 2004; Ma et al., 2017; Wang et al., 2019). The quality and quantity of reference data used to label crop types fundamentally affects classification accuracy (Foody et al., 2016; Kavzoglu, 2009; Van Niel et al., 2005). The common sources for these reference data include field surveys, census data, or visual interpretation of remote sensing products (Dong et al., 2016; Kun et al., 2013; Wardlow et al., 2007). However, conventional ground truthing is time-consuming, labor-intensive, and costly. The lack of a low-cost and efficient method for producing ground reference data results in pervasively limited cropland information, particularly for large-scale and long periods (Phalke and Özdoğan, 2018; Wang et al., 2019; Zhong et al., 2019b).

Many satellite-derived global land cover products are available, but very few provide detailed crop type information (Buchhorn et al., 2019; Friedl et al., 2010; Gong et al., 2013). One possible reason is the lack of ground truth crop type data, which has hindered crop growth monitoring and yield prediction at large scales. Annual cropland data layer (CDL) products released by the United States Department of Agriculture (USDA) are one of the most successful crop type maps to date in terms of nationwide coverage, annual updating frequency, and high mapping accuracy (85–95%) (Boryan et al., 2011). Since 2008, many studies have relied on CDL products for geo-referenced and crop-specific maps (Howard and Wylie, 2014; King et al., 2017; Skakun et al., 2017; Torbick et al., 2018). However, many regions and countries are incapable of producing long-term, large-scale, and accurate crop type mapping products. The extremely limited amount of publicly available ground reference data is a critical obstacle of crop type mapping, especially for developing countries (Wang et al., 2020b). Therefore, frequent updating of large-scale crop type maps with high spatial resolution remains a great challenge (You et al., 2014).

Efficient acquisition and sharing of sufficiently high-quality ground truthing observations are therefore goals for both the scientific and practical applications of crop type mapping. Aside from CDL products, a recent crowdsource-based project attempted to initiate collaborations between

scientists and citizens to collect and distribute geo- and time-referenced field photographs on a global scale (Xiao et al., 2011). As of 2020, the resulting data portal stores more than 180,000 land cover images. Another crowdsourced project, GeoWiki recruited volunteers to review and improve global land cover map products using the Google Earth platform (Fritz et al., 2009). Citizen science thus provides unconventional solutions for generating ground truth data. However, encouraging citizens to participate remains a challenge, as does quality assurance.

Google Street View (GSV) images offer an unprecedented high-quality data source that directly captures land cover information. GSV; was launched in 2007 in the US and has been developing rapidly, with international coverage including several major crop producing regions, including America, Europe, and parts of Asia (Fig. 16). A vast number of panoramic images containing detailed geographic coordinates and time information are now available. These data hold great potential for scientific studies and are surprisingly underexploited for land cover applications. Ringland et al. (2019) applied a pre-trained convolutional neural network (CNN) model to GSV images to characterize food production along roads. Gebru et al. (2017) also employed a CNN model to analyze socioeconomic profiles across 200 American cities using GSV images. Deep learning, especially in CNN models, has been successfully applied to image classification tasks (Ciresan et al., 2011; Sharif et al., 2014). Applying a CNN model to GSV images is a promising alternative for the efficient and cost-effective production of large amounts of ground reference data. Moreover, the widely available of GSV images have already shown great scalable potential for urban land use studies (Li et al., 2017; Srivastava et al., 2019; Srivastava et al., 2020; Zhang et al., 2017). Nevertheless, to the best of our knowledge, GSV images have not been explored or demonstrated as a feasible and robust proxy for generating broadly representative ground reference data for continuous crop type mapping at large spatial and temporal scales.

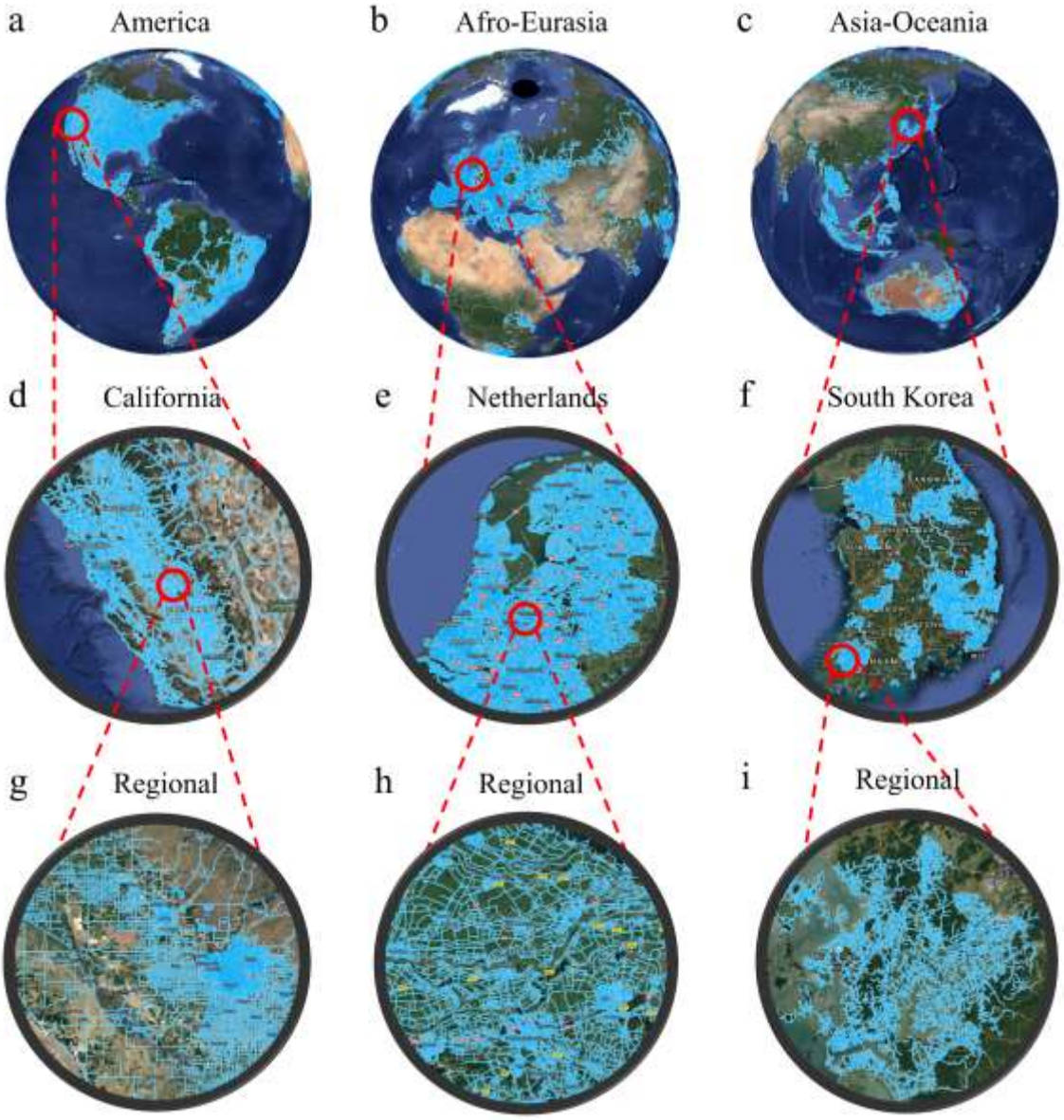

Figure 16 Examples of the availability and spatial distribution of GSV images across the globe, indicated in light blue. Note that the red circles show the approximate location of the inset areas. Image copyright: Google Inc.

The objective of this study is to develop an effective crop type referencing method using off-the-shelf GSV images. A successful method should be location-independent and have the ability to be upscaled efficiently to large areas where GSV images are available. To assess the performance of

the GSV based method, we validate the GSV derived crop type maps with other renowned land cover products such as CDL, particularly for the years without GSV as reference (see detailed description in the Method sections (2.6–2.7)).

Here, we address the following two key questions:

1. Can we use GSV images to efficiently produce low-cost, sufficient, and reliable crop type ground reference data covering large areas?

2. Can we use GSV-derived reference data as "ground truth" to map crop types for large areas spanning many years?

2. Materials and Methods

2.1 Study area

To demonstrate the reliability and generality of the proposed method, we use two large and representative farming regions in the US. Study area I is the Central Valley in California, covering approximately 46,620 km² (Fig. 17). According to recent CDL products (2011–2017), the majority of cropland in California is concentrated in the Central Valley region. This is one of the most diverse crop regions in the US; producing alfalfa, corn, cotton, wheat, almonds, grape, pistachios, as well as other crops varying annually. The Central Valley has two growing seasons with a common rotation practice, e.g., winter wheat and summer maize. Study area II is the entire state of Illinois, covering approximately 149,998 km² (Fig. 17). This area is at the core of the US Corn Belt; its major crops are soybean and maize. The general practice in this region is single-season cropping.

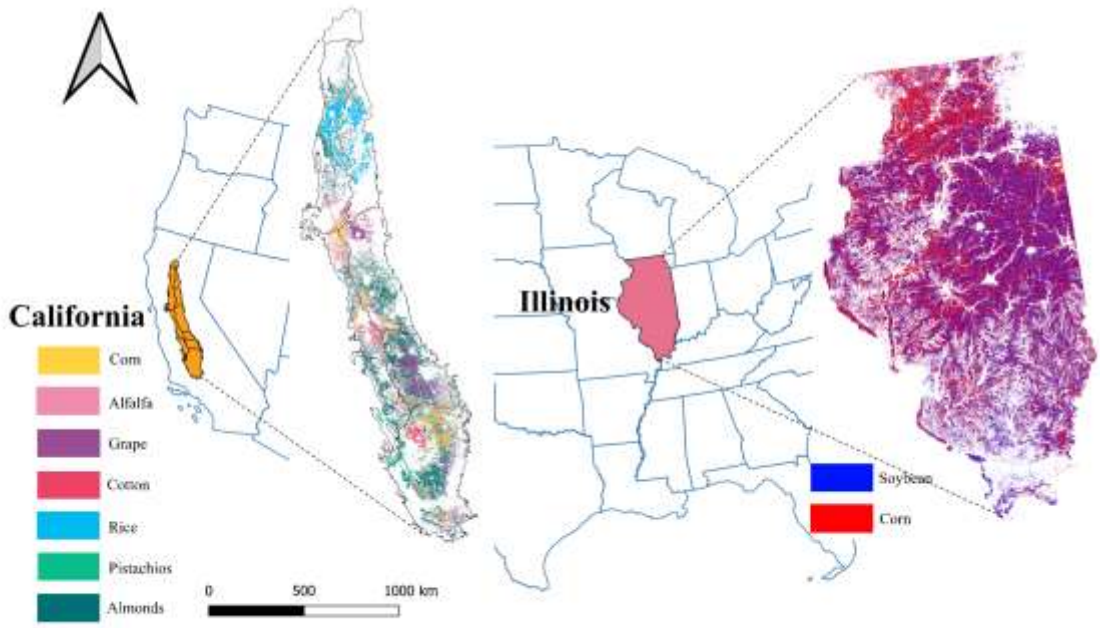

Figure 17 Study area I and II, the Central Valley in California and the state of Illinois, and their major crop types distribution from the CDL.

2.2 General methodology

This research involves the following steps: GSV image acquisition, GSV image classification, crop type referencing, and crop type mapping. Figure 3 presents an overall flowchart of our proposed methodology. To make an automatic image classifier, we trained a convolutional neural network (CNN) model with labeled GSV images. To produce point ground reference data, we subsequently applied the CNN model to classify GSV images. To evaluate the usefulness of the GSV-derived crop type ground reference on a large scale, we applied a random forest (RF) classifier with the CNN derived-references and Landsat satellite imagery to produce state-level crop type maps over multiple years. Finally, we compared the mapping results with the USDA CDL.

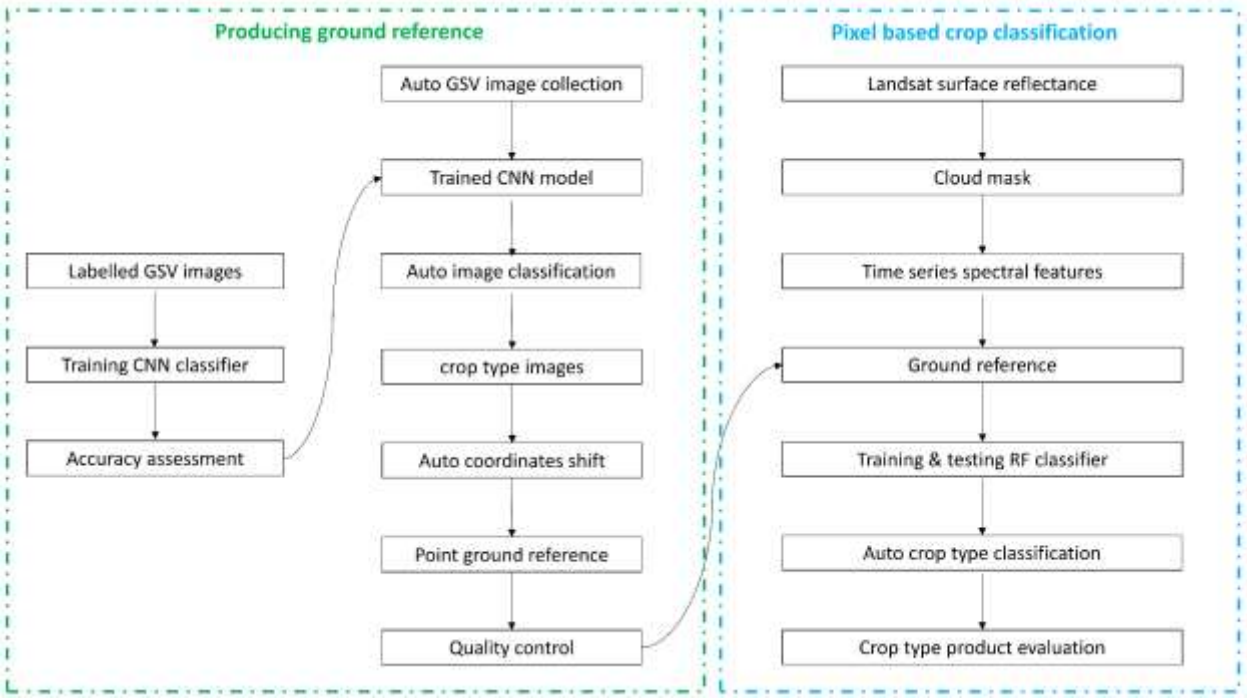

Figure 18 Flowchart of the convolutional neural network (CNN)-based ground referencing and pixel-based crop type classification.

2.3 Google Street View image collection

GSV images were automatically downloaded from Google Maps with an HTTP URL request using the GSV API via a Python script (Fig. 19). When we accessed these images in May 2020, the cost was $7 USD per 1000 images. Upon user-specification of the latitude and longitude information, the GSV API searches for the photographs within a 50-m radius and provides panoramic images where available. To decompose the images, we used a heading parameter to identify images facing four directions: north, east, south, and west. We collected GSV images by specifying latitude and longitude coordinates around the two study areas. Time information is also preserved for each image. Detailed information on the retrieval of GSV images is available in the Google Developer Guide (https://developers.google.com/maps/documentation/streetview). The code that we used for collecting GSV images is available here: http://environment.snu.ac.kr/ground_truth//.

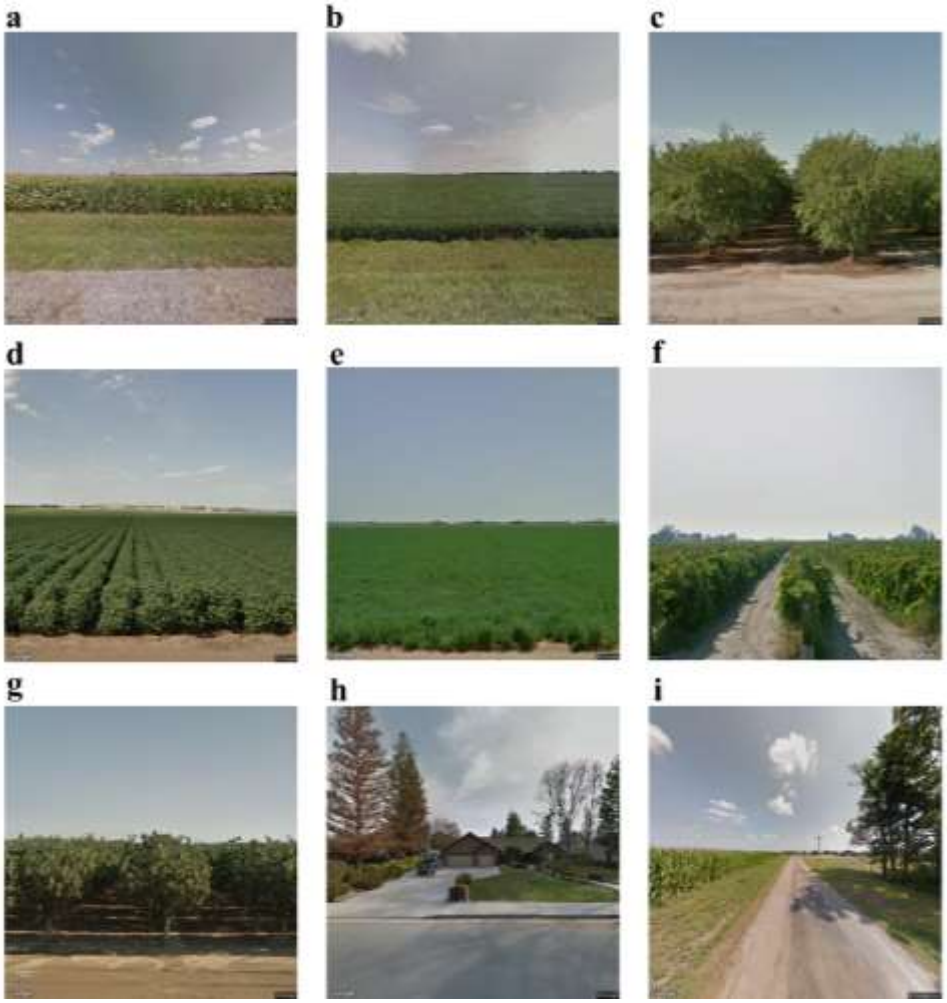

Figure 19 GSV image samples randomly collected in this study: (a) corn, (b) soybean, (c) almond, (d) cotton, (e) alfalfa, (f) grape, (g) pistachio, (h) and (i) are classified as “other”. Image copyright: Google Inc.

2.4 CNN model training and validation

We applied a CNN model to automatically classify all collected GSV images into three classes in Illinois (corn, soybean and “other”), and eight classes in the Central Valley (alfalfa, almonds, corn, cotton, grape, pistachios, rice, and “other”). The “other” category includes forest, grassland, man-made structures, and water bodies. Because the target land cover type in the study areas is cropland, we did not further classify “other” according to land cover type. The key structure of the CNN

model is presented in Fig. 20. The Input layer (a GSV image) with dimensions 30×30×3 of the CNN model includes three color channels (R, G, B), with an image width and height of 30. Cov2D is a two-dimensional convolution layer that results in feature maps from the previous input. We applied the Rectified Linear Unit (ReLU) activation function for the convolutional operation. The Max Pooling layer is a downsampling process that takes the maximum value in each patch through the feature maps. To prevent over-fitting, we applied four dropout layers. The full connection layer calculates the final probabilities for each class, which is activated by the *softmax* function. For a more detailed explanation of the CNN model structure and technical terms, see Krizhevsky et al. (2012).

To prepare training datasets for the CNN model, we labeled approximately 500–1000 GSV images for each crop type, with 7 classes for the Central Valley and 2 classes for Illinois, and 1 class representing "other". To simplify this task, we targeted only ideal images containing a single homogeneous crop type (Fig. 19a–g). Images like the one in Fig 19i, containing both corn and forest, were classified as "other". Because preparing a training dataset is usually time-consuming at the initial model setup phase, we share all of our classified images to facilitate potential future studies here: http://environment.snu.ac.kr/ground_truth//. The images were later randomly separated into three groups (60%, 20%, and 20%) for training (parameter fitting), validation (hyper-parameter tuning), and test (performance evaluation), respectively.

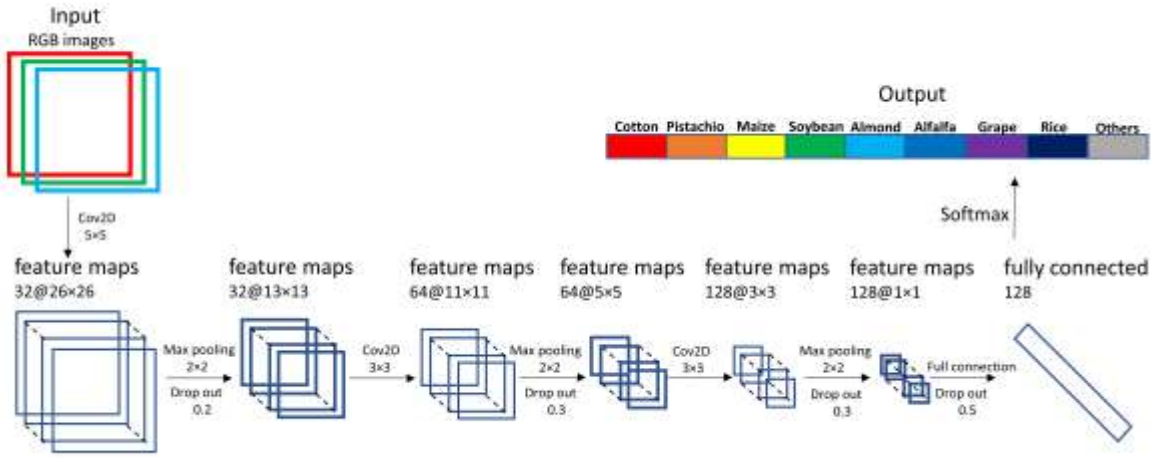

Figure 20 Architecture of the CNN model used for Google Street View (GSV) image classification.

2.5 Producing ground reference data and quality control

We applied the CNN model to filter out crop images automatically from GSV images, which contained detailed geographic coordinate and time information. We first conducted quality control to remove minor images (<10%) that were incorrectly classified by the CNN model (Table 1 & 2). The quality control is optional but valuable for the region with lower CNN performance. Currently, we still have to do quality control by human intervention, but the post-processing is marginal. In Appendix Table 1, we present the quantitative impacts of quality control on the performance of the land cover classification model. The coordinates of the image represent the location of the GSV vehicle, which is not identical to that of the crop parcel of interest (Fig. 21). Therefore, we shifted the coordinates of the GSV car by considering the width of the road and size of the crop parcel; an example of the process is shown in Fig. 21.

We applied a buffer zone to avoid the reference points locating in the Landsat pixels mixing with road and crop parcels. Thus, the coordinates of targeted GSV images were moved 0.5y (6 m) away from the car and approximately x (30 m) away from a parcel edge (Fig. 21). To produce many reference points as possible, we moved the coordinates 2–3 times in the same direction with an interval of 30 m, thereby producing reference points at 30 m, 60 m and 90 m away from the road edge. By considering the field sizes of US cropland (Fritz et al., 2015), we assumed that the crop type would not change within approximately 100 m of the GSV car in the study areas.

Although road width varies considerably, based on random checks of road widths in the two study areas we applied a fixed value of 12 m. The fixed distance x value of 30 m between adjacent reference points is related to the spatial resolution of the Landsat 7 and 8 surface reflectance products used for mapping. For smaller parcel, a value of 10 m would be more suitable to produce the reference points, if higher spatial resolution remote sensing products such as Sentinel are available. To test the generality of our method, we used the same x- and y-values for both the

Central Valley and Illinois. To simplify the procedure, we considered images captured from the four absolute cardinal directions only: north, south, east, and west.

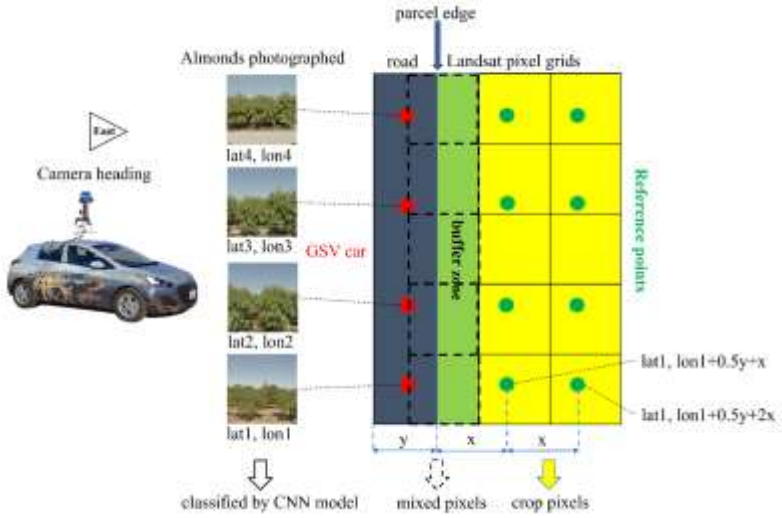

Figure 21 GSV vehicle coordinates were shifted to generate ground reference points. The buffer zone indicates potential mixed pixels near the parcel edge. Red dots indicate the position of the GSV car; green dots indicate reference points; y is road width; x is Landsat pixel resolution. Image copyright: Google Inc.

2.6 Mapping crop types

To demonstrate the reliability and usefulness of the GSV-derived ground reference across spatial and temporal domains, we conducted crop type mapping at the scale of the Central Valley and all the state of Illinois over a period of years with and without GSV-derived reference data. We performed the pixel-based crop type classification using the cloud-based Google Earth Engine (GEE) platform with the RF classifier. For a detailed description of GEE and RF classifier for land cover classification, see Gorelick et al. (2017) and Pal (2005).

Intuitively, a model trained with multiple years of data should result in better performance. We trained the RF classifier with all available GSV image data through all study periods. In Appendix, Fig. A1 shows the sensitivity of the RF classifier to the training dataset size. Table A2 shows the

overall accuracy of the RF classifier in Illinois when trained with different years of data. As expected, the performance of the RF classifier substantially increases with more training data, and eventually saturates. To train the RF classifier, we randomly divided all the reference as 80% for training and 20% for validation. To test the generic performance of the trained model in the case of data scarcity, we applied the classifier for years without GSV images as reference.

Temporal and spectral features from remote sensing surface reflectance products are commonly used to map crop types (Arvor et al., 2011; Foerster et al., 2012; Wardlow and Egbert, 2008). However, different crop types with similar spectral information can hinder classification (Cai et al., 2018). We therefore combined time series (for each year) of spectral reflectance data (Blue, Green, NIR, Red, SWIR1, and SWIR2), and normalized difference vegetation index (NDVI) (Tucker, 1979) for use as input for the RF classification model. NDVI was derived from Landsat 7 Collection 1 Level-2 scene product (surface reflectance) for the Central Valley, and Landsat 8 surface reflectance for Illinois. We used the "pixel_qa" band to mask out cloud contaminated data generated from the C Function of Mask (CFMask) algorithm (Foga et al., 2017). In accordance with the availability of Landsat products and GSV images, we mapped the crop types in the Central Valley (using Landsat 7) from 2011–2017, and in Illinois (using Landsat 8) from 2013–2019. Our code for performing landcover classification on the GEE platform is available here: http://environment.snu.ac.kr/ground_truth//.

2.7 Mapping results evaluation

The annual CDL products provided by the USDA is one of the most successful cropland datasets available in terms of nationwide coverage, annual updating frequency, and overall accuracy. Fig. A2 presents the producer and user accuracies of CDL for our investigated crop types in the Central Valley and Illinois, for the entire study periods. Detailed crop type mapping accuracy assessments of the CDL from 2008–2019 are freely available at nass.usda.gov/Research_and_Science/Cropland/SARS1a.php.

We assessed the mapping results using CDL by sampling the number of pixels for each crop type with a 5-km^2 resolution for both the study areas, using the following equation:

$$Y_{i,k,p} = \alpha X_{i,k,p} + b + \varepsilon \quad \text{Eq. 1}$$

where $Y_{i,k,p}$ ($X_{i,k,p}$) is the number of pixels for crop type k at year p derived from CDL (this study) respectively, for grid i across the entire study area; α is the linear-fit coefficient, b is the linear fit intercept; and ε is the error. To evaluate the spatial distribution of crop types in our methods against CDL, we calculated the difference in pixel numbers of each crop type from the mapping results every 5km^2, using the following equation:

$$D_{i,k,p} = \frac{X_{i,k,p} - Y_{i,k,p}}{N} \times 100 \quad \text{Eq. 2}$$

where $D_{i,k,p}$ is the disagreement (%) between the CDL and mapping results of this study for crop type k in grid i for year p; and N is the total number of pixels per 5km^2.

2.8 Additional test case

To demonstrate the applicational value of the aforementioned method in other countries, we further apply the proposed method in South Korea and map the rice paddy for the year 2014-2018. Landscape in South Korea is much more heterogeneous and fragmented compared to Illinois and Central Valley, which could be a representative study area to showcase the practical value of our approach. To transfer the CNN model into a new study area, we use the rice paddy images prepared in Central Valley with only limited additional images in South Korea. Due to the absence of CDL alike products, we evaluate the mapping results with Dong et al. (2016) rice paddy map for the year 2014.

3. Results

3.1 GSV image classification

Tables 1 and 2 present the performance of the CNN model for differentiating GSV images in the Central Valley and Illinois, respectively. The CNN model demonstrates considerable capacity for crop type image classification in both simple (3 classes in Illinois) and complex (8 classes in the Central Valley) situations. In the Central Valley (Table 1), the overall accuracy is 92%. All producer accuracy results exceed 90%, except for alfalfa (82%) and almonds (82%). All user accuracy results exceed 90% except for rice (76%) and "other" (84%). The CNN model occasionally misclassified alfalfa and rice, especially for images of crop land with remote distance and low resolution. In Illinois (Table 2), the CNN model performed better, with an overall accuracy of 97% and producer and user accuracy both exceeding 94%. In South Korea, the CNN model achieved an overall accuracy of 92%, for the detailed results see Supplementary Table 1.

Table 1 Performance of the CNN model for GSV image classification in the Central Valley, displayed as a confusion matrix. PA: producer accuracy; UA: user accuracy; OA: overall accuracy.

Central Valley	*Alfalfa*	*Almonds*	*Corn*	*Cotton*	*Grape*	*Other*	*Pistachios*	*Rice*	*UA*
Alfalfa	185	0	0	0	0	0	0	3	98%
Almonds	0	127	0	0	3	1	3	0	95%
Corn	6	0	110	2	1	0	1	0	92%
Cotton	0	0	0	116	0	0	0	0	100%
Grape	0	0	1	0	121	0	0	0	99%
Other	4	25	0	0	1	182	0	4	84%
Pistachios	0	3	0	0	3	2	119	0	94%
Rice	31	0	0	2	0	0	0	104	76%
PA	82%	82%	99%	97%	94%	98%	97%	94%	OA = 92%

Table 2 Performance of the CNN model for GSV image classification in Illinois, displayed as a confusion matrix. PA: producer accuracy; UA: user accuracy; OA: overall accuracy.

Illinois	*Corn*	*Other*	*Soybean*	*UA*
Corn	118	3	5	94%
Other	0	139	0	100%
Soybean	1	4	119	96%
PA	99%	95%	96%	OA = 97%

3.2 Producing ground reference data from classified GSV images

We applied the trained CNN model to automatically screen crop images. In the Central Valley, we found 4,811 out of a total of 42,485 GSV images belonging to 7 crop classes: 613 alfalfa, 1,682 almond, 777 pistachio, 348 corn, 250 cotton, 796 grape, and 113 rice. In Illinois, we found 4,593 out of a total of 85,635 GSV images for 2 classes: 3093 corn and 1500 soybean. Subsequently, we produced reference points with the classified GSV images by shifting the geocoordinates (Fig. 21). In South Korea, we found 1,488 rice paddy images from 43,536 GSV images. Supplementary Fig. 1b shows the temporal and spatial distribution of the produced reference points. We retrieved rice images in two years (2015, 2018) but with a biased sample size, which is the nature of GSV.

In total, we produced 31,829 crop reference points within parcels, 14,471 in the Central Valley, and 17,358 in Illinois (Fig. 22). Due to the unequal spatial-temporal availability of GSV image, as well as the varied areas of different crop types, the consequent GSV image derived reference points present an imbalanced distribution. For instance, in Illinois (Fig. 22h & 22i) the majority of reference points are located in the center of the state, whereas the reference point density is relatively low in north and southeast of Illinois; this may affect subsequent mapping results using these reference data.

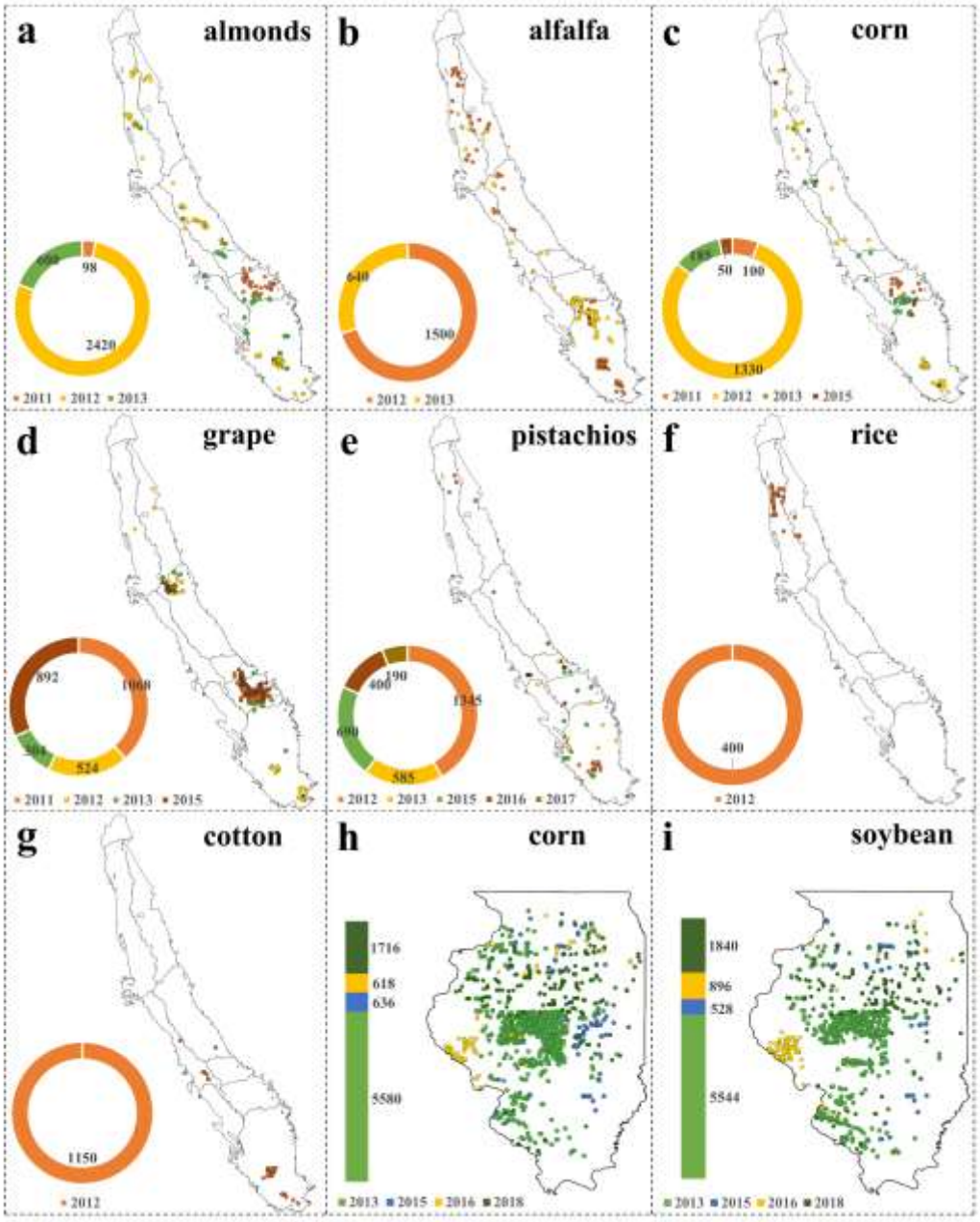

Figure 22 Temporal and spatial distribution of crop type reference points derived from GSV images for the Central Valley (a-g) and Illinois (h-i). The doughnut plots and bar plots indicate the number and proportion of reference points for each year.

3.3 Mapping using the GSV derived ground reference

Tables 3 and 4 present the accuracy assessment of the RF classifier for landcover classification in the Central Valley and Illinois, respectively. The RF classifier trained with GSV-derived reference points demonstrates good performance for crop type mapping in both study areas. However, using GSV derived data itself for both training and validation would result in potential biased accuracy. Therefore, the performance was further assessed with independent CDL products, as described next. In South Korea, we found the RF classifier shows comparable performance as Illinois and Central Valley. The detailed accuracy assessment is available in Supplementary Table 2.

Table 3 Performance of the RF model for land cover classification in the Central Valley indicated as a confusion matrix. PA: producer accuracy; UA: user accuracy; OA: overall accuracy.

Central Valley	*Alfalfa*	*Almonds*	*Corn*	*Cotton*	*Grape*	*Other*	*Pistachios*	*Rice*	*UA*
Alfalfa	534	8	10	1	2	11	2	1	94%
Almonds	1	1428	0	0	6	21	4	0	98%
Corn	4	1	450	3	4	21	2	0	93%
Cotton	4	1	1	234	2	3	1	0	95%
Grape	1	5	0	0	427	7	6	0	96%
Other	14	30	5	3	15	1192	9	2	94%
Pistachios	1	23	0	1	1	10	865	0	96%
Rice	0	0	1	0	0	2	0	70	96%
PA	96%	95%	96%	97%	93%	94%	97%	96 %	OA= 95 %

Table 4 Performance of the RF model for land cover classification in Illinois indicated as a confusion matrix. PA: producer accuracy; UA: user accuracy; OA: overall accuracy.

Illinois	*Corn*	*Others*	*Soybean*	*UA*
Corn	1168	47	41	93%

Others	45	1194	55	92%
Soybean	52	61	938	89%
PA	92%	92%	91%	OA =92 %

Figure 8 and 9 present the examples of the overall mapping results compared with the CDL products in the Central Valley for 2017, and in Illinois for 2014, respectively. Mapping results are notably consistent with CDL products for both study areas. The crop type mapping model (RF classifier) trained with GSV derived reference data (Fig. 22) captured the overall spatial pattern of crop types when applied to the years with very few GSV images. Note that only 190 reference points were available for pistachio crop in the Central Valley in 2017 (Fig. 22e), while no reference data were obtained via GSV images in Illinois in 2014. In South Korea, we also found a comparable rice paddy distribution map for the year without GSV as reference (Supplementary Fig. 2 & 3).

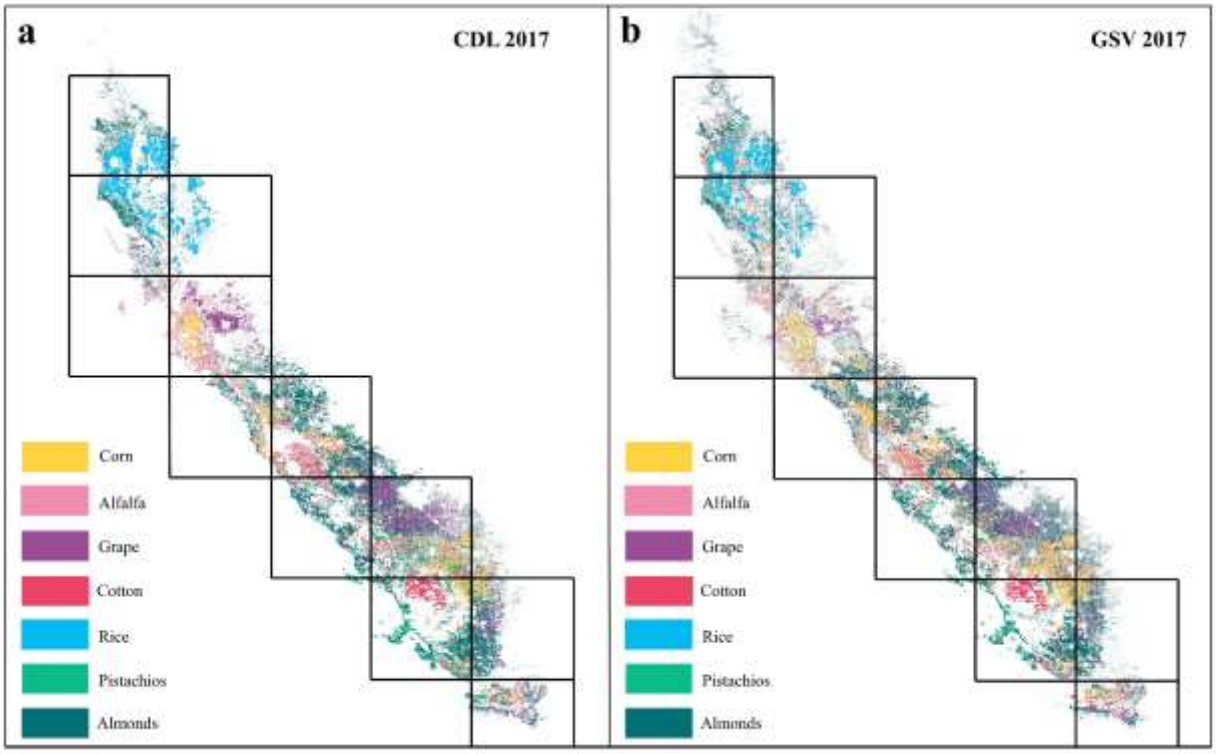

Figure 23 Comparison between the CDL and GSV-derived crop type maps for the Central Valley in 2017 (a, b, respectively), a year with only 190 reference points. Black squares serve as guide grids to facilitate visual comparison.

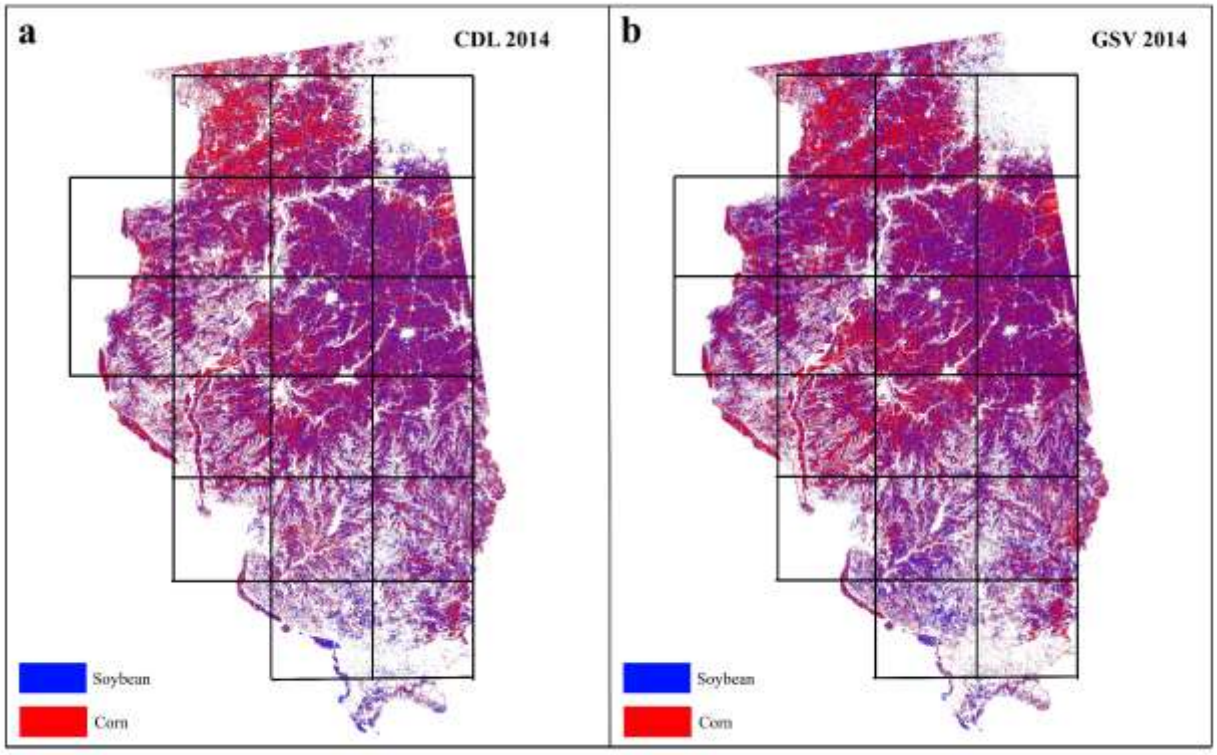

Figure 24 Comparison between the CDL and GSV-derived crop type maps for Illinois in 2014 (a, b, respectively), a year without reference GSV images. Black squares serve as guide grids to facilitate visual comparison.

Table 5 presents a detailed, long-term, quantitative comparison between the CDL and GSV-derived crop type maps for the Central Valley from 2011–2017. Overall, the RF classifier trained with GSV-derived reference data is capable of mapping heterogenous and diverse land cover types at a large scale and over multiple years. Furthermore, the RF classifier still demonstrates comparatively promising performance for the years when GSV images are unavailable, e.g., 2014. As expected, the model generally achieves higher agreement for the years with more GSV images, e.g., 2012. Mapping results are more consistent for rice and cotton, although relatively fewer reference points were used for training. The CDL assessment also yielded similar mapping

performance for rice and cotton over time (Fig. A2). In contrast, the agreement was lower for pistachio, which could be explained by the higher uncertainties of the CDL for pistachio classification. For a more comprehensive evaluation, Fig. 25 presents a comparison of the mapping results with the CDL-derived results for a year with almost no ground reference data (2017). For the years 2011–2016, see Appendix Fig. A3.

Table 5 Comparison of GSV-derived and CDL-derived crop type distribution maps for each crop type in the Central Valley using a 5-km^2 grid resolution. The number of references indicates data available for training and testing the random forest classifier for each year.

		2011	*2012*	*2013*	*2014*	*2015*	*2016*	*2017*
Alfalfa	R^2	0.79	0.82	0.79	0.77	0.79	0.73	0.66
	number of references	0	1500	640	0	0	0	0
Almonds	R^2	0.85	0.82	0.87	0.80	0.85	0.79	0.84
	number of references	98	2420	600	0	0	0	0
Cotton	R^2	0.89	0.92	0.93	0.79	0.84	0.92	0.93
	number of references	0	1150	0	0	0	0	0
Grape	R^2	0.88	0.87	0.82	0.75	0.81	0.78	0.83
	number of references	1068	524	304	0	892	0	0
Corn	R^2	0.76	0.80	0.84	0.84	0.72	0.67	0.79
	number of references	100	1330	185	0	50	0	0
Pistachios	R^2	0.60	0.59	0.61	0.44	0.66	0.63	0.61
	number of references	0	1345	585	0	690	400	190
Rice	R^2	0.98	0.99	0.99	0.99	0.99	0.99	0.99
	number of references	0	400	0	0	0	0	0

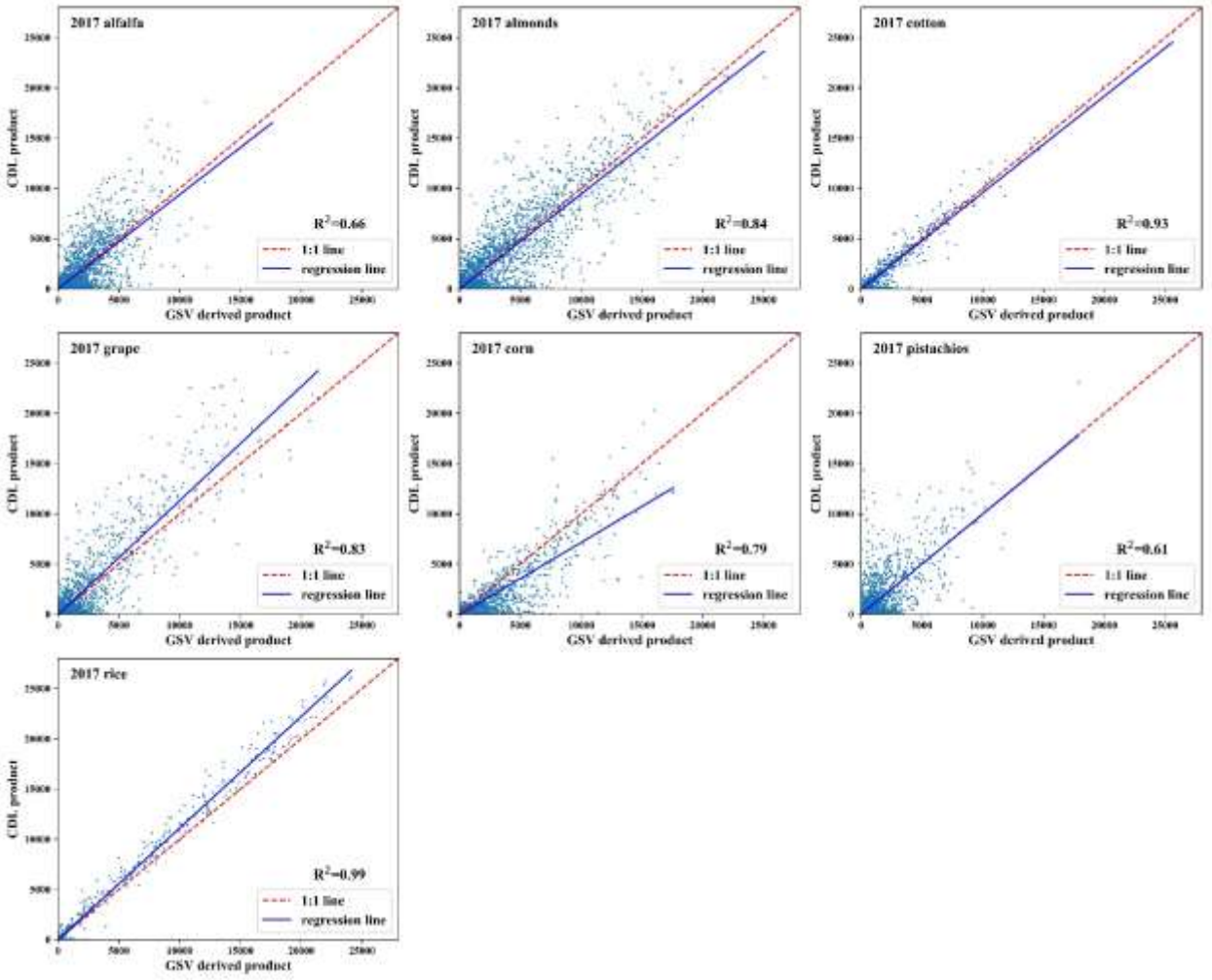

Figure 25 Comparison between GSV-derived and CDL-derived crop type distribution for the Central Valley in 2017. The x and y axes show the pixel numbers of each crop type for a 5-km^2 grid resolution for the entire study area.

Figure 26 and Fig. A4 present the detailed mapping assessment for corn and soybean in Illinois during 2013–2019. We found consistent mapping results for Illinois from 2013–2019, however, we found better overall agreement between GSV-derived and CDL crop type maps for the entire study period and domain. Comparable to the Central Valley, the RF classifier trained with multiple years of GSV-derived reference points (Fig. 22) can still be applied and has promising mapping results for both corn and soybean for years without GSV images as reference data, i.e., 2014, 2017,

and 2019. For the detailed quantitatively mapping assessment for rice paddy in South Korea, see Fig. 27.

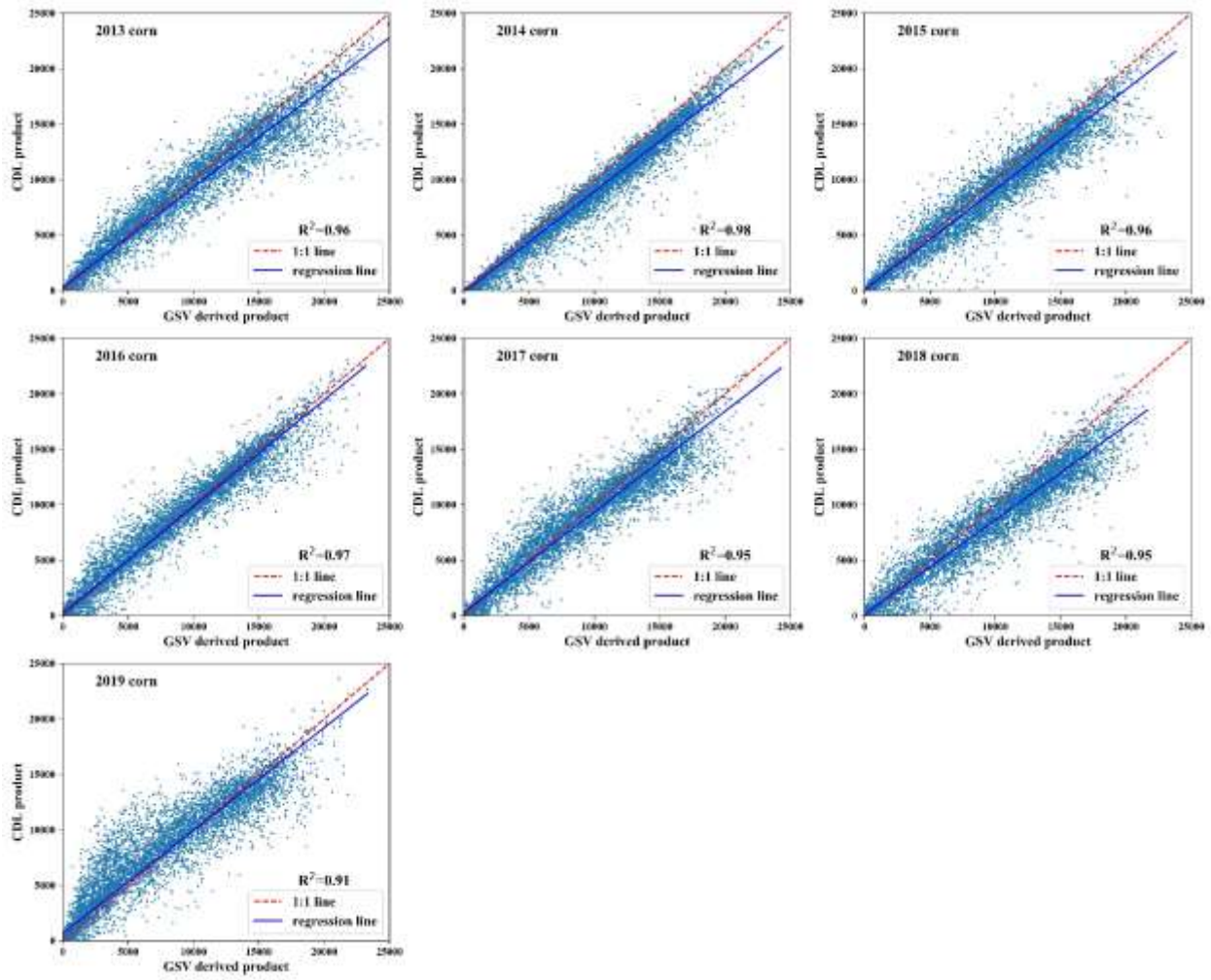

Figure 26 Comparison between GSV-derived and CDL-derived corn distribution for Illinois from 2013–-2019. The x and y axes show the pixel numbers of corn for a 5-km^2 grid resolution for the entire study area.

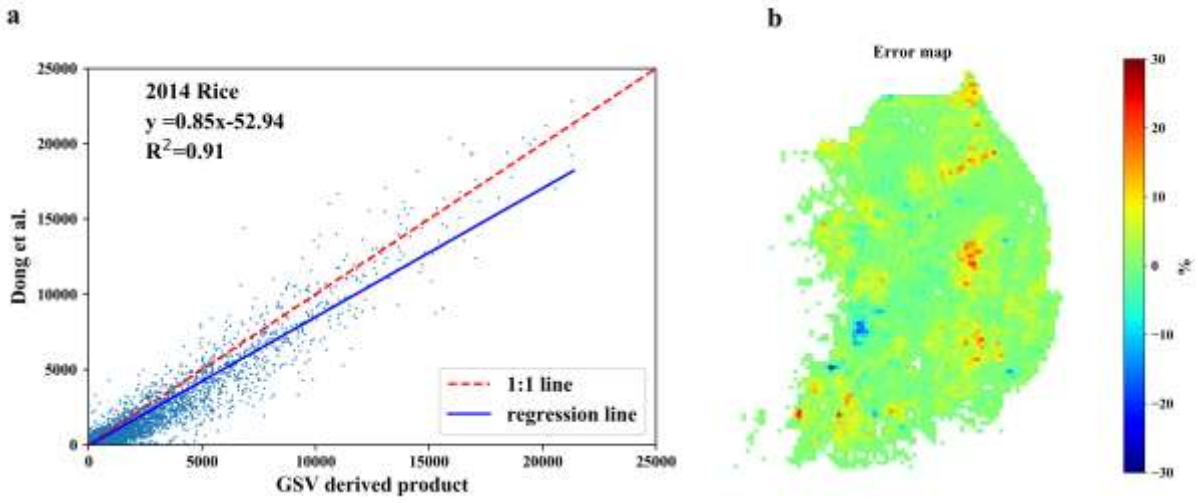

Figure 27 Comparison between GSV-derived and Dong et al., (2016) -derived rice paddy distribution for South Korea in 2014 (a). The x and y axes show the pixel numbers of rice paddy for a 5-km2 grid resolution for the entire study area. And rice paddy distribution error (%) map, expressed as the percentage difference in pixel numbers per $5km^2$ (b).

For a more detailed spatial comparison, we present the zoomed-in views of mapping results for different regions from 2011–2017 (Fig. 28 and Fig. A5). The location of each region is shown in Fig. A5g. We found an overall consistent spatial pattern of the crop types between CDL- and GSV-derived results. The reference points produced alongside the road are representative of "ground truth", and can adequately map crop types at large scales in the Central Valley for complex scenarios, e.g., mapping the potential heterogeneity of the cropland within a field that would not be observable from the road.

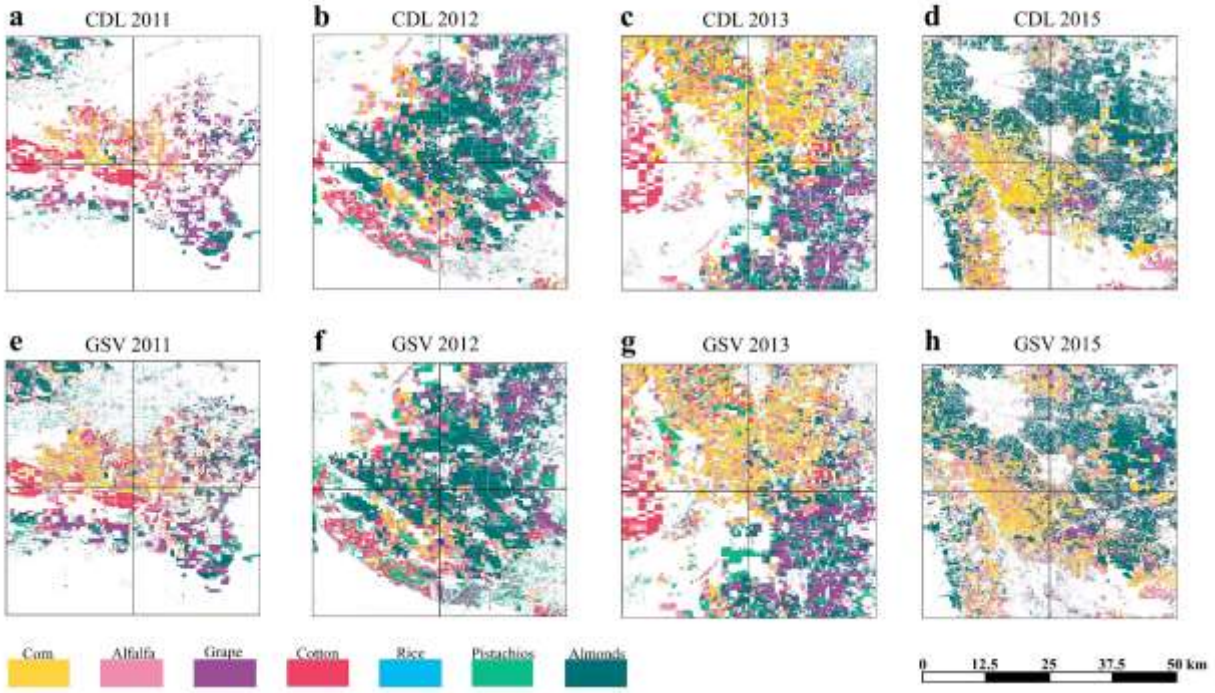

Figure 28 Regional-scale crop type mapping comparison for the Central Valley for years with GSV as reference data. Each subplot covers approximately 2500 km^2. Black squares serve as guide grids to facilitate visual comparison.

Figure 29 and Fig. A6 provide the zoomed-in views of Illinois results for years with and without GSV-derived reference data, respectively. The location of each region is shown in Fig. A6g. We found better general agreement and less noisy mapping results across the study regions than for the Central Valley, which may be due to higher CDL accuracy (Fig. A2), and relatively homogeneous and simple land cover types. Moreover, the zoomed-in views for rice paddy in South Korea show fairly well agreement (Supplementary Fig. 3).

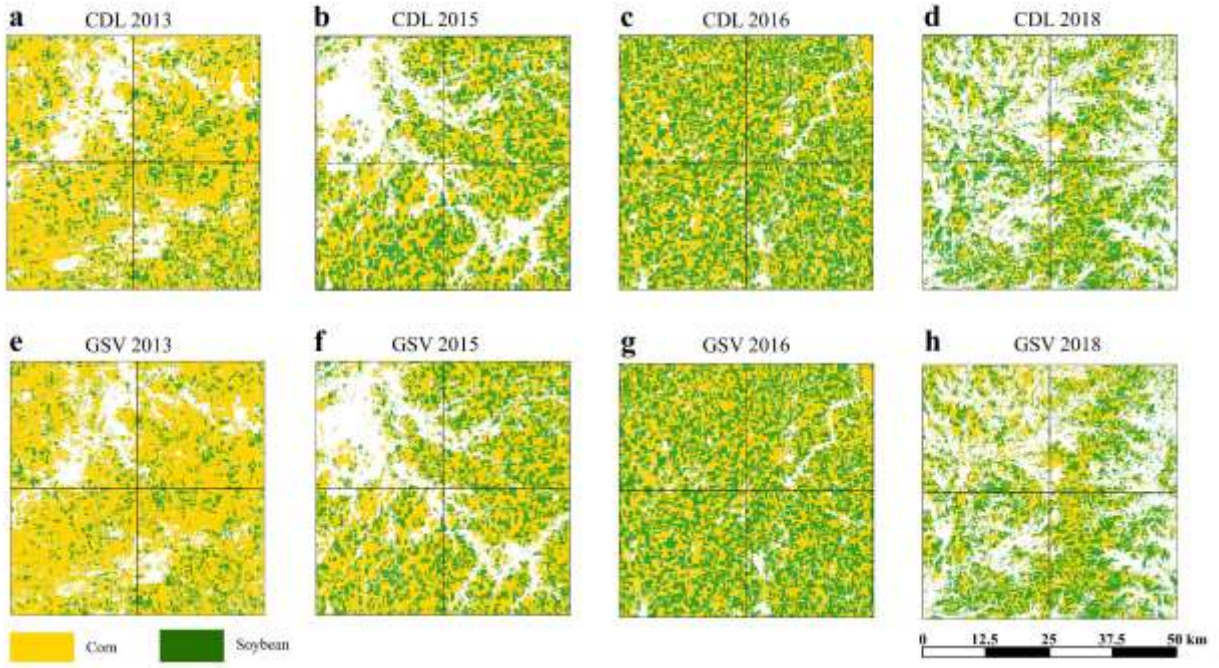

Figure 29 Regional-scale crop type mapping comparison for Illinois, for the years with GSV used as reference data. Each subplot covers approximately 2500 km^2. Black squares serve as guide grids to facilitate visual comparison.

The spatial errors in the mapping results for soybean and corn are shown in Fig. 30 and 31, respectively, for each study year for Illinois and in Fig. A7 for 2017 for the Central Valley, and in Fig. 27b for South Korea. The extent of the disagreement varies considerably over time. There is no clear correlation between reference data density and degree of error; for example, for Illinois in 2013, the year with the most abundant reference data, the error is not lower than for 2014, the year without reference data. This may affect by the performance of the RF classifier and the availability of the Landsat products (e.g., cloud cover).

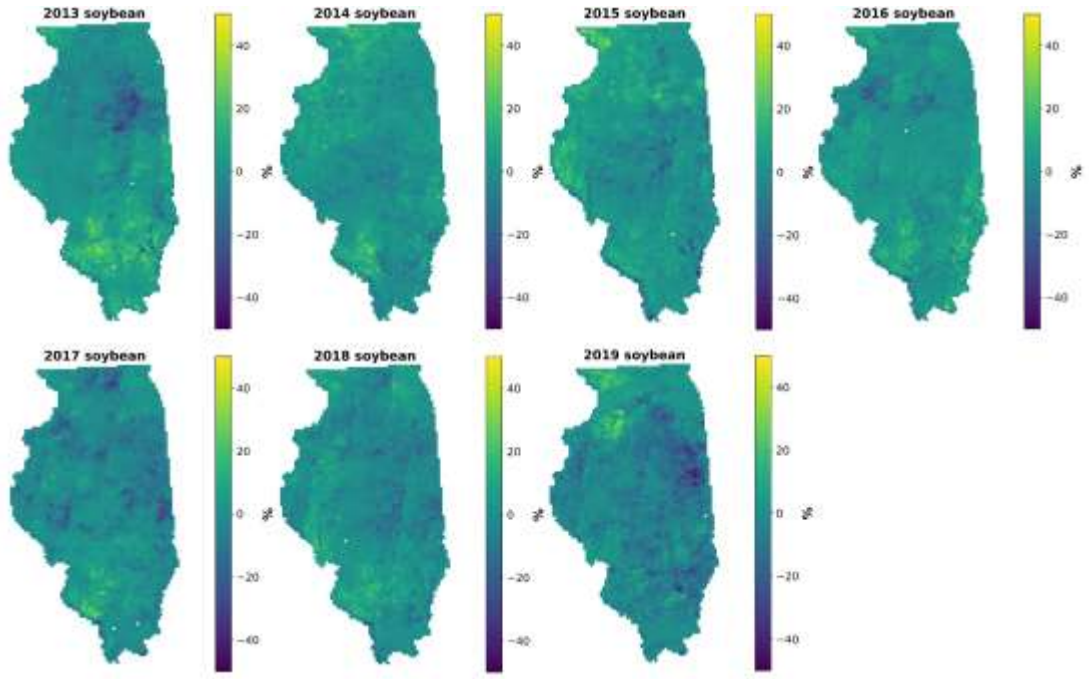

Figure 30 Soybean distribution error (%) map between GSV-derived and CDL-derived soybean maps for Illinois from 2013–2019, expressed as the percentage difference in pixel numbers per 5km^2.

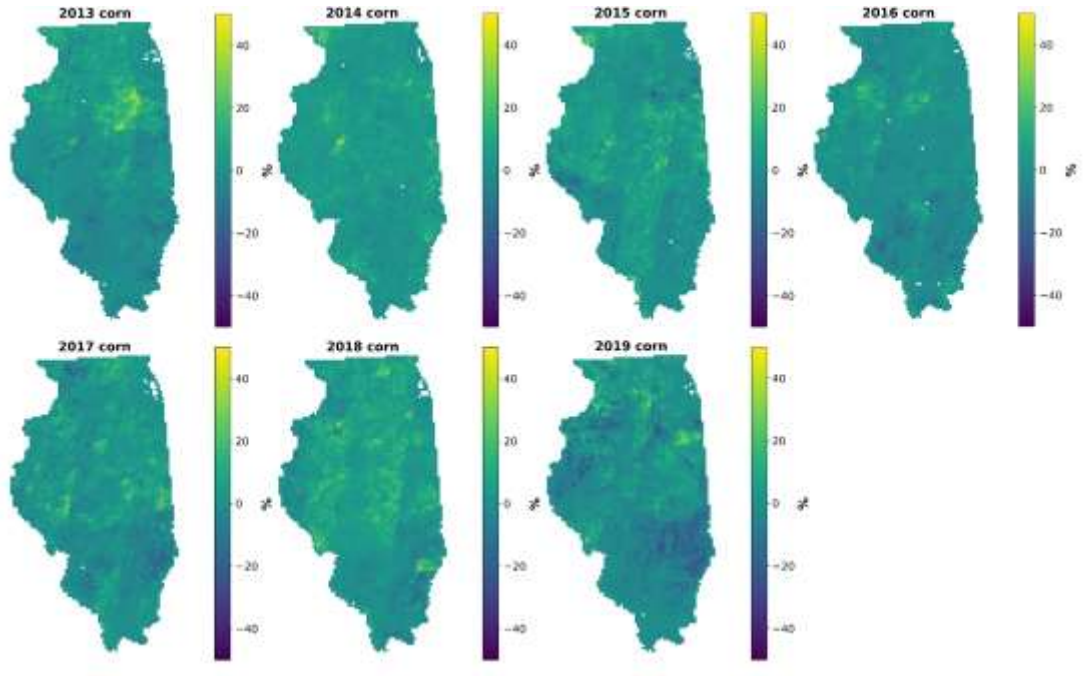

Figure 31 Corn distribution error (%) map between GSV-derived and CDL-derived corn maps for Illinois from 2013–2019, expressed as the percentage difference in pixel numbers per 5km^2.

4. Discussion

4.1 Can we use GSV images to efficiently produce low-cost, sufficient, and reliable crop type ground reference data covering large areas?

Currently, there are more than 100 countries have partial or full coverage of GSV. Except for the USA and Canada, most of the countries in the world do not have CDL alike high-quality crop type maps. At a cost of only $7 USD per 1000 images, GSV provides substantial opportunities to produce coherent ground reference points for different regions. To date, the potential for cost-effective upscaling at the national scale has been underexplored for crop type and landcover mapping. By applying a CNN model (Fig. 20) and a simple shift in geocoordinates (Fig. 21) for three large study areas, we provide an effective method for producing ground reference points from GSV images over heterogeneous regions for multiple years (Fig. 22). A post-processing quality control step is necessary to reduce the uncertainties of the CNN model. For example, the distinction between crop types in GSV images is generally robust but less effective at the early phenological stages (e.g., for seedlings). Seedling morphology is nearly identical across crop types due to low image resolution and short canopy height, and neural network performance is susceptible to the image quality (Dodge and Karam, 2016). To reduce uncertainties in image classification, an ideal strategy would be to use images taken during the peak growing season in the model training process.

In this study, we built a simple architecture-based CNN and trained the model using only a few thousand labeled GSV images. To further improve the performance of the CNN model in complex regions such as the Central Valley, future studies could also use a pretrained state-of-the-art CNN model (e.g. ResNeXt) with more training data containing seasonal crop morphology variations. Future studies could also explore generating object-based (instead of point-based) ground references by detecting cropland parcels along roads (e.g., edge extraction) (Graesser and Ramankutty, 2017). These could be connected with classified GSV images, which would fully utilize the image information and greatly benefit regions with fragmented and small parcel sizes.

4.2 Can we use GSV-derived reference data as "ground truth" to map crop types for large areas spanning many years?

The GSV-derived reference points must be representative of subsequent crop type mapping (Campbell and Wynne, 2011). Heterogeneity within croplands might not be captured by GSV images that are taken from the roadside. Using a simple geocoordinate shift (Fig. 21) and based on assessments of the regional cropland mapping results (Figs. 25–27), we found that roadside sampling via GSV images is likely sufficient to account for potential environmental and management induced within-field variability. This is consistent with a previous assessment of roadside sampling strategy for crop mapping (Waldner et al., 2019).

By mapping crop types for Illinois and the Central Valley (Figs. 25 and 26), we demonstrated the usefulness and reliability of GSV derived reference points at a large scale and over long periods. The multi-year crop type distribution maps are consistent when compared to CDL products for both large study areas, demonstrating the robustness of our proposed ground referencing method. To test the applicability of our method in the other region, we applied it for rice paddy mapping in South Korea, which showed comparable performance with the results from California and Illinois (Fig. 27 and Supplementary Information). GSV images certainly offer an unprecedented rich data source as ground truth for crop type mapping, but to date this has been underexplored. We only tested the proposed ground referencing method for croplands in the Central Valley, Illinois, and South Korea. More studies are needed to explore the usefulness of GSV images for land cover mapping in other regions of the world.

The assessment of different ground sampling strategies is crucial to achieving credible mapping results. One study reported that a random sampling method (regardless of sample location) is superior to roadside sampling (Waldner et al., 2019), and another proposed a sequential exploration method for efficient *in situ* data collection (Fowler et al., 2020). However, constrained by the availability of GSV data, random or more sophisticated sampling for GSV image collection currently seems infeasible and impractical. Although we found that the random roadside sampling strategy (where we enumerate GSV images) is robust for producing "ground truth", future studies

investigating different GSV image sampling methods would help the community collect data more efficiently, rather than enumerating the images.

We also demonstrated that increasing the sample size temporally and spatially is an effective approach to improve the final crop type mapping results (Fig. A1 and Table. A2). However, the optimal size of training dataset needed to map crop types accurately is still the subject of debate (Lillesand et al., 2015; Van Niel et al., 2005; Waldner et al., 2019). For example, we found only 400 reference points for rice in the Central Valley, and this was sufficient to achieve good mapping performance (Table. 5). It is challenging to give universal quantitative suggestions for the density of reference data because mapping results are strongly affected by the quality of the reference data, the performance of the classifier, the complexity of the landcover type, and also the availability of remote sensing products (Heydari and Mountrakis, 2018; Khatami et al., 2016; Ma et al., 2017). Nevertheless, we conclude that increasing the sample size temporally and spatially is highly desirable for collecting GSV images to enhance the representativeness.

Another current limitation of using GSV image is that the update frequency remains uncertain, and ranges from months to years, and also varies spatially. Images recorded during non-growing seasons usually provide little to no useful information unless special traits related to the specific crops are exhibited, such as standing rice stem residues after harvesting. It is a common to train a classifier using one or more years of reference data and apply this to other years without the training reference (Massey et al., 2017; Wang et al., 2020a; Zhong et al., 2016a; Zhong et al., 2019a). We adopted this idea and demonstrated the performance of the RF classifier when applied to the years without reference data (Figs. A5 and A6).

Another limitation is that GSV still has large data gaps in China, India, and Germany due to privacy concerns and local restrictions (Rakower, 2011). Additional street view maps, such as the Baidu map, Tencent map, and OpenStreetMap, are available in these countries (Haklay and Weber, 2008; Liang et al., 2017; Long and Liu, 2017; Munoz et al., 2020; Zhang et al., 2019a). Recent trends in mining vast amounts of geo-tagged social media data for urban land use and tourist behavior

studies could provide another potential solution for crop type ground truthing (Frias-Martinez and Frias-Martinez, 2014; Liu et al., 2017; Wood et al., 2013). Although we show the reliability of GSV images for production-level crop type mapping, we believe GSV is one of the useful sources but not the solution for all the countries. For instance, a recent study mapped crop types in India (where GSV image is unavailable) with smartphone crowdsourcing data (Wang et al., 2020b). Social media users continually generate recent land use information and "big data" in the form of texts, images, and videos. These processes should be further investigated because these types of information are now far more timely and abundant than GSV images. In summary, we suggest that future studies use a hybrid method that fuses GSV images, social media data, and census data (Zhong et al., 2019b), which would be valuable at the global level, for both crop type and land cover ground truthing.

Appendix

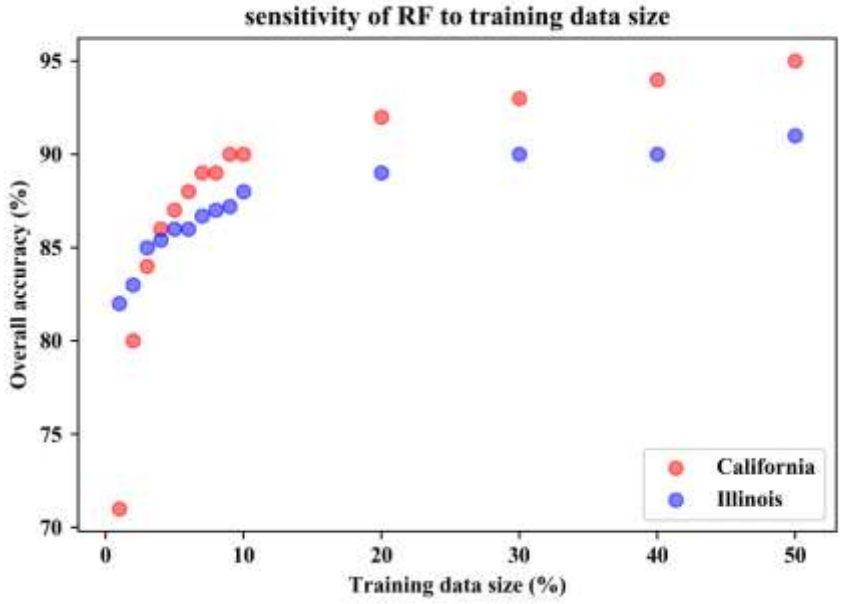

Fig. A1 Sensitivity of the RF classifier to the size of training dataset (expressed as a percentage of the total reference dataset) for crop type classification. We assessed the overall accuracy with a fixed validation dataset (20% of the total dataset).

Table A1. Performance of the RF model for land cover classification in South Korea assessed with GSV derived reference in the absence of quality control. PA: producer accuracy; UA: user accuracy; OA: overall accuracy

South Korea	*Rice paddy*	*Other*	*UA*
Rice paddy	250	33	89%
Other	38	244	85%
PA	87%	88%	OA = 87%

Table A2. Performance of the RF classifier when trained with multiple years of data for Illinois. Higher accuracy is achieved when longer periods of data are used for training.

Number of years	1	2	3	4
Overall accuracy	76%	81%	83%	92%

Fig. A2 Accuracy of the CDL for the Central Valley during 2011–2017, and for Illinois from 2013–2019; PA is producer accuracy and UA is user accuracy.

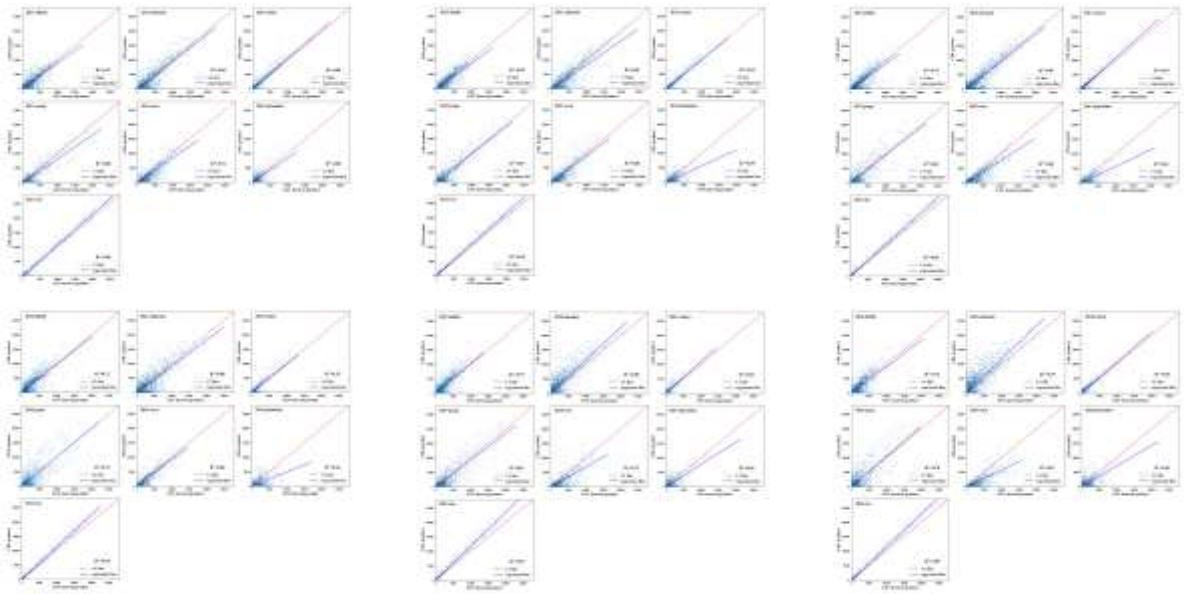

Fig. A3 Comparison between GSV-derived and CDL-derived crop type distribution for the Central Valley from 2011–2016. The x and y axes are the pixel numbers of each crop type at a 5-km^2 grid resolution for the whole study area. The R^2 values are given in Table 5.

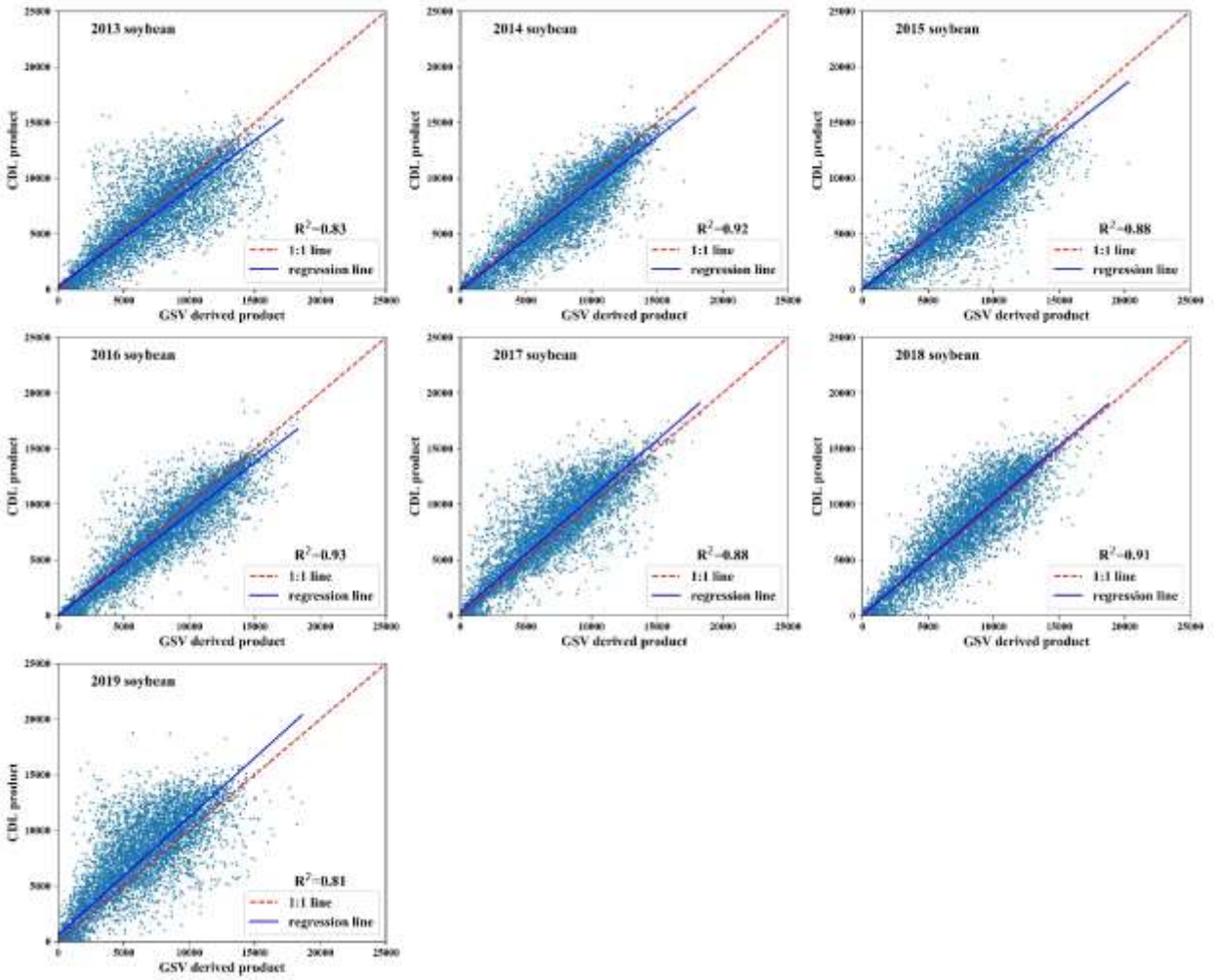

Fig. A4 Comparison between GSV-derived and CDL-derived soybean distribution for Illinois from 2013–2019. The x and y axes are the pixel numbers of soybean at a resolution of 5-km^2 grid for the whole study area.

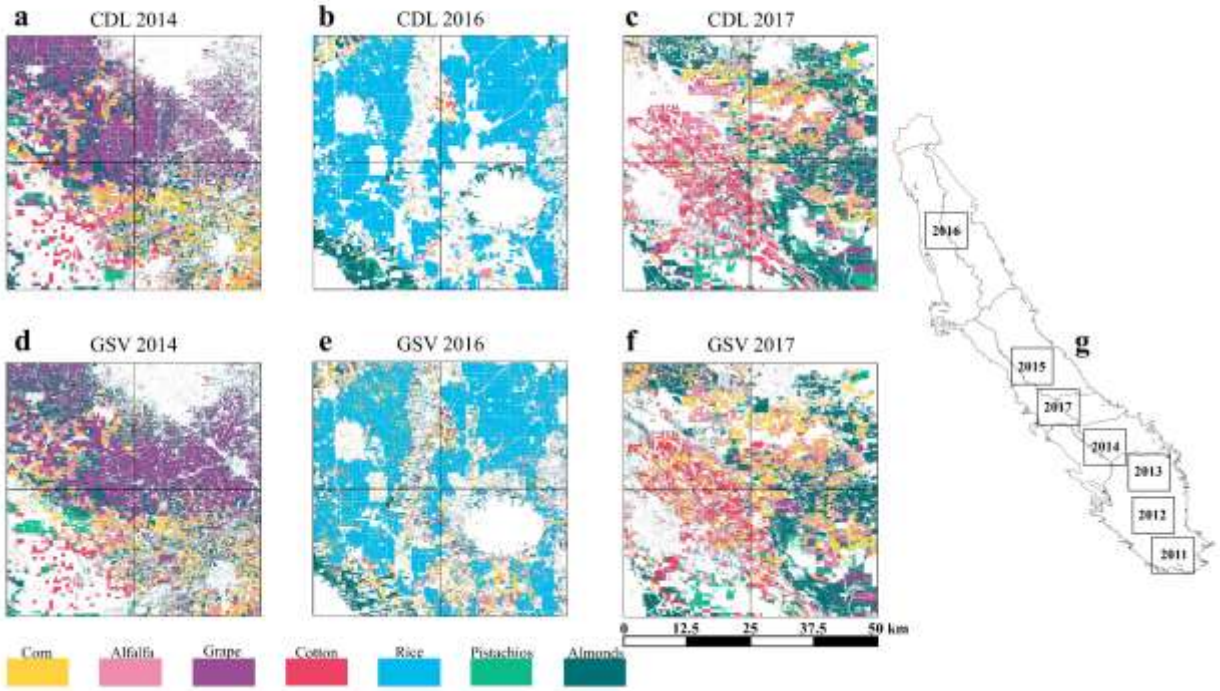

Fig. A5 Regional-scale crop type mapping comparison for the Central Valley, for years with few or no GSV images as reference data. Each subplot covers approximately 2500 km^2.

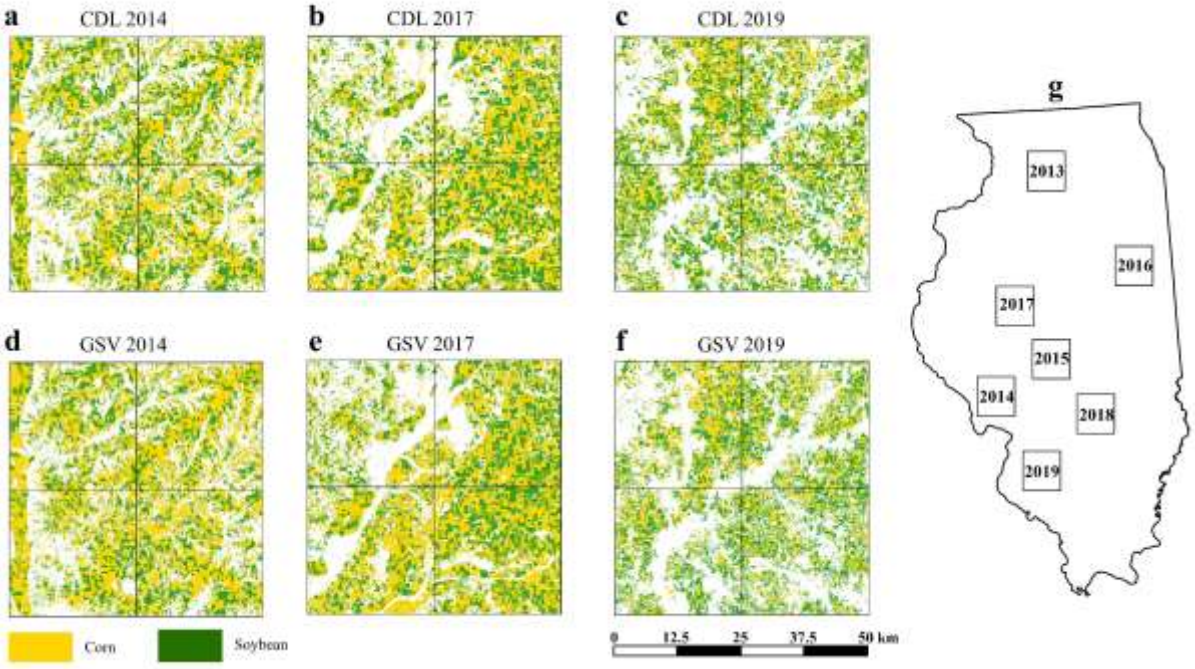

Fig. A6 Regional-scale crop type mapping comparison for Illinois, for years without GSV images as reference data. Each subplot covers approximately 2500 km^2.

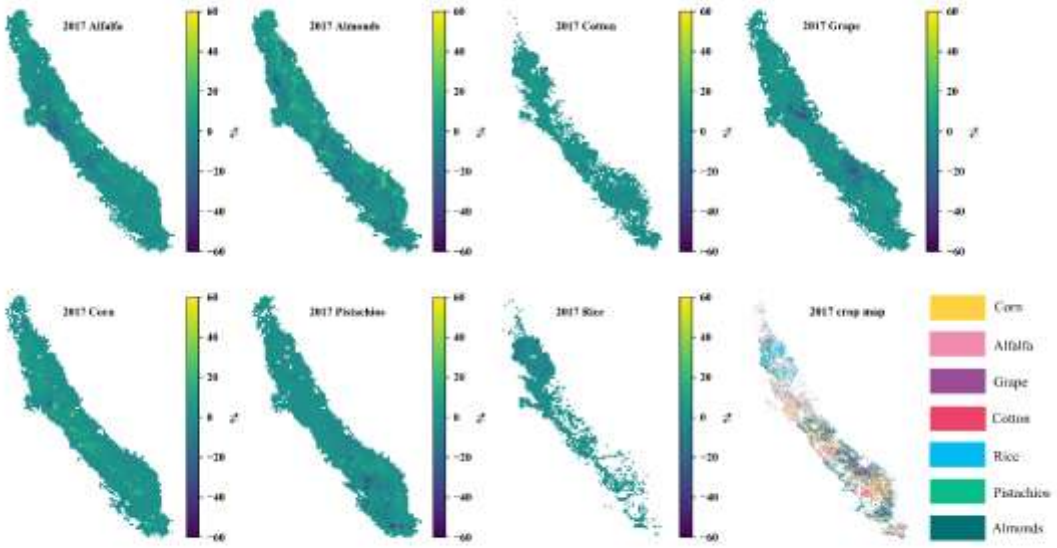

Fig. A7 Disagreement (%) between GSV-derived and CDL-derived crop type distribution maps for the Central Valley in 2017, expressed as the percentage difference in pixel numbers for each crop type per $5km^2$. White color indicates the non-cultivation area derived from both CDL and GSV mapping results for each crop type.

References

Acharjee, T.K., van Halsema, G., Ludwig, F., Hellegers, P., Supit, I. (2019) Shifting planting date of Boro rice as a climate change adaptation strategy to reduce water use. Agricultural Systems 168, 131-143.

Arvor, D., Jonathan, M., Meirelles, M.S.P., Dubreuil, V., Durieux, L. (2011) Classification of MODIS EVI time series for crop mapping in the state of Mato Grosso, Brazil. International Journal of Remote Sensing 32, 7847-7871.

Auchincloss, L., Easlon, H.M., Levine, D., Donovan, L., Richards, J.H. (2014) Pre-dawn stomatal opening does not substantially enhance early-morning photosynthesis in Helianthus annuus. Plant, Cell & Environment 37, 1364-1370.

Barbour, M.M., Cernusak, L.A., Whitehead, D., Griffin, K.L., Turnbull, M.H., Tissue, D.T., Farquhar, G.D. (2005) Nocturnal stomatal conductance and implications for modelling 18O of leaf-respired CO2 in temperate tree species. Functional Plant Biology 32, 1107-1121.

Bo, Y., Jägermeyr, J., Yin, Z., Jiang, Y., Xu, J., Liang, H., Zhou, F. (2022) Global benefits of non-continuous flooding to reduce greenhouse gases and irrigation water use without rice yield penalty. Global change biology n/a.

Boryan, C., Yang, Z., Mueller, R., Craig, M. (2011) Monitoring US agriculture: the US Department of Agriculture, National Agricultural Statistics Service, Cropland Data Layer Program. Geocarto International 26, 341-358.

Bouman, B.A.M., Tuong, T.P. (2001) Field water management to save water and increase its productivity in irrigated lowland rice. Agricultural Water Management 49, 11-30.

Bouwman, A.F. (1998) Nitrogen oxides and tropical agriculture. Nature 392, 866-867.

Buchhorn, M., Smets, B., Bertels, L., Lesiv, M., Tsendbazar, N., Herold, M., Fritz, S.J.V.V. (2019) Copernicus Global Land Service: Land Cover 100m: Epoch 2015: Globe.

Cai, Y., Guan, K., Peng, J., Wang, S., Seifert, C., Wardlow, B., Li, Z. (2018) A high-performance and in-season classification system of field-level crop types using time-series Landsat data and a machine learning approach. Remote Sensing of Environment 210, 35-47.

Caird, M.A., Richards, J.H., Donovan, L.A. (2007) Nighttime Stomatal Conductance and Transpiration in C3 and C4 Plants. Plant Physiology 143, 4-10.

Campbell, J.B., Wynne, R.H. (2011) Introduction to remote sensing. Guilford Press.

Chen, H., Yu, C., Li, C., Xin, Q., Huang, X., Zhang, J., Yue, Y., Huang, G., Li, X., Wang, W. (2016) Modeling the impacts of water and fertilizer management on the ecosystem service of rice rotated cropping systems in China. Agriculture, Ecosystems & Environment 219, 49-57.

Chieppa, J., Brown, T., Giresi, P., Juenger, T.E., Resco de Dios, V., Tissue, D.T., Aspinwall, M.J. (2021) Climate and stomatal traits drive covariation in nighttime stomatal conductance and daytime gas exchange rates in a widespread C4 grass. New Phytologist 229, 2020-2034.

Chowdhury, F.I., Arteaga, C., Alam, M.S., Alam, I., Resco de Dios, V. (2021) Drivers of nocturnal stomatal conductance in C3 and C4 plants. Science of The Total Environment, 151952.

Ciresan, D.C., Meier, U., Masci, J., Gambardella, L.M., Schmidhuber, J., (2011) Flexible, high performance convolutional neural networks for image classification, Twenty-Second International Joint Conference on Artificial Intelligence.

Coleman, K., Muhammed, S.E., Milne, A.E., Todman, L.C., Dailey, A.G., Glendining, M.J., Whitmore, A.P. (2017) The landscape model: A model for exploring trade-offs between agricultural production and the environment. Science of The Total Environment 609, 1483-1499.

Collalti, A., Prentice, I.C. (2019) Is NPP proportional to GPP? Waring's hypothesis 20 years on. Tree Physiology 39, 1473-1483.

Daley, M.J., Phillips, N.G. (2006) Interspecific variation in nighttime transpiration and stomatal conductance in a mixed New England deciduous forest. Tree Physiology 26, 411-419.

Daloso, D.M., dos Anjos, L., Fernie, A.R. (2016) Roles of sucrose in guard cell regulation. New Phytologist 211, 809-818.

Darwin, F. (1898) IX. Observations on stomata. Philosophical Transactions of the Royal Society of London. Series B, Containing Papers of a Biological Character 190, 531-621.

de Weck, O. (2004) Multiobjective Optimization: History and Promise. Invited Keynote Paper, GL2-2, the Third China-Japan-Korea Joint Symposium on Optimization of Structural and Mechanical Systems 2.

Deng, F., Zhang, C., He, L., Liao, S., Li, Q., Li, B., Zhu, S., Gao, Y., Tao, Y., Zhou, W., Lei, X., Wang, L., Hu, J., Chen, Y., Ren, W. (2022) Delayed sowing date improves the quality of mechanically transplanted rice by optimizing temperature conditions during growth season. Field Crops Research 281, 108493.

Ding, Y., Wang, W., Zhuang, Q., Luo, Y. (2020) Adaptation of paddy rice in China to climate change: The effects of shifting sowing date on yield and irrigation water requirement. Agricultural Water Management 228, 105890.

Dodd, A., N., Salathia, N., Hall, A., Kévei, E., Tóth, R., Nagy, F., Hibberd Julian, M., Millar Andrew, J., Webb Alex, A.R. (2005) Plant Circadian Clocks Increase Photosynthesis, Growth, Survival, and Competitive Advantage. Science 309, 630-633.

Dodge, S., Karam, L., (2016) Understanding how image quality affects deep neural networks, 2016 Eighth International Conference on Quality of Multimedia Experience (QoMEX), pp. 1-6.

Dong, J., Xiao, X. (2016) Evolution of regional to global paddy rice mapping methods: A review. ISPRS Journal of Photogrammetry and Remote Sensing 119, 214-227.

Dong, J., Xiao, X., Menarguez, M.A., Zhang, G., Qin, Y., Thau, D., Biradar, C., Moore, B. (2016) Mapping paddy rice planting area in northeastern Asia with Landsat 8 images, phenology-based algorithm and Google Earth Engine. Remote Sensing of Environment 185, 142-154.

Drake, P.L., Froend, R.H., Franks, P.J. (2013) Smaller, faster stomata: scaling of stomatal size, rate of response, and stomatal conductance. Journal of Experimental Botany 64, 495-505.

Emmerich, M.T.M., Deutz, A.H. (2018) A tutorial on multiobjective optimization: fundamentals and evolutionary methods. Natural Computing 17, 585-609.

Epps, T.W., Singleton, K.J. (1986) An omnibus test for the two-sample problem using the empirical characteristic function. Journal of Statistical Computation and Simulation 26, 177-203.

Flagg, J.A. (2015) Aiming for zero: what makes nations adopt carbon neutral pledges? Environmental Sociology 1, 202-212.

Flütsch, S., Santelia, D. (2021) Mesophyll-derived sugars are positive regulators of light-driven stomatal opening. New Phytologist 230, 1754-1760.

Flütsch, S., Wang, Y., Takemiya, A., Vialet-Chabrand, S.R.M., Klejchová, M., Nigro, A., Hills, A., Lawson, T., Blatt, M.R., Santelia, D. (2020) Guard Cell Starch Degradation Yields Glucose for Rapid Stomatal Opening in Arabidopsis[CC-BY]. The Plant Cell 32, 2325-2344.

Foerster, S., Kaden, K., Foerster, M., Itzerott, S. (2012) Crop type mapping using spectral–temporal profiles and phenological information. Computers and Electronics in Agriculture 89, 30-40.

Foga, S., Scaramuzza, P.L., Guo, S., Zhu, Z., Dilley, R.D., Beckmann, T., Schmidt, G.L., Dwyer, J.L., Joseph Hughes, M., Laue, B. (2017) Cloud detection algorithm comparison and validation for operational Landsat data products. Remote Sensing of Environment 194, 379-390.

Foody, G., Mathur, A. (2004) Toward intelligent training of supervised image classifications: directing training data acquisition for SVM classification. Remote Sensing of Environment 93, 107-117.

Foody, G., Pal, M., Rocchini, D., Garzon-Lopez, X.C., Bastin, L. (2016) The Sensitivity of Mapping Methods to Reference Data Quality: Training Supervised Image Classifications with Imperfect Reference Data. ISPRS International Journal of Geo-Information 5.

Forster, M.A. (2014) How significant is nocturnal sap flow? Tree Physiology 34, 757-765.

Fowler, J., Waldner, F., Hochman, Z.J.I.J.o.A.E.O., Geoinformation (2020) All pixels are useful, but some are more useful: Efficient in situ data collection for crop-type mapping using sequential exploration methods. 91, 102114.

Frias-Martinez, V., Frias-Martinez, E. (2014) Spectral clustering for sensing urban land use using Twitter activity. Engineering Applications of Artificial Intelligence 35, 237-245.

Fricke, W. (2019) Night-Time Transpiration – Favouring Growth? Trends in Plant Science 24, 311-317.

Friedl, M.A., Sulla-Menashe, D., Tan, B., Schneider, A., Ramankutty, N., Sibley, A., Huang, X. (2010) MODIS Collection 5 global land cover: Algorithm refinements and characterization of new datasets. Remote Sensing of Environment 114, 168-182.

Fritz, S., McCallum, I., Schill, C., Perger, C., Grillmayer, R., Achard, F., Kraxner, F., Obersteiner, M. (2009) Geo-Wiki.Org: The Use of Crowdsourcing to Improve Global Land Cover. Remote Sensing 1.

Fritz, S., See, L., McCallum, I., You, L., Bun, A., Moltchanova, E., Duerauer, M., Albrecht, F., Schill, C., Perger, C., Havlik, P., Mosnier, A., Thornton, P., Wood-Sichra, U., Herrero, M., Becker-Reshef, I., Justice, C., Hansen, M., Gong, P., Abdel Aziz, S., Cipriani, A., Cumani, R., Cecchi, G., Conchedda, G., Ferreira, S., Gomez, A., Haffani, M., Kayitakire, F., Malanding, J., Mueller, R., Newby, T., Nonguierma, A., Olusegun, A., Ortner, S., Rajak, D.R., Rocha, J., Schepaschenko, D., Schepaschenko, M., Terekhov, A., Tiangwa, A., Vancutsem, C., Vintrou, E., Wenbin, W., van der Velde, M., Dunwoody, A., Kraxner, F., Obersteiner, M. (2015) Mapping global cropland and field size. Global change biology 21, 1980-1992.

Fuller, D.Q., Qin, L., Zheng, Y., Zhao, Z., Chen, X., Hosoya, L.A., Sun, G.-P. (2009) The Domestication Process and Domestication Rate in Rice: Spikelet Bases from the Lower Yangtze. Science 323, 1607.

Fumoto, T., Yanagihara, T., Saito, T., Yagi, K. (2010) Assessment of the methane mitigation potentials of alternative water regimes in rice fields using a process-based biogeochemistry model. Global change biology 16, 1847-1859.

Gansert, D. (2003) Xylem sap flow as a major pathway for oxygen supply to the sapwood of birch (Betula pubescens Ehr.). Plant, Cell & Environment 26, 1803-1814.

Gebru, T., Krause, J., Wang, Y., Chen, D., Deng, J., Aiden, E.L., Fei-Fei, L. (2017) Using deep learning and Google Street View to estimate the demographic makeup of neighborhoods across the United States. Proceedings of the National Academy of Sciences 114, 13108.

Gilhespy, S.L., Anthony, S., Cardenas, L., Chadwick, D., del Prado, A., Li, C., Misselbrook, T., Rees, R.M., Salas, W., Sanz-Cobena, A., Smith, P., Tilston, E.L., Topp, C.F.E., Vetter, S., Yeluripati, J.B. (2014) First 20 years of DNDC (DeNitrification DeComposition): Model evolution. Ecological Modelling 292, 51-62.

Giltrap, D.L., Li, C., Saggar, S. (2010) DNDC: A process-based model of greenhouse gas fluxes from agricultural soils. Agriculture, Ecosystems & Environment 136, 292-300.

Gong, P., Wang, J., Yu, L., Zhao, Y., Zhao, Y., Liang, L., Niu, Z., Huang, X., Fu, H., Liu, S., Li, C., Li, X., Fu, W., Liu, C., Xu, Y., Wang, X., Cheng, Q., Hu, L., Yao, W., Zhang, H., Zhu, P., Zhao, Z., Zhang, H., Zheng, Y., Ji, L., Zhang, Y., Chen, H., Yan, A., Guo, J., Yu, L., Wang, L., Liu, X., Shi, T., Zhu, M., Chen, Y., Yang, G., Tang, P., Xu, B., Giri, C., Clinton, N., Zhu, Z., Chen, J., Chen,

J. (2013) Finer resolution observation and monitoring of global land cover: first mapping results with Landsat TM and ETM+ data. International Journal of Remote Sensing 34, 2607-2654.

Gorelick, N., Hancher, M., Dixon, M., Ilyushchenko, S., Thau, D., Moore, R. (2017) Google Earth Engine: Planetary-scale geospatial analysis for everyone. Remote Sensing of Environment 202, 18-27.

Gosling, S.N., Arnell, N.W. (2016) A global assessment of the impact of climate change on water scarcity. Climatic Change 134, 371-385.

Graesser, J., Ramankutty, N. (2017) Detection of cropland field parcels from Landsat imagery. Remote Sensing of Environment 201, 165-180.

Groot, J.C.J., Oomen, G.J.M., Rossing, W.A.H. (2012) Multi-objective optimization and design of farming systems. Agricultural Systems 110, 63-77.

Gross, B.L., Zhao, Z. (2014) Archaeological and genetic insights into the origins of domesticated rice. Proceedings of the National Academy of Sciences 111, 6190.

Gutaker, R.M., Groen, S.C., Bellis, E.S., Choi, J.Y., Pires, I.S., Bocinsky, R.K., Slayton, E.R., Wilkins, O., Castillo, C.C., Negrão, S., Oliveira, M.M., Fuller, D.Q., Guedes, J.A.d.A., Lasky, J.R., Purugganan, M.D. (2020) Genomic history and ecology of the geographic spread of rice. Nature Plants 6, 492-502.

Haklay, M., Weber, P. (2008) Openstreetmap: User-generated street maps. IEEE Pervasive Computing 7, 12-18.

Haque, M.M., Kim, G.W., Kim, P.J., Kim, S.Y. (2016) Comparison of net global warming potential between continuous flooding and midseason drainage in monsoon region paddy during rice cropping. Field Crops Research 193, 133-142.

Heydari, S.S., Mountrakis, G. (2018) Effect of classifier selection, reference sample size, reference class distribution and scene heterogeneity in per-pixel classification accuracy using 26 Landsat sites. Remote Sensing of Environment 204, 648-658.

Hong, J.-K., et al. (2009) Standardization of KoFlux Eddy-Covariance Data Processing. Korean Journal of Agricultural and Forest Meteorology 11, 19-26.

Howard, D.M., Wylie, B.K. (2014) Annual Crop Type Classification of the US Great Plains for 2000 to 2011. Photogrammetric Engineering & Remote Sensing 80, 537-549.

Huang, C.-W., Domec, J.-C., Ward, E.J., Duman, T., Manoli, G., Parolari, A.J., Katul, G.G. (2017) The effect of plant water storage on water fluxes within the coupled soil–plant system. New Phytologist 213, 1093-1106.

Huang, M., Fang, S., Cao, F., Chen, J., Shan, S., Liu, Y., Lei, T., Tian, A., Tao, Z., Zou, Y. (2020) Early sowing increases grain yield of machine-transplanted late-season rice under single-seed sowing. Field Crops Research 253, 107832.

Huang, Y., Ryu, Y., Jiang, C., Kimm, H., Kim, S., Kang, M., Shim, K. (2018) BESS-Rice: A remote sensing derived and biophysical process-based rice productivity simulation model. Agricultural and Forest Meteorology 256-257, 253-269.

Hussain, S., Peng, S., Fahad, S., Khaliq, A., Huang, J., Cui, K., Nie, L. (2015) Rice management interventions to mitigate greenhouse gas emissions: a review. Environmental Science and Pollution Research 22, 3342-3360.

Hwang, Y., Ryu, Y., Huang, Y., Kim, J., Iwata, H., Kang, M. (2020) Comprehensive assessments of carbon dynamics in an intermittently-irrigated rice paddy. Agricultural and Forest Meteorology 285-286, 107933.

Ishfaq, M., Farooq, M., Zulfiqar, U., Hussain, S., Akbar, N., Nawaz, A., Anjum, S.A. (2020) Alternate wetting and drying: A water-saving and ecofriendly rice production system. Agricultural Water Management 241, 106363.

Islam, S.F.-u., van Groenigen, J.W., Jensen, L.S., Sander, B.O., de Neergaard, A. (2018) The effective mitigation of greenhouse gas emissions from rice paddies without compromising yield by early-season drainage. Science of The Total Environment 612, 1329-1339.

Jiang, R., Yang, J.Y., Drury, C.F., He, W., Smith, W.N., Grant, B.B., He, P., Zhou, W. (2021) Assessing the impacts of diversified crop rotation systems on yields and nitrous oxide emissions in Canada using the DNDC model. Science of The Total Environment 759, 143433.

Jiang, Y., Carrijo, D., Huang, S., Chen, J., Balaine, N., Zhang, W., van Groenigen, K.J., Linquist, B. (2019a) Water management to mitigate the global warming potential of rice systems: A global meta-analysis. Field Crops Research 234, 47-54.

Jiang, Y., Qian, H., Huang, S., Zhang, X., Wang, L., Zhang, L., Shen, M., Xiao, X., Chen, F., Zhang, H., Lu, C., Li, C., Zhang, J., Deng, A., van Groenigen, K.J., Zhang, W. (2019b) Acclimation of methane emissions from rice paddy fields to straw addition. Science Advances 5, eaau9038.

Jung, M., Reichstein, M., Ciais, P., Seneviratne, S.I., Sheffield, J., Goulden, M.L., Bonan, G., Cescatti, A., Chen, J., de Jeu, R., Dolman, A.J., Eugster, W., Gerten, D., Gianelle, D., Gobron, N., Heinke, J., Kimball, J., Law, B.E., Montagnani, L., Mu, Q., Mueller, B., Oleson, K., Papale, D., Richardson, A.D., Roupsard, O., Running, S., Tomelleri, E., Viovy, N., Weber, U., Williams, C., Wood, E., Zaehle, S., Zhang, K. (2010) Recent decline in the global land evapotranspiration trend due to limited moisture supply. Nature 467, 951-954.

Kang, M., et al. (2018) Changes and Improvements of the Standardized Eddy Covariance Data Processing in KoFlux. Korean Journal of Agricultural and Forest Meteorology 20, 5-17.

Katayanagi, N., Furukawa, Y., Fumoto, T., Hosen, Y. (2012) Validation of the DNDC-Rice model by using CH4 and N2O flux data from rice cultivated in pots under alternate wetting and drying irrigation management. Soil Science and Plant Nutrition 58, 360-372.

Kavzoglu, T. (2009) Increasing the accuracy of neural network classification using refined training data. Environmental Modelling & Software 24, 850-858.

Khatami, R., Mountrakis, G., Stehman, S.V. (2016) A meta-analysis of remote sensing research on supervised pixel-based land-cover image classification processes: General guidelines for practitioners and future research. Remote Sensing of Environment 177, 89-100.

Kim, G.-Y., Gutierrez, J., Jeong, H.-C., Lee, J.-S., Haque, M.D.M., Kim, P.J. (2014) Effect of intermittent drainage on methane and nitrous oxide emissions under different fertilization in a temperate paddy soil during rice cultivation. Journal of the Korean Society for Applied Biological Chemistry 57, 229-236.

King, L., Adusei, B., Stehman, S.V., Potapov, P.V., Song, X.-P., Krylov, A., Di Bella, C., Loveland, T.R., Johnson, D.M., Hansen, M.C. (2017) A multi-resolution approach to national-scale cultivated area estimation of soybean. Remote Sensing of Environment 195, 13-29.

Klefoth, R.R., Clough, T.J., Oenema, O., Van Groenigen, J.-W. (2014) Soil Bulk Density and Moisture Content Influence Relative Gas Diffusivity and the Reduction of Nitrogen-15 Nitrous Oxide. Vadose Zone Journal 13, vzj2014.2007.0089.

Kritee, K., Nair, D., Zavala-Araiza, D., Proville, J., Rudek, J., Adhya, T.K., Loecke, T., Esteves, T., Balireddygari, S., Dava, O., Ram, K., S. R, A., Madasamy, M., Dokka, R.V., Anandaraj, D., Athiyaman, D., Reddy, M., Ahuja, R., Hamburg, S.P. (2018) High nitrous oxide fluxes from rice indicate the need to manage water for both long- and short-term climate impacts. Proceedings of the National Academy of Sciences 115, 9720.

Krizhevsky, A., Sutskever, I., Hinton, G.E., (2012) Imagenet classification with deep convolutional neural networks, Advances in neural information processing systems, pp. 1097-1105.

Kropp, I., Nejadhashemi, A.P., Deb, K., Abouali, M., Roy, P.C., Adhikari, U., Hoogenboom, G. (2019) A multi-objective approach to water and nutrient efficiency for sustainable agricultural intensification. Agricultural Systems 173, 289-302.

Kudo, Y., Noborio, K., Shimoozono, N., Kurihara, R. (2014) The effective water management practice for mitigating greenhouse gas emissions and maintaining rice yield in central Japan. Agriculture, Ecosystems & Environment 186, 77-85.

Kun, J., Bingfang, W., Qiangzi, L. (2013) Crop classification using HJ satellite multispectral data in the North China Plain. Journal of Applied Remote Sensing 7, 1-13.

Kupper, P., Rohula, G., Saksing, L., Sellin, A., Lõhmus, K., Ostonen, I., Helmisaari, H.-S., Sõber, A. (2012) Does soil nutrient availability influence night-time water flux of aspen saplings? Environmental and Experimental Botany 82, 37-42.

LaHue, G.T., Chaney, R.L., Adviento-Borbe, M.A., Linquist, B.A. (2016) Alternate wetting and drying in high yielding direct-seeded rice systems accomplishes multiple environmental and agronomic objectives. Agriculture, Ecosystems & Environment 229, 30-39.

Lampayan, R.M., Rejesus, R.M., Singleton, G.R., Bouman, B.A.M. (2015) Adoption and economics of alternate wetting and drying water management for irrigated lowland rice. Field Crops Research 170, 95-108.

Leitgeb, H. (1886) Beiträge zur Physiologie der Spaltöffnungsapparate. Mittheilungen aus dem Botanischen Institute zu Graz, 123-184.

Lewis, J.D., Phillips, N.G., Logan, B.A., Hricko, C.R., Tissue, D.T. (2011) Leaf photosynthesis, respiration and stomatal conductance in six Eucalyptus species native to mesic and xeric environments growing in a common garden. Tree Physiology 31, 997-1006.

Li, C., Frolking, S., Frolking, T.A. (1992) A model of nitrous oxide evolution from soil driven by rainfall events: 1. Model structure and sensitivity. Journal of Geophysical Research: Atmospheres 97, 9759-9776.

Li, C., Frolking, S., Xiao, X., Moore Iii, B., Boles, S., Qiu, J., Huang, Y., Salas, W., Sass, R. (2005) Modeling impacts of farming management alternatives on CO2, CH4, and N2O emissions: A case study for water management of rice agriculture of China. Global Biogeochemical Cycles 19.

Li, C., Salas, W., DeAngelo, B., Rose, S. (2006a) Assessing Alternatives for Mitigating Net Greenhouse Gas Emissions and Increasing Yields from Rice Production in China Over the Next Twenty Years. Journal of Environmental Quality 35, 1554-1565.

Li, C., Zhou, A., Sang, T. (2006b) Rice Domestication by Reducing Shattering. Science 311, 1936.

Li, G., Chen, T., Xu, K., Liu, Y., Dai, Q., Huo, Z., Wei, H. (2021) Early sowing increases grain yield and cooking and eating quality of machine-transplanted rice in eastern China. Crop Science 61, 4383-4401.

Li, X., Zhang, C., Li, W. (2017) Building block level urban land-use information retrieval based on Google Street View images. GIScience & Remote Sensing 54, 819-835.

Liang, J., Gong, J., Sun, J., Zhou, J., Li, W., Li, Y., Liu, J., Shen, S. (2017) Automatic Sky View Factor Estimation from Street View Photographs—A Big Data Approach. Remote Sensing 9.

Liang, K., Zhong, X., Huang, N., Lampayan, R.M., Pan, J., Tian, K., Liu, Y. (2016) Grain yield, water productivity and CH4 emission of irrigated rice in response to water management in south China. Agricultural Water Management 163, 319-331.

Lillesand, T., Kiefer, R.W., Chipman, J. (2015) Remote sensing and image interpretation. John Wiley & Sons.

Lilley, J.M., Fukai, S. (1994) Effect of timing and severity of water deficit on four diverse rice cultivars III. Phenological development, crop growth and grain yield. Field Crops Research 37, 225-234.

Lima, V.F., Medeiros, D.B., Dos Anjos, L., Gago, J., Fernie, A.R., Daloso, D.M. (2018) Toward multifaceted roles of sucrose in the regulation of stomatal movement. Plant Signaling & Behavior 13, e1494468.

Linquist, B.A., Anders, M.M., Adviento-Borbe, M.A.A., Chaney, R.L., Nalley, L.L., da Rosa, E.F.F., van Kessel, C. (2015) Reducing greenhouse gas emissions, water use, and grain arsenic levels in rice systems. Global change biology 21, 407-417.

Liu, X., He, J., Yao, Y., Zhang, J., Liang, H., Wang, H., Hong, Y. (2017) Classifying urban land use by integrating remote sensing and social media data. International Journal of Geographical Information Science 31, 1675-1696.

Liu, X., Zhou, T., Liu, Y., Zhang, X., Li, L., Pan, G. (2019) Effect of mid-season drainage on CH4 and N2O emission and grain yield in rice ecosystem: A meta-analysis. Agricultural Water Management 213, 1028-1035.

Long, Y., Liu, L. (2017) How green are the streets? An analysis for central areas of Chinese cities using Tencent Street View. PLOS ONE 12, e0171110.

Ma, L., Li, M., Ma, X., Cheng, L., Du, P., Liu, Y. (2017) A review of supervised object-based land-cover image classification. ISPRS Journal of Photogrammetry and Remote Sensing 130, 277-293.

Massey, R., Sankey, T.T., Congalton, R.G., Yadav, K., Thenkabail, P.S., Ozdogan, M., Meador, A.J.S. (2017) MODIS phenology-derived, multi-year distribution of conterminous US crop types. Remote Sensing of Environment 198, 490-503.

McAusland, L., Smith, K.E., Williams, A., Molero, G., Murchie, E.H. (2021) Nocturnal stomatal conductance in wheat is growth-stage specific and shows genotypic variation. New Phytologist 232, 162-175.

Meijide, A., Gruening, C., Goded, I., Seufert, G., Cescatti, A. (2017) Water management reduces greenhouse gas emissions in a Mediterranean rice paddy field. Agriculture, Ecosystems & Environment 238, 168-178.

Mekonnen, M.M., Hoekstra, A.Y. (2016) Four billion people facing severe water scarcity. Science Advances 2, e1500323.

Minamikawa, K., Fumoto, T., Iizumi, T., Cha-un, N., Pimple, U., Nishimori, M., Ishigooka, Y., Kuwagata, T. (2016) Prediction of future methane emission from irrigated rice paddies in central Thailand under different water management practices. Science of The Total Environment 566-567, 641-651.

Munoz, J.E.V., Srivastava, S., Tuia, D., Falcao, A.X. (2020) OpenStreetMap: Challenges and Opportunities in Machine Learning and Remote Sensing. IEEE Geoscience and Remote Sensing Magazine, 0-0.

Naylor, R.L., Battisti, D.S., Vimont, D.J., Falcon, W.P., Burke, M.B. (2007) Assessing risks of climate variability and climate change for Indonesian rice agriculture. Proceedings of the National Academy of Sciences 104, 7752.

Neue, H.-U. (1993) Methane Emission from Rice Fields. BioScience 43, 466-474.

Ogle, K., Lucas, R.W., Bentley, L.P., Cable, J.M., Barron-Gafford, G.A., Griffith, A., Ignace, D., Jenerette, G.D., Tyler, A., Huxman, T.E., Loik, M.E., Smith, S.D., Tissue, D.T. (2012) Differential daytime and night-time stomatal behavior in plants from North American deserts. New Phytologist 194, 464-476.

Pal, M. (2005) Random forest classifier for remote sensing classification. International Journal of Remote Sensing 26, 217-222.

Palet, A., Ribas-Carbó, M., Argilés, J.M., Azcón-Bieto, J. (1991) Short-Term Effects of Carbon Dioxide on Carnation Callus Cell Respiration 1. Plant Physiology 96, 467-472.

Pandey, A., Dou, F., Morgan, C.L.S., Guo, J., Deng, J., Schwab, P. (2021) Modeling organically fertilized flooded rice systems and its long-term effects on grain yield and methane emissions. Science of The Total Environment 755, 142578.

Peng, S., Bouman, B., Visperas, R.M., Castañeda, A., Nie, L., Park, H.-K. (2006) Comparison between aerobic and flooded rice in the tropics: Agronomic performance in an eight-season experiment. Field Crops Research 96, 252-259.

Phalke, A.R., Özdoğan, M. (2018) Large area cropland extent mapping with Landsat data and a generalized classifier. Remote Sensing of Environment 219, 180-195.

Prina, M.G., Cozzini, M., Garegnani, G., Manzolini, G., Moser, D., Filippi Oberegger, U., Pernetti, R., Vaccaro, R., Sparber, W. (2018) Multi-objective optimization algorithm coupled to EnergyPLAN software: The EPLANopt model. Energy 149, 213-221.

Rainville, F.-M.D., Fortin, F.-A., Gardner, M.-A., Parizeau, M., Gagné, C., (2012) DEAP: a python framework for evolutionary algorithms, Proceedings of the 14th annual conference companion on Genetic and evolutionary computation. Association for Computing Machinery, Philadelphia, Pennsylvania, USA, pp. 85–92.

Rakower, L.H.J.B.J.I.l.L. (2011) Blurred line: zooming in on Google Street View and the global right to privacy. Brook. J. Int'l L 37, 317.

Ray, D.K., Mueller, N.D., West, P.C., Foley, J.A. (2013) Yield Trends Are Insufficient to Double Global Crop Production by 2050. PLOS ONE 8, e66428.

Rea, A.C. (2020) Sugar Is Sweeter: Plants Open Their “Mouths” for Glucose, Not Malate, in the Morning[OPEN]. The Plant Cell 32, 2071-2072.

Resco de Dios, V., Chowdhury, F.I., Granda, E., Yao, Y., Tissue, D.T. (2019) Assessing the potential functions of nocturnal stomatal conductance in C3 and C4 plants. 223, 1696-1706.

Resco de Dios, V., Loik, M.E., Smith, R., Aspinwall, M.J., Tissue, D.T. (2016) Genetic variation in circadian regulation of nocturnal stomatal conductance enhances carbon assimilation and growth. Plant, Cell & Environment 39, 3-11.

Resco de Dios, V., Loik, M.E., Smith, R.A., Tissue, D.T. (2018) Effects of a Heat Wave on Nocturnal Stomatal Conductance in Eucalyptus camaldulensis. Forests 9.

Ringland, J., Bohm, M., Baek, S.-R. (2019) Characterization of food cultivation along roadside transects with Google Street View imagery and deep learning. Computers and Electronics in Agriculture 158, 36-50.

Saini, H.S., Westgate, M.E., (1999) Reproductive Development in Grain Crops during Drought, in: Sparks, D.L. (Ed.), Advances in Agronomy. Academic Press, pp. 59-96.

Saunois, M., Stavert, A.R., Poulter, B., Bousquet, P., Canadell, J.G., Jackson, R.B., Raymond, P.A., Dlugokencky, E.J., Houweling, S., Patra, P.K., Ciais, P., Arora, V.K., Bastviken, D., Bergamaschi, P., Blake, D.R., Brailsford, G., Bruhwiler, L., Carlson, K.M., Carrol, M., Castaldi, S., Chandra, N., Crevoisier, C., Crill, P.M., Covey, K., Curry, C.L., Etiope, G., Frankenberg,

C., Gedney, N., Hegglin, M.I., Höglund-Isaksson, L., Hugelius, G., Ishizawa, M., Ito, A., Janssens-Maenhout, G., Jensen, K.M., Joos, F., Kleinen, T., Krummel, P.B., Langenfelds, R.L., Laruelle, G.G., Liu, L., Machida, T., Maksyutov, S., McDonald, K.C., McNorton, J., Miller, P.A., Melton, J.R., Morino, I., Müller, J., Murguia-Flores, F., Naik, V., Niwa, Y., Noce, S., O'Doherty, S., Parker, R.J., Peng, C., Peng, S., Peters, G.P., Prigent, C., Prinn, R., Ramonet, M., Regnier, P., Riley, W.J., Rosentreter, J.A., Segers, A., Simpson, I.J., Shi, H., Smith, S.J., Steele, L.P., Thornton, B.F., Tian, H., Tohjima, Y., Tubiello, F.N., Tsuruta, A., Viovy, N., Voulgarakis, A., Weber, T.S., van Weele, M., van der Werf, G.R., Weiss, R.F., Worthy, D., Wunch, D., Yin, Y., Yoshida, Y., Zhang, W., Zhang, Z., Zhao, Y., Zheng, B., Zhu, Q., Zhu, Q., Zhuang, Q. (2020) The Global Methane Budget 2000–2017. Earth Syst. Sci. Data 12, 1561-1623.

Schellenberg, H.C. (1896) Beiträge zur Kenntnis von Bau und Funktion der Spaltöffnungen. Botanische Zeitung 1, 169.

Schneider, C.A., Rasband, W.S., Eliceiri, K.W. (2012) NIH Image to ImageJ: 25 years of image analysis. Nature Methods 9, 671-675.

Shang, Z., Abdalla, M., Xia, L., Zhou, F., Sun, W., Smith, P. (2021) Can cropland management practices lower net greenhouse emissions without compromising yield? Global change biology 27, 4657-4670.

Sharif, R.A., Azizpour, H., Sullivan, J., Carlsson, S., (2014) CNN features off-the-shelf: an astounding baseline for recognition, Proceedings of the IEEE conference on computer vision and pattern recognition workshops, pp. 806-813.

Sharkey, T.D. (2016) What gas exchange data can tell us about photosynthesis. Plant, Cell & Environment 39, 1161-1163.

Skakun, S., Franch, B., Vermote, E., Roger, J.-C., Becker-Reshef, I., Justice, C., Kussul, N. (2017) Early season large-area winter crop mapping using MODIS NDVI data, growing degree days information and a Gaussian mixture model. Remote Sensing of Environment 195, 244-258.

Snyder, K.A., Richards, J.H., Donovan, L.A. (2003) Night-time conductance in C3 and C4 species: do plants lose water at night? Journal of Experimental Botany 54, 861-865.

Srivastava, S., Vargas-Muñoz, J.E., Tuia, D. (2019) Understanding urban landuse from the above and ground perspectives: A deep learning, multimodal solution. Remote Sensing of Environment 228, 129-143.

Srivastava, S., Vargas Muñoz, J.E., Lobry, S., Tuia, D. (2020) Fine-grained landuse characterization using ground-based pictures: a deep learning solution based on globally available data. International Journal of Geographical Information Science 34, 1117-1136.

Stahl, E., (1897) Über den Pflanzenschlaf und verwandte Erscheinungen. A. Förstner.

Stinziano, J.R., McDermitt, D.K., Lynch, D.J., Saathoff, A.J., Morgan, P.B., Hanson, D.T. (2019) The rapid A/Ci response: a guide to best practices. New Phytologist 221, 625-627.

Stinziano, J.R., Morgan, P.B., Lynch, D.J., Saathoff, A.J., McDermitt, D.K., Hanson, D.T. (2017) The rapid A–Ci response: photosynthesis in the phenomic era. Plant, Cell & Environment 40, 1256-1262.

Stuerz, S., Asch, F. (2021) Responses of Rice Growth to Day and Night Temperature and Relative Air Humidity—Leaf Elongation and Assimilation. Plants 10.

Sun, L., Lu, Y., Yu, F., Kronzucker, H.J., Shi, W. (2016) Biological nitrification inhibition by rice root exudates and its relationship with nitrogen-use efficiency. New Phytologist 212, 646-656.

Tian, Z., Fan, Y., Wang, K., Zhong, H., Sun, L., Fan, D., Tubiello, F.N., Liu, J. (2021) Searching for "Win-Win" solutions for food-water-GHG emissions tradeoffs across irrigation regimes of paddy rice in China. Resources, Conservation and Recycling 166, 105360.

Tilman, D., Balzer, C., Hill, J., Befort, B.L. (2011) Global food demand and the sustainable intensification of agriculture. Proceedings of the National Academy of Sciences 108, 20260.

Torbick, N., Huang, X., Ziniti, B., Johnson, D., Masek, J., Reba, M. (2018) Fusion of Moderate Resolution Earth Observations for Operational Crop Type Mapping. Remote Sensing 10.

Towprayoon, S., Smakgahn, K., Poonkaew, S. (2005) Mitigation of methane and nitrous oxide emissions from drained irrigated rice fields. Chemosphere 59, 1547-1556.

Tu, D., Jiang, Y., Liu, M., Zhang, L., Chen, L., Cai, M., Ling, X., Zhan, M., Li, C., Wang, J., Cao, C. (2020) Improvement and stabilization of rice production by delaying sowing date in

irrigated rice system in central China. Journal of the Science of Food and Agriculture 100, 595-606.

Tucker, C.J. (1979) Red and photographic infrared linear combinations for monitoring vegetation. Remote Sensing of Environment 8, 127-150.

Van Niel, T.G., McVicar, T.R., Datt, B. (2005) On the relationship between training sample size and data dimensionality: Monte Carlo analysis of broadband multi-temporal classification. Remote Sensing of Environment 98, 468-480.

Van Oijen, M., Schapendonk, A., Höglind, M. (2010) On the relative magnitudes of photosynthesis, respiration, growth and carbon storage in vegetation. Annals of Botany 105, 793-797.

Waldner, F., Bellemans, N., Hochman, Z., Newby, T., de Abelleyra, D., Verón, S.R., Bartalev, S., Lavreniuk, M., Kussul, N., Le Maire, G. (2019) Roadside collection of training data for cropland mapping is viable when environmental and management gradients are surveyed. International Journal of Applied Earth Observation and Geoinformation 80, 82-93.

Wang, S., Azzari, G., Lobell, D.B. (2019) Crop type mapping without field-level labels: Random forest transfer and unsupervised clustering techniques. Remote Sensing of Environment 222, 303-317.

Wang, S., Di Tommaso, S., Deines, J.M., Lobell, D.B. (2020a) Mapping twenty years of corn and soybean across the US Midwest using the Landsat archive. Scientific Data 7, 307.

Wang, S., Di Tommaso, S., Faulkner, J., Friedel, T., Kennepohl, A., Strey, R., Lobell, D.B. (2020b) Mapping Crop Types in Southeast India with Smartphone Crowdsourcing and Deep Learning. Remote Sensing 12.

Wang, Y., Anderegg, W.R.L., Venturas, M.D., Trugman, A.T., Yu, K., Frankenberg, C. (2021) Optimization theory explains nighttime stomatal responses. New Phytologist 230, 1550-1561.

Wardlow, B.D., Egbert, S.L. (2008) Large-area crop mapping using time-series MODIS 250 m NDVI data: An assessment for the U.S. Central Great Plains. Remote Sensing of Environment 112, 1096-1116.

Wardlow, B.D., Egbert, S.L., Kastens, J.H. (2007) Analysis of time-series MODIS 250 m vegetation index data for crop classification in the U.S. Central Great Plains. Remote Sensing of Environment 108, 290-310.

Wenting, W., Wenpei, C., Ke, X., Hui, G., Haiyan, W., Hongcheng, Z. (2021) Effects of Early- and Late-Sowing on Starch Accumulation and Associated Enzyme Activities During Grain Filling Stage in Rice. Rice Science 28, 191-199.

Wood, S.A., Guerry, A.D., Silver, J.M., Lacayo, M. (2013) Using social media to quantify nature-based tourism and recreation. Scientific Reports 3, 2976.

Woodward, F.I. (1987) Climate and plant distribution. Cambridge University Press.

Xiao, X., Dorovskoy, P., Biradar, C., Bridge, E. (2011) A library of georeferenced photos from the field. Eos, Transactions American Geophysical Union 92, 453-454.

You, L., Wood, S., Wood-Sichra, U., Wu, W. (2014) Generating global crop distribution maps: From census to grid. Agricultural Systems 127, 53-60.

Yu, K., Goldsmith, G.R., Wang, Y., Anderegg, W.R.L. (2019) Phylogenetic and biogeographic controls of plant nighttime stomatal conductance. New Phytologist 222, 1778-1788.

Zeppel, M.J.B., Lewis, J.D., Phillips, N.G., Tissue, D.T. (2014) Consequences of nocturnal water loss: a synthesis of regulating factors and implications for capacitance, embolism and use in models. Tree Physiology 34, 1047-1055.

Zhang, F., Wu, L., Zhu, D., Liu, Y. (2019a) Social sensing from street-level imagery: A case study in learning spatio-temporal urban mobility patterns. ISPRS Journal of Photogrammetry and Remote Sensing 153, 48-58.

Zhang, J., Zhang, S., Cheng, M., Jiang, H., Zhang, X., Peng, C., Lu, X., Zhang, M., Jin, J. (2018) Effect of Drought on Agronomic Traits of Rice and Wheat: A Meta-Analysis. International Journal of Environmental Research and Public Health 15.

Zhang, Q., Yang, Y., Peng, S., Li, Y. (2021) Nighttime transpirational cooling enabled by circadian regulation of stomatal conductance is related to stomatal anatomy and leaf morphology in rice. Planta 254, 12.

Zhang, W., Li, W., Zhang, C., Hanink, D.M., Li, X., Wang, W. (2017) Parcel-based urban land use classification in megacity using airborne LiDAR, high resolution orthoimagery, and Google Street View. Computers, Environment and Urban Systems 64, 215-228.

Zhang, W., Liu, C., Zheng, X., Wang, K., Cui, F., Wang, R., Li, S., Yao, Z., Zhu, J. (2019b) Using a modified DNDC biogeochemical model to optimize field management of a multi-crop (cotton, wheat, and maize) system: a site-scale case study in northern China. Biogeosciences 16, 2905-2922.

Zhao, C., Liu, B., Piao, S., Wang, X., Lobell, D.B., Huang, Y., Huang, M., Yao, Y., Bassu, S., Ciais, P., Durand, J.-L., Elliott, J., Ewert, F., Janssens, I.A., Li, T., Lin, E., Liu, Q., Martre, P., Müller, C., Peng, S., Peñuelas, J., Ruane, A.C., Wallach, D., Wang, T., Wu, D., Liu, Z., Zhu, Y., Zhu, Z., Asseng, S. (2017) Temperature increase reduces global yields of major crops in four independent estimates. Proceedings of the National Academy of Sciences 114, 9326.

Zhao, Z., Cao, L., Deng, J., Sha, Z., Chu, C., Zhou, D., Wu, S., Lv, W. (2020) Modeling CH4 and N2O emission patterns and mitigation potential from paddy fields in Shanghai, China with the DNDC model. Agricultural Systems 178, 102743.

Zhong, L., Hu, L., Yu, L., Gong, P., Biging, G.S. (2016a) Automated mapping of soybean and corn using phenology. ISPRS Journal of Photogrammetry and Remote Sensing 119, 151-164.

Zhong, L., Hu, L., Zhou, H. (2019a) Deep learning based multi-temporal crop classification. Remote Sensing of Environment 221, 430-443.

Zhong, L., Hu, L., Zhou, H., Tao, X. (2019b) Deep learning based winter wheat mapping using statistical data as ground references in Kansas and northern Texas, US. Remote Sensing of Environment 233, 111411.

Zhong, Y., Wang, X., Yang, J., Zhao, X., Ye, X. (2016b) Exploring a suitable nitrogen fertilizer rate to reduce greenhouse gas emissions and ensure rice yields in paddy fields. Science of The Total Environment 565, 420-426.

Zong, Y., Chen, Z., Innes, J.B., Chen, C., Wang, Z., Wang, H. (2007) Fire and flood management of coastal swamp enabled first rice paddy cultivation in east China. Nature 449, 459-462.

Chapter V. Conclusions

Nocturnal stomatal conductance (g_{sn}) in rice plants accounts for a non-negligible portion of the daytime stomatal conductance (g_{sd}) and surprisingly showed no strong response to abiotic stress. In chapter II, we identify the coordinated leaf traits ($Rn - g_{sn} - g_{sd} - A$) as the primary mechanism of g_{sn} in rice plants. We found g_{sn} is acting as a "bridge" to link the prior Rn and photosynthesis next dawn. The proposed coordination hypothesis explains the considerable observed variation of g_{sn}, early-morning g_{sd}, early-morning *A*, and leaf cooling results, which could not fully be explained with the circadian regulation. We demonstrated the coordinated leaf traits hold firm under drought, nutrient scarcity, and the combination of these two abiotic stressors. Circadian priming, nutrient uptake, water conservation, and excessive CO_2 flushing are only the secondary explanations of g_{sn} in rice as we did not find clear evidence to deny these hypotheses as well.

By proposing a simple heuristic and holistic method, chapter III optimized rice farming beyond previous most emphasized irrigation regimes, while also exploring niches from other pivotal farm managements regarding sowing window, fertilization rate, tillage depth, and their interactions. Specifically, we validated and coupled the DNDC model with the NSGA-III algorithm to maximize crop yield, minimize water consumption, and minimize N_2O, CH_4 emissions. By approaching four objectives on its paired Pareto fronts, we quantified the gaps in current farming practices in South Korea to achieve optimal solutions. Our results indicate that the optimized holistic farm management would maintain or even increase current crop yield while reducing more than 50% irrigation demand and GHGs emissions. Furthermore, this new method also tackled the dilemma of simultaneously reducing CH_4 and N_2O emissions. Our study clearly shows that the present rice farming system in the study site not only has not achieved its potential yield level but also comes at a great environmental cost to water resources and GHGs emissions. More importantly, this simple method could further be applied to evaluate the environmental sustainability of a rice farming system under various climate and local conditions and to guide policymakers and farming practices with detailed solutions.

Ground reference data are essential for supervised crop type mapping. In chapter IV, we developed a novel alternative method for nearly automated ground truthing by integrating a CNN model and GSV images. We demonstrated the general applicability of this new method by evaluation with CDL products at two large distinct farming areas in the Central Valley and Illinois from 2011–2019 and the additional test case in South Korea. The CNN model revealed considerable capability for GSV image classification, with an accuracy of 92% for the Central Valley, and 97% for Illinois. The ground reference points derived from GSV images taken along roads are representative and suitable for conducting state- and country- level crop type classification, with R^2 of 0.44-0.99 for the Central Valley, 0.81-0.98 for Illinois, and 0.91 for South Korea. The strong performance of the CNN model indicates upscaling potential for coherent ground truthing when GSV images are available. We have demonstrated that GSV is a useful data source which has been overlooked in generating massive ground truth data and making crop type maps. However, GSV is not a universal solution, we strongly encourage future studies to explore vast amounts of geo-tagged social media data in tandem with GSV if available. Furthermore, we would like to highlight that the coverage and data size in GSV and relevant street view images will expand and grow rapidly.

Supplementary Information Chapter II

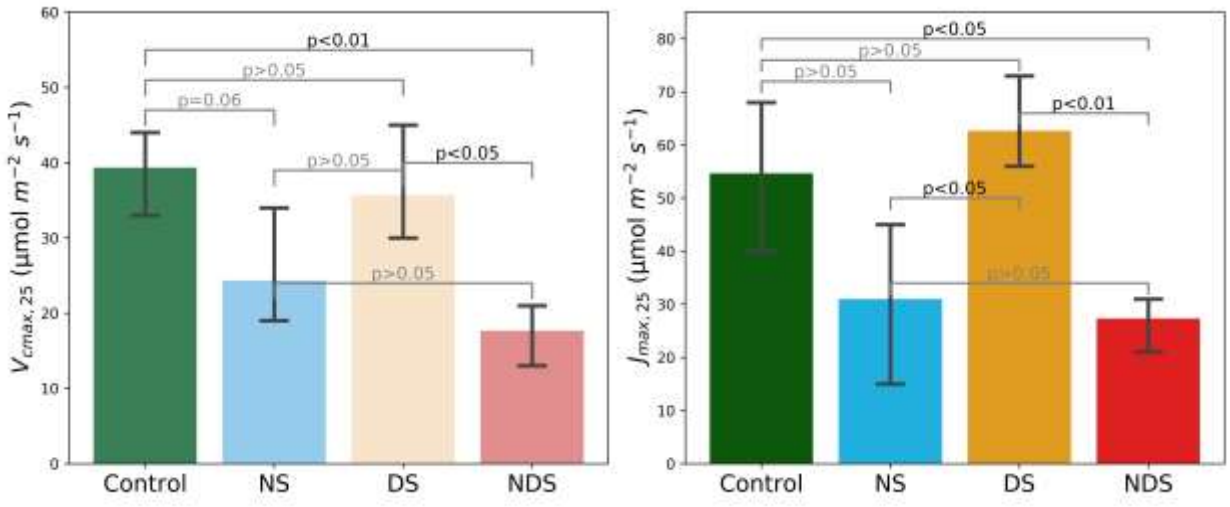

Fig. S1 Variation (n = 3) of the maximum velocity of carboxylation ($V_{c,max}$) and maximum electron transport rate (J_{max}) normalized at 25°C across treatments on DOY 224 and 225.

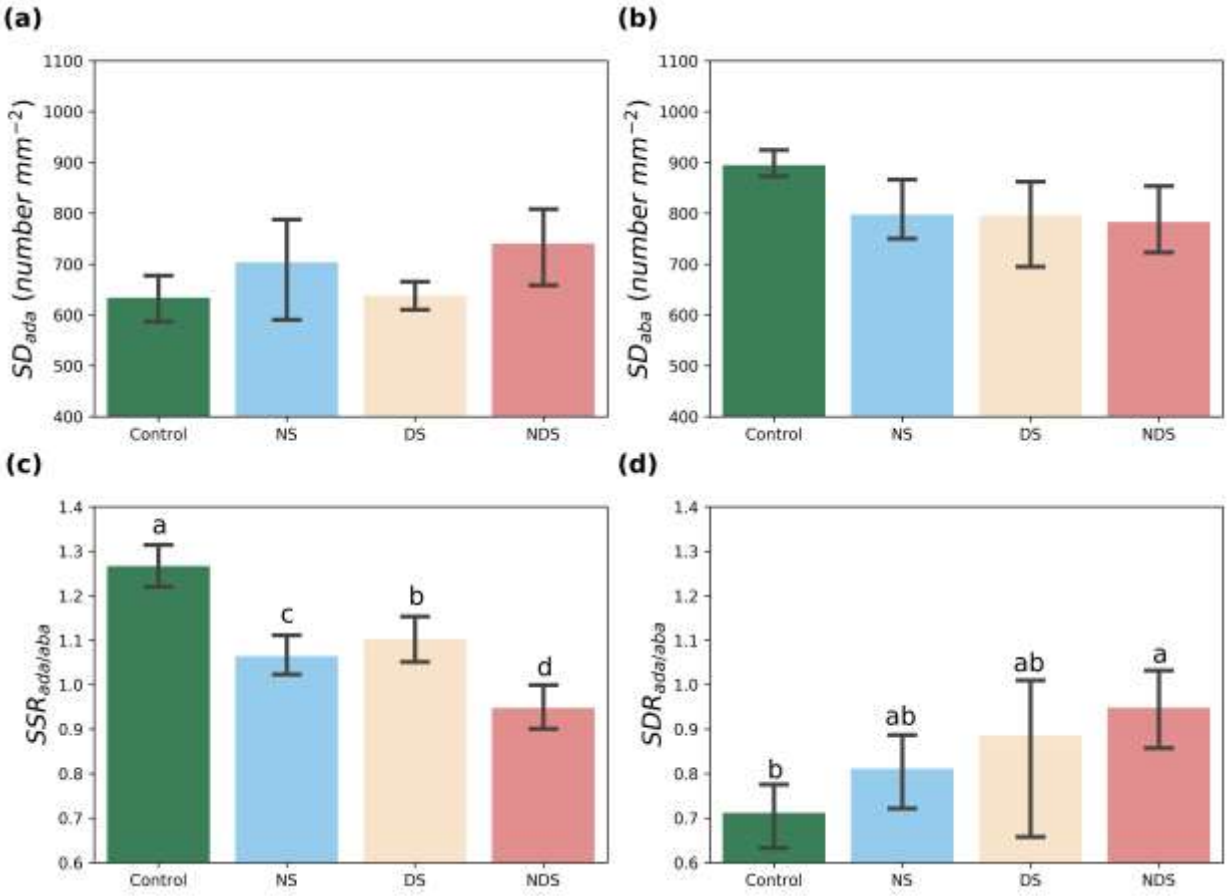

Fig. S2 Stomatal density (SD) on the adaxial and abaxial surfaces (a & b), stomatal size ratio (SSRada/aba) (c), and stomatal density ratio (SDRada/aba) across treatments (d). The error bars indicate one standard deviation of uncertainty. The lowercase letters in each panel indicate the significance level of differences between mean values and data distributions. Nonsignificant results are unlabeled.

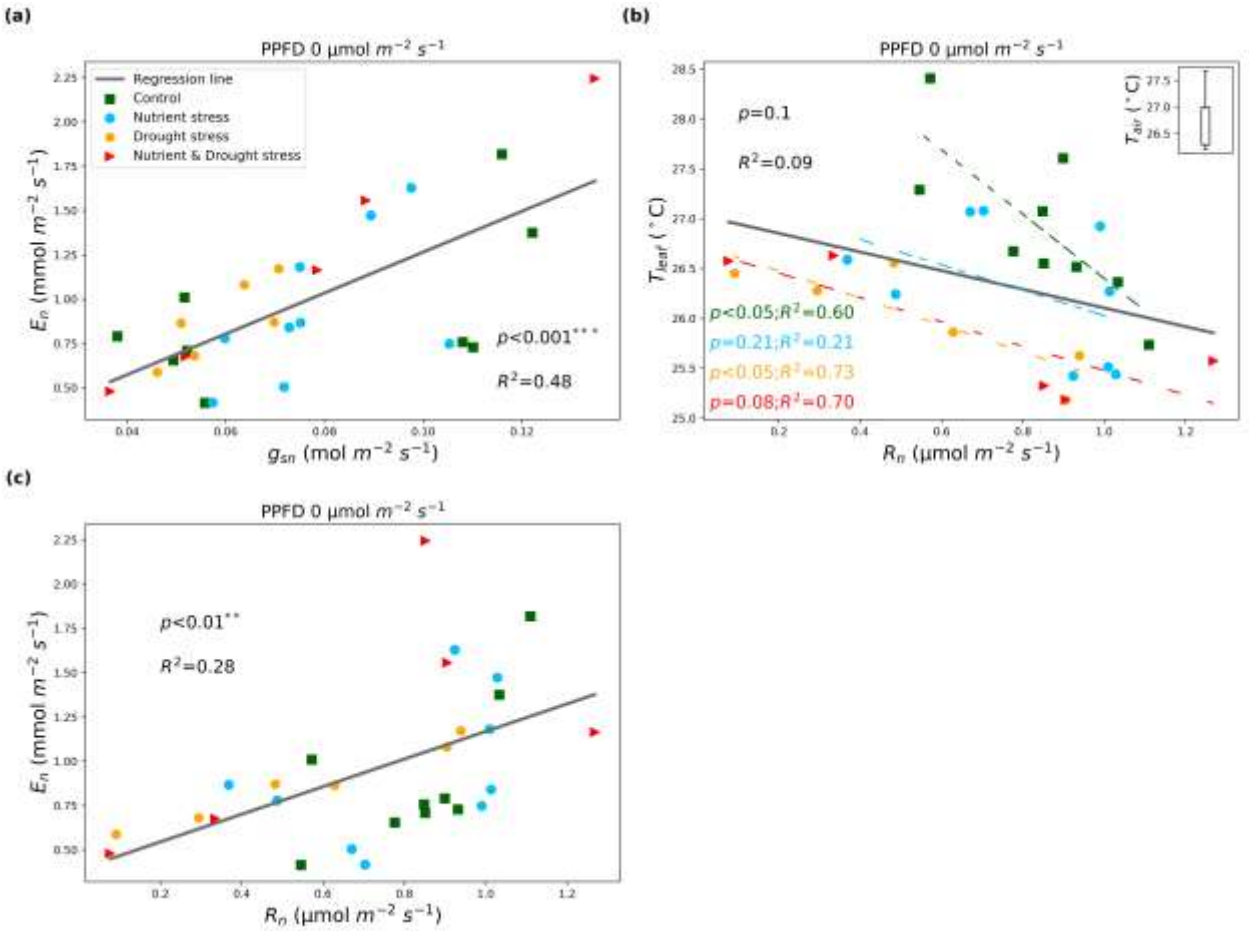

Fig. S3 Correlations between nocturnal stomatal conductance (g_{sn}) and nocturnal transpiration (E_n) (a), nocturnal respiration (R_n) and leaf temperature (T_{leaf}) (b), and R_n and E_n (c). The grey regression line denotes the slope for all data points, while the dotted regression lines denote the slopes for individual treatments.

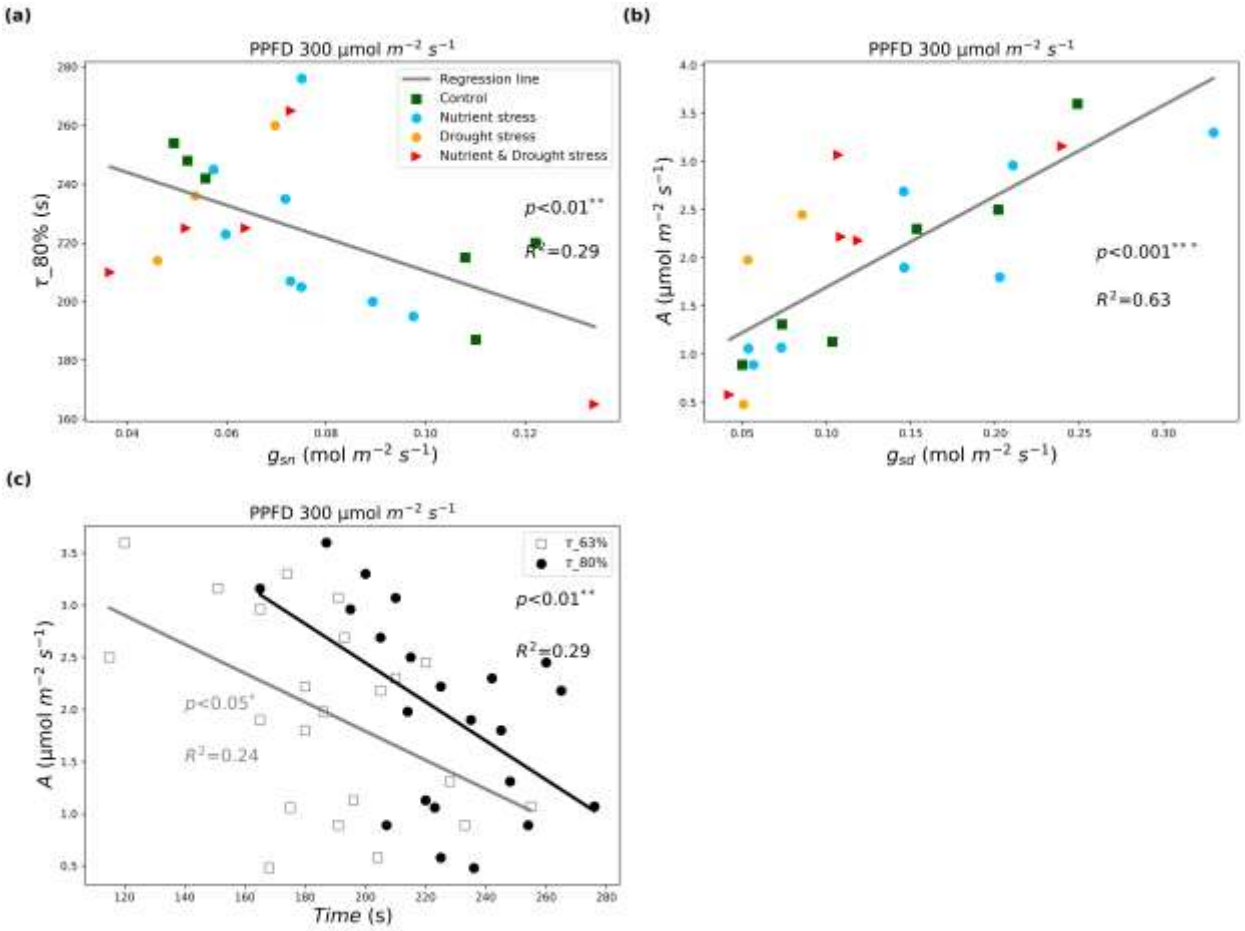

Fig. S4 Correlations between nocturnal stomatal conductance (g_{sn}) and time to reach 80% of the early morning (PPFD = 300 µmol m^{-2} s^{-1}) maximum *A* within a 5-min period (a), early morning non-steady-state maximum stomatal conductance (g_{sd}) and the maximum assimilation rate (*A*) within a 5-min period (b), and the stomatal response time and early morning maximum *A* (c).

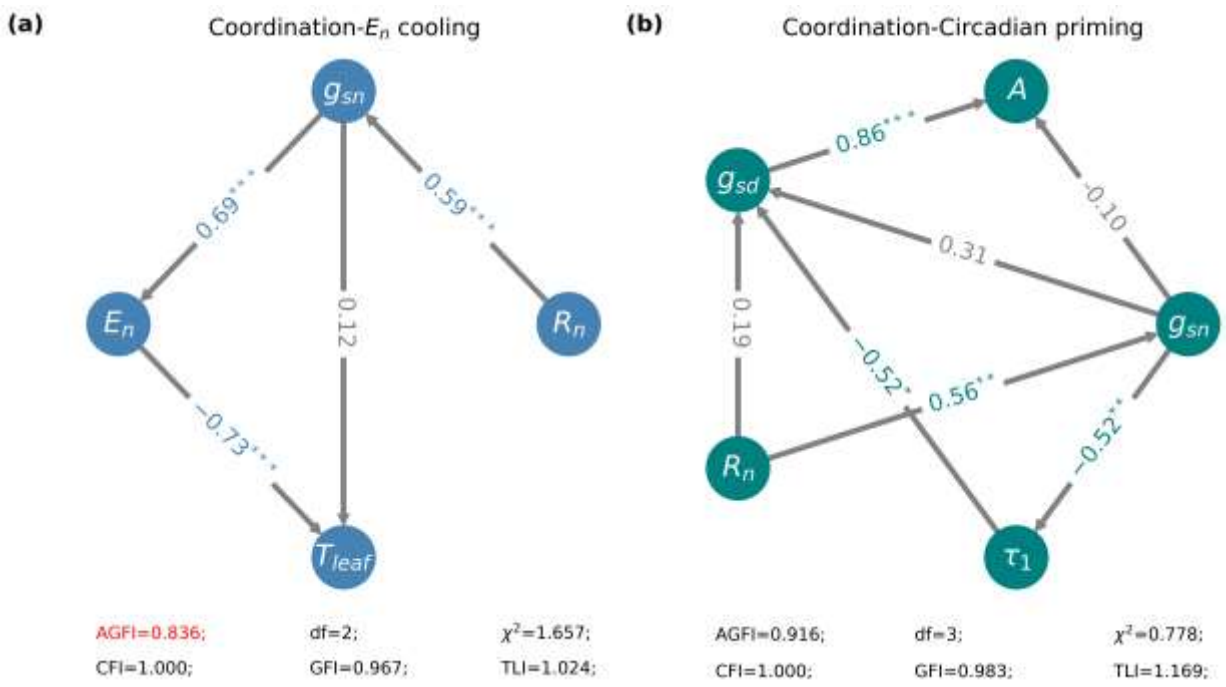

Fig. S5 Additional path analyses with higher degrees of freedom (df) for the coordination-E_n cooling hypothesis (n = 29) (a), and for the coordination-circadian priming hypothesis (early morning and non-steady-state conditions) (n = 22), where τ_1 denotes the time to reach 63% of the maximum early morning A within a 5-min period (b). The arrows denote the speculative interactions between two leaf traits. Path coefficients were normalized from −1 to 1 and are shown in between traits; significant relationships (*P < 0.05, **P < 0.01, ***P < 0.001) are indicated by blue or green numbers. GFI, goodness of fit; AGFI, adjusted goodness of fit; CFI, comparative fit index; TLI, Tucker-Lewis index. Red text indicates poor model fit indices. Ranges of good model fit indices were defined as follows: AGFI > 0.90, CFI > 0.90, GFI > 0.95, and TLI > 0.97.

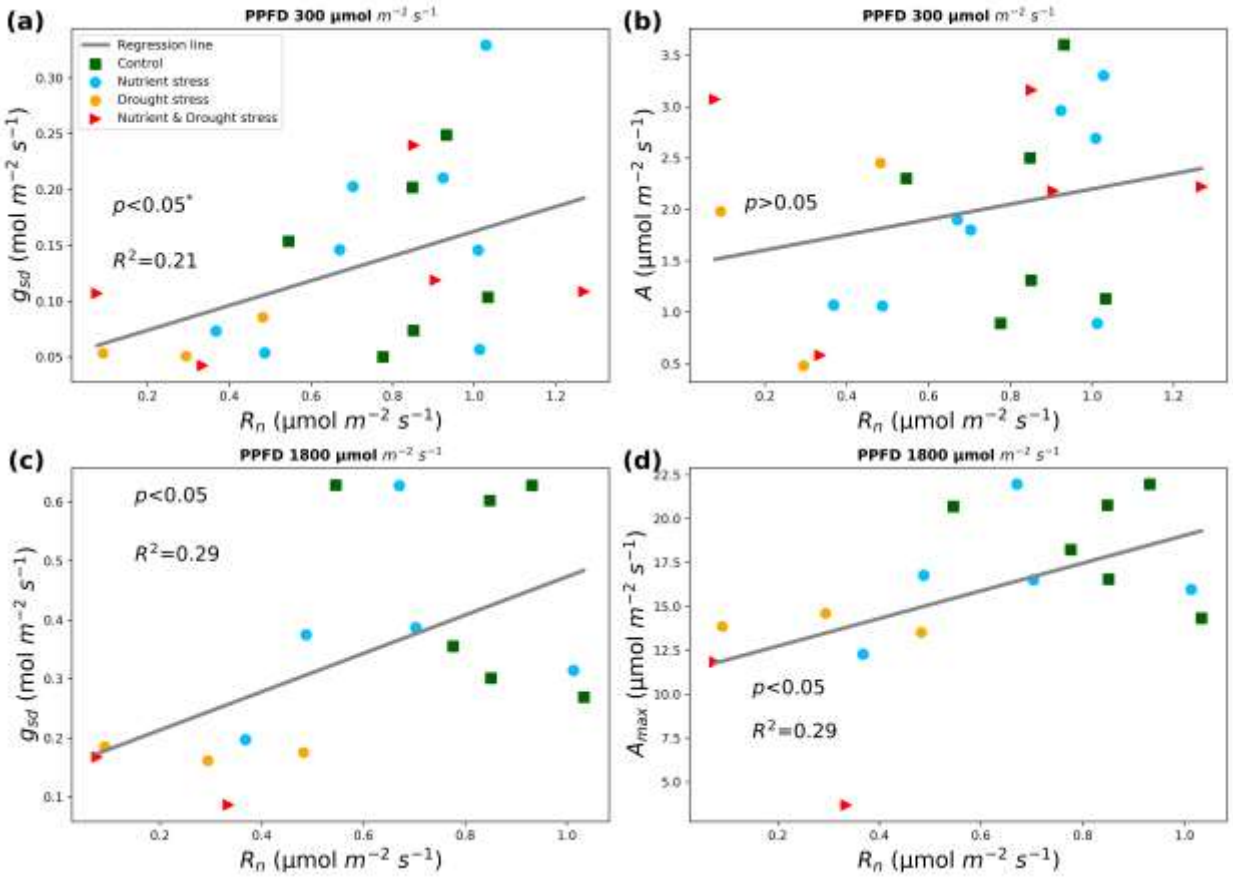

Fig. S6 Correlation between nocturnal respiration (R_n) and early morning (300 µmol m^{-2} s^{-1} PPFD) non-steady-state stomatal conductance (g_{sd}) (a), assimilation rate (b), correlation between R_n and steady-state light-saturated (1,800 µmol m^{-2} s^{-1} PPFD) stomatal conductance (g_{sd}) (c), and assimilation rate (d).

Supplementary Information Chapter III

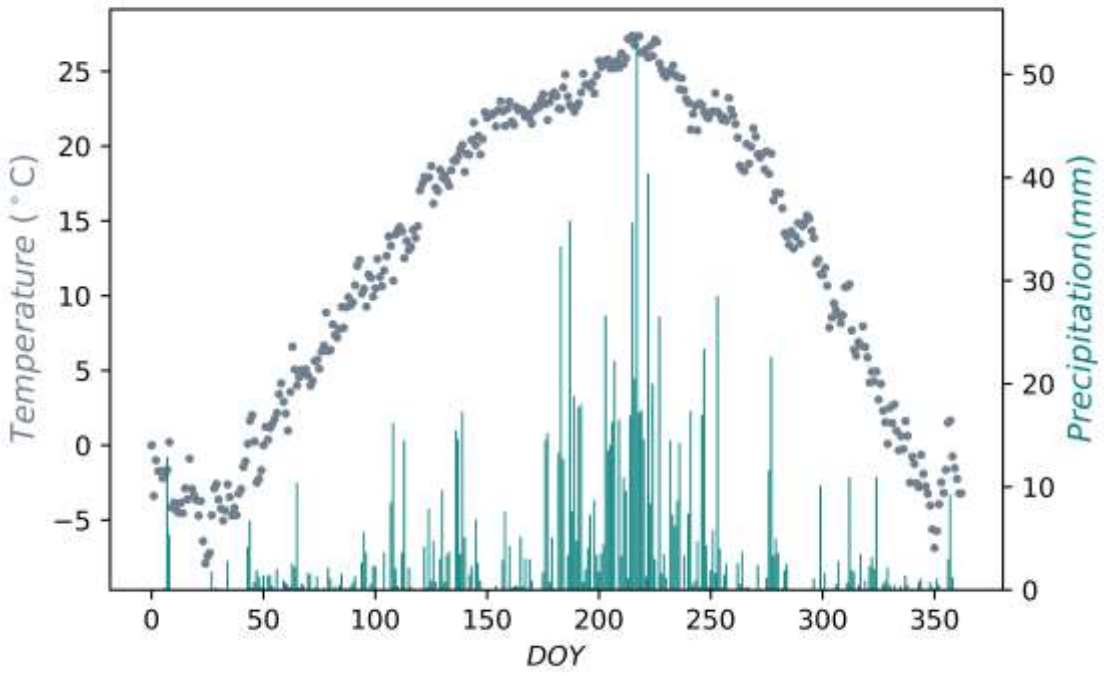

Supplementary Fig. 1 Mean daily climate conditions (surface temperature & precipitation) during 2016-2020 in the study area.

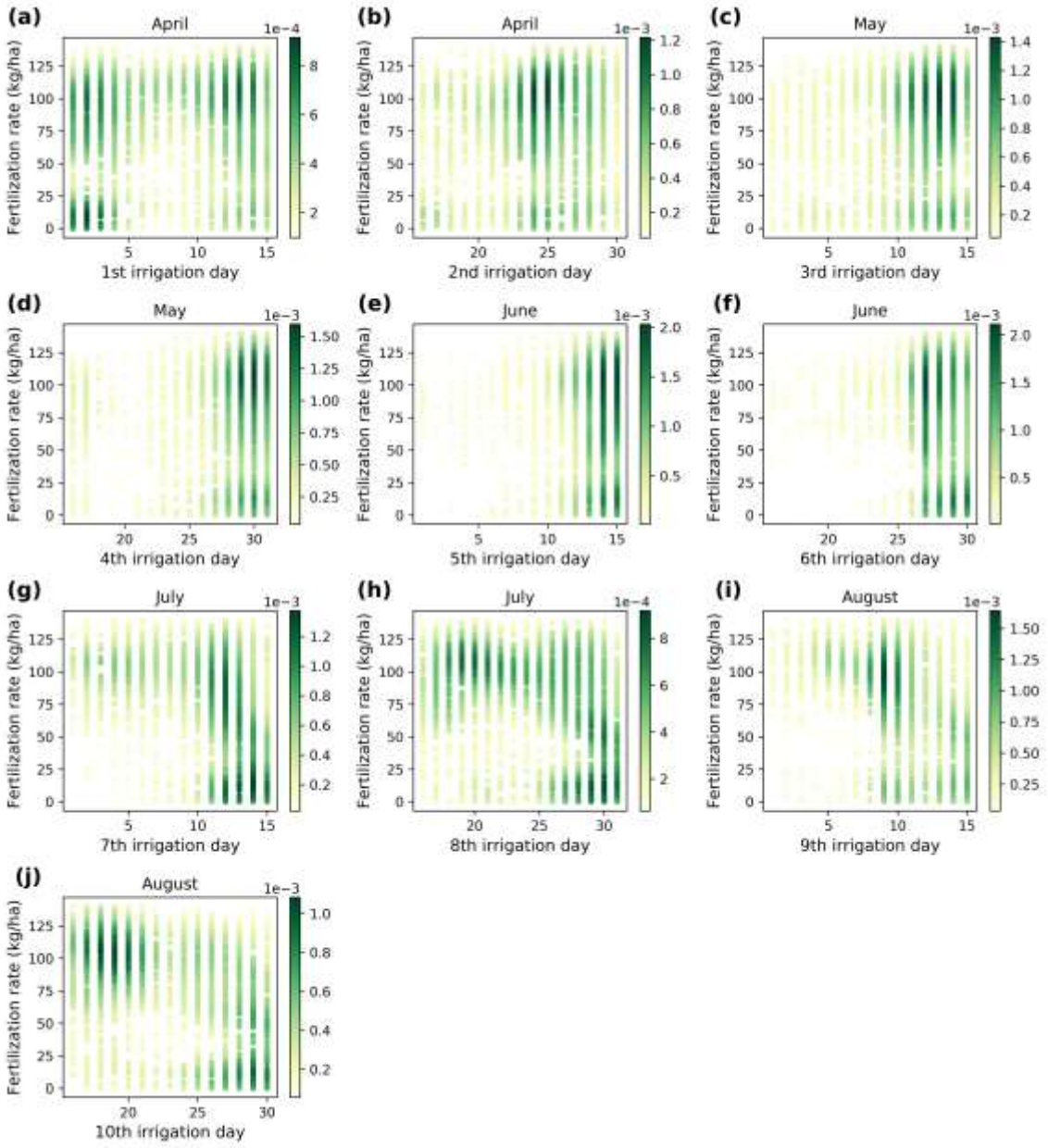

Supplementary Fig. 2 Probability density distribution of the interaction between the non-dominated fertilization rate and non-dominated half-monthly irrigation schedule.

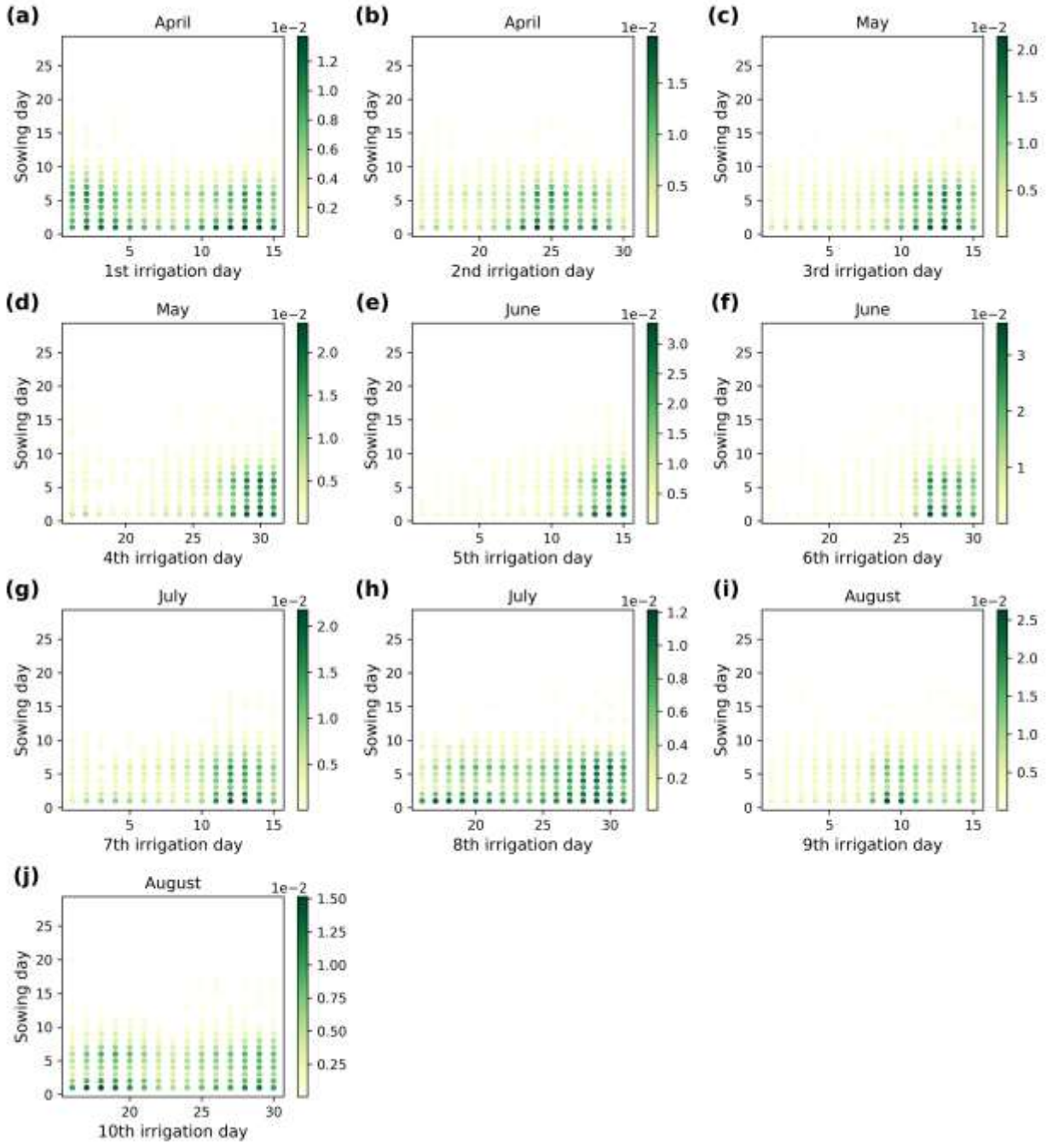

Supplementary Fig. 3 Probability density distribution of the interaction between the non-dominated sowing day and non-dominated monthly irrigation schedule.

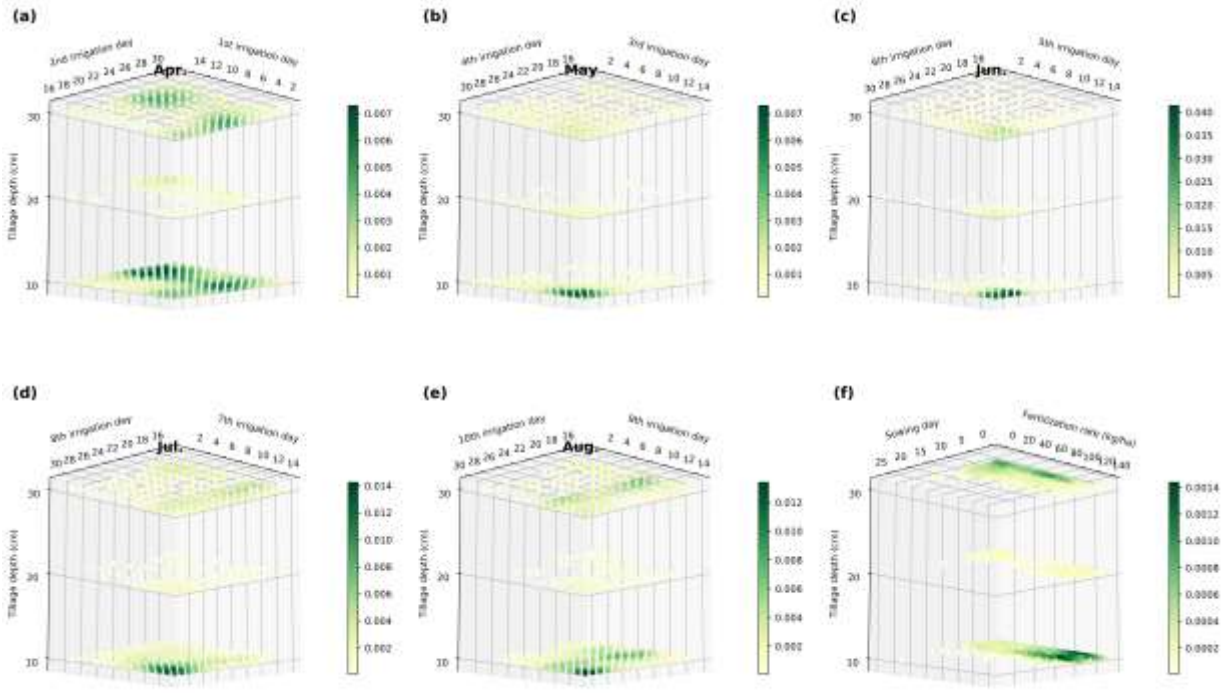

Supplementary Fig. 4 (a-e) Probability density distribution of the interaction between the non-dominated tillage depth and non-dominated monthly irrigation schedule. (f) Probability density distribution of the interaction between the non-dominated tillage depth, sowing day, and fertilization rate.

Supplementary Information Chapter IV

Method

To demonstrate the applicational value of the proposed method in other countries, we further apply the proposed method in South Korea and map the rice paddy for the year 2014-2018. To transfer the CNN model into a new study area, we use the rice paddy images prepared at California with only limited additional images in South Korea. Due to the absence of CDL alike products, we evaluate the mapping results with Dong et al. (2016) rice paddy map for the year 2014.

Results

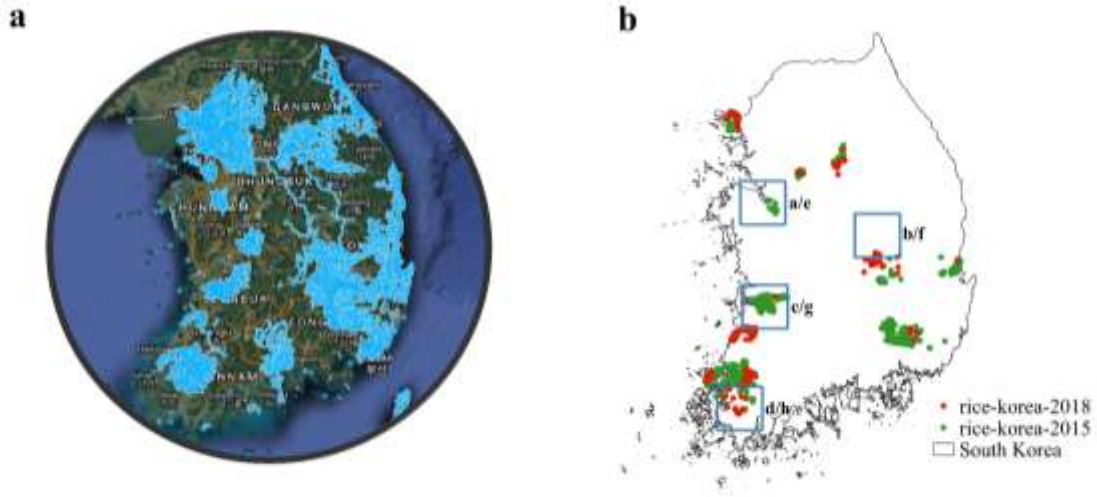

Supplementary Fig. 1 Availability and spatial distribution of GSV images across South Korea (a), produced rice paddy reference points (b) which include 1219 for 2015 (green) and 269 for 2018 (red). The blue squares indicate the location of regional-scale rice paddy mapping comparison against a reference rice paddy map (Dong et al., 2016) which appears at Supplementary Fig. 3.

Supplementary Table 1. Performance of the CNN model for GSV image classification in South Korea, displayed as a confusion matrix. PA: producer accuracy; UA: user accuracy; OA: overall accuracy.

South Korea	*Rice paddy*	*Other*	*UA*
Rice paddy	210	5	98%
Other	27	177	87%
PA	89%	97%	OA = 92%

Supplementary Table 2. Performance of the RF model for land cover classification in South Korea indicated as a confusion matrix. PA: producer accuracy; UA: user accuracy; OA: overall accuracy

South Korea	*Rice paddy*	*Other*	*UA*
Rice paddy	279	17	94%
Other	27	263	91%
PA	91%	94%	OA =92 %

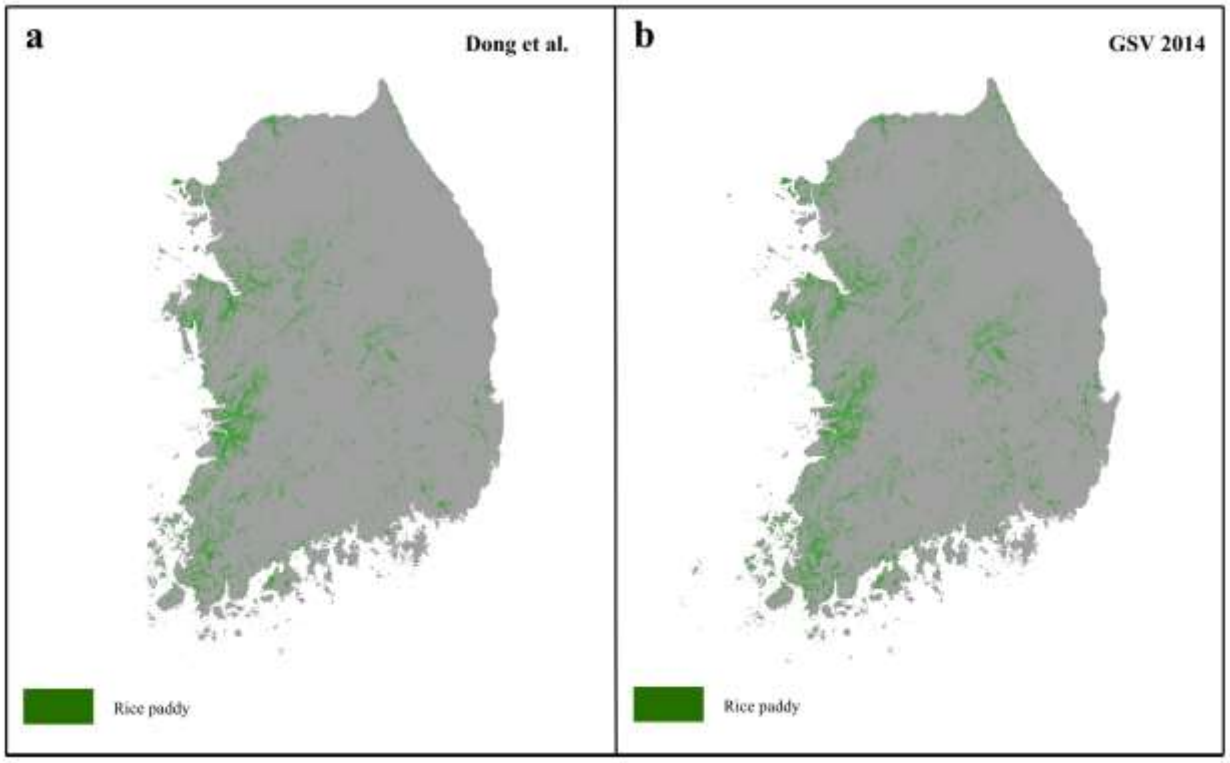

Supplementary Fig. 2 Comparison between the Dong et al. (a) and GSV-derived (b) rice paddy maps in 2014, a year without reference GSV images.

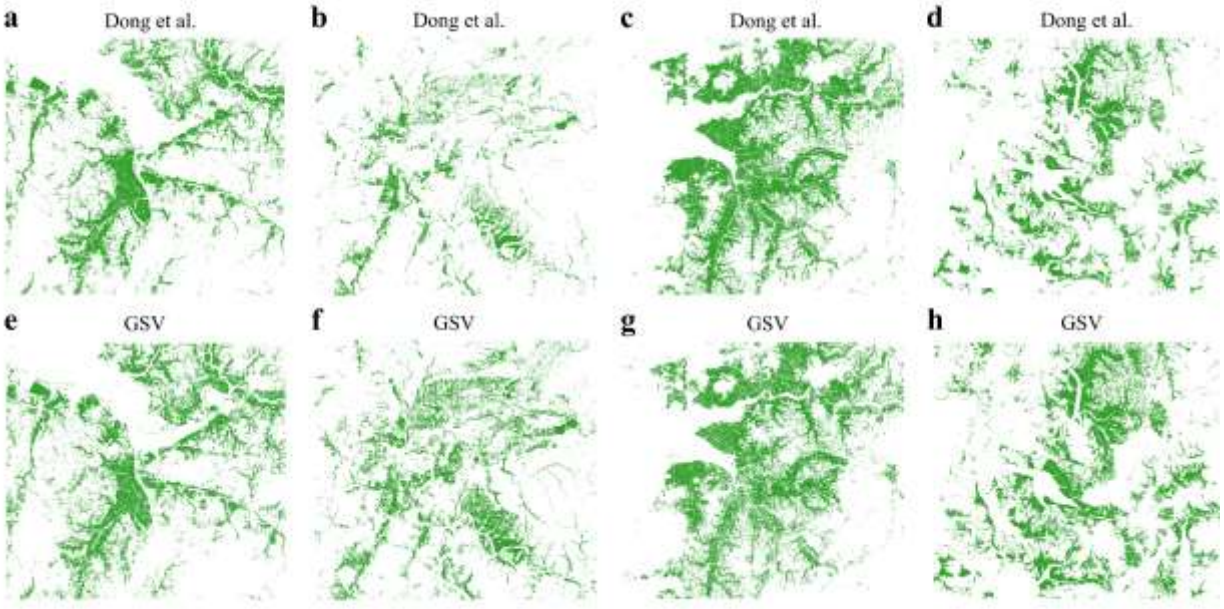

Supplementary Fig. 3 Regional-scale rice paddy mapping comparison for South Korea in 2014. Each subplot covers approximately 2500 km2. The location of each region is available in Supplementary Fig. 1b.

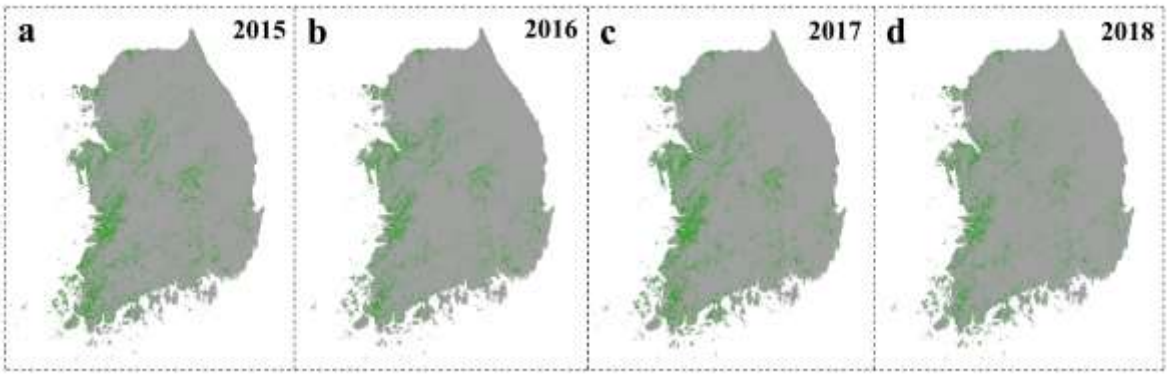

Supplementary Fig. 4 GSV- and Landsat8- derived rice paddy maps (green) for South Korea between 2015-2018.

5. Abstract in Korean

쌀(오리자 사티바)은 세계 인구의 50% 이상을 먹여 살리는 중요한 곡물 작물이다. 그러나 전통적인 혐기성 관리는 쌀 생산으로 관개수의 40%를 소비하고 전 세계 인공 메탄의 10%를 배출한다. 식량 수요 증가, 물 부족, 온실가스 배출 감소 등의 과제 속에서 지속 가능한 벼농사를 위한 새로운 패러다임이 시급하다. 벼는 하룻밤 사이에 상당한 양의 물을 내뿜는다. 야간 수분 손실을 줄이는 것은 바람직하지만, 먼저 야간 기공 개방의 기본 메커니즘을 이해할 필요가 있다. 야간과 별도로 주간 경영의 최적화는 환경적으로 지속 가능한 벼농사 시스템을 설계하는 데 매우 중요하다. 장기 전략에서, 새로운 잎 수준 발견과 현장 수준 방법을 지역적 또는 전역적 규모로 상향 조정하려면 상세하고 신뢰할 수 있는 작물 유형 맵이 필수적이다. 따라서, 본 논문에서 우리는 벼농사의 야간 기공 전도도에 대한 기계적 이해를 향상시켰다(제 2 장). 환경적으로 지속 가능한 벼농사 시스템을 설계하기 위한 학제 간 및 휴리스틱 접근법 제공(제 3 장). 그리고 새로운 작물 유형 참조 방법을 개발했다. 기성품인 Google Street View 이미지를 마이닝하여 자르기 유형을 매핑합니다.

2 장에서 우리는 벼의 야행성 기공 전도도(g_{sn})의 생태학적 메커니즘을 설명하기 위해 "협동된 잎 형질" 가설을 제안했습니다. 가뭄, 영양 결핍 및 가뭄-영양소 결핍 복합 스트레스를 적용하여 노지 실험을 수행했습니다. 우리는 g_{sn} 이 가뭄에 의해 크게 감소하지도 않고 영양 결핍에 의해 지속적으로 증가하지도 않는다는 것을 발견했습니다. 무생물적 스트레스를 무작위 효과로 사용하여 g_{sn} 은 야간 호흡(Rn)과 강한 양의 상관관계를 보였습니다. 특히, g_{sn} 은 $R_n(\uparrow) \rightarrow g_{sn}(\uparrow) \rightarrow g_{sd}$(주간 기공 전도도)$(\uparrow) \rightarrow A$(동화)$(\uparrow)$와 같이 이른 아침 광합성을 프라이밍했습니다. 이 광합성 프라이밍 효과는 오전 중반 이후에 감소했습니다. 잎은 g_{sn} 에 의해 다음과 같이 냉각되었습니다: $g_{sn}(\uparrow) \rightarrow$ E(증산)$(\uparrow) \rightarrow T_{leaf}$(잎 온도)$(\downarrow)$. 그러나 우리의 결과는 증발 냉각이 Rn 비용을 감소시키지 않았다는 것을 분명히 시사합니다. 우리의 결과는 g_{sn} 이 물 및 영양소 가용성보다 탄소 호흡 및 동화와 더 밀접하게 관련되어 있으며 잎 형질 조정(R_n - g_{sn} - g_{sd} - A)이 g_{sn} 을 제어하는 주요 메커니즘일 가능성이 있음을 나타냅니다.

제 3 장에서 우리는 현재의 작물 수확량을 늘리고 관개 용수 소비를 줄이며 침수된 쌀 생산 시스템에서 CH_4 와 N_2O 배출량을 동시에 줄이는 딜레마를 해결하는 것을 목표로 했다. 휴리스틱하고 전체론적 방법을 제안함으로써, 우리는 이전에 가장 강조되었던 관개 체제를 넘어 농장 관리를 최적화함과 동시에 파종 창, 수정률, 경작 깊이 및 이들의 상호 작용과 관련된 다른 중추적 옵션의 틈새를 탐색했다. 구체적으로, 우리는 5 년간의 와류 공분산 관찰로 프로세스 기반 DNDC 모델을 교정하고 검증했다. DNDC 모델은 나중에 다중 객관적 최적화 문제를 해결하기 위해 비지배적 정렬 유전 알고리듬(NSGA-III)과 통합되었다. 우리는 최적화된 관리를 통해 50% 이상의 관개 수요와 GHG(CH_4 & N_2O) 배출량을 줄이면서 현재 농작물 수확량을 잠재력(~10t/ha)까지 유지하거나 증가시킬 수 있다는 것을 발견했습니다. 우리의 결과는 더 이른 파종 기간과 관개 관개 관행의 개선이 환경적 이익을 유지하면서 농작물 수확량을 최대화하는 데 중추적일 것이라는 것을 보여준다. 우리는 홍수 없는 날의 최적 부분이 성장기 길이의 약 54%였고 최적의 시간 분포는 주로 식물 단계에 있다는 것을 발견했다. 우리의 연구는 연구 현장의 현재 농장 수확량(8.3-8.9 t/ha)이 잠재적 수준을 달성했을 뿐만 아니라 수자원(604-810 mm/yr)과 GHGs 배출(CH_4: 186-220 kg C/ha/yr; N_2O: 0.3-1.6 kg C/ha/yr)에 막대한 환경 비용을 초래한다는 것을 보여준다. 또한, 이 간단한 방법은 다양한 기후 및 지역 조건 하에서 농업 시스템의 환경 지속 가능성을 평가하고 정책 입안자와 농업 관행을 포괄적인 해결책으로 안내하는 데 추가로 적용될 수 있다.

제 4 장에서는 컨볼루션 신경망(CNN) 모델을 적용하여 두 개의 구별되는 농업 지역에서 구글 스트리트 뷰(GSV) 이미지를 통해 자동 지상 트러싱의 효과를 탐구한다. 일리노이와 캘리포니아의 센트럴 밸리. 지상 참조 데이터는 감독된 작물 매핑을 위한 필수 전제 조건이다. 저렴하고 효율적인 지상 참조 방법이 없기 때문에 참조 데이터가 광범위하게 제한되고 작물 분류를 방해한다. 본 연구에서는 클라우드 기반 Google 어스 엔진 플랫폼을 사용하여 상태 수준에서 픽셀 기반 크롭 매핑을 수행하여 새로운 지상 참조 기술의 실현 가능성과 신뢰성을 입증한다. 매핑 결과는 미국 농무부(USDA) 작물 데이터층(CDL) 제품을 사용하여 평가된다. 약 130,000 개의 GSV 이미지에서 CNN 모델은 약 9,400 개의 목표 크롭

이미지를 식별했다. 이 이미지들은 알팔파, 아몬드, 옥수수, 면화, 포도, 쌀, 콩, 피스타치오 등의 작물 유형으로 잘 분류된다. 전체 GSV 이미지 분류 정확도는 센트럴 밸리의 경우 92%, 일리노이 주의 경우 97%이다. 그 후 이미지 지리적 좌표를 특정 방향으로 2~3 회 이동하여 31,829 개의 크롭 기준점을 생성했다. 즉, 일리노이에서 17,358 개, 센트럴 밸리에서 14,471 개였다. CDL 제품으로 매핑 결과를 평가한 결과 만족스러운 일관성이 나타났다. GSV 에서 파생된 매핑 결과는 2011-2019 년 작물 유형 분포의 일반적인 패턴을 포착한다. CDL 제품과 우리의 매핑 결과 사이의 전체 합치는 센트럴 밸리의 경우 0.44–0.99 의 R^2 값과 일리노이 주의 경우 0.81–0.98 의 R2 값으로 표시된다. 제안된 방법의 다른 국가에서 적용 가치를 보여주기 위해, 꽤 좋은 결과를 얻은 한국의 논(2014–2018)을 추가로 매핑했다(R^2=0.91). 이러한 결과는 딥 러닝 모델과 함께 사용되는 GSV 이미지가 세계의 많은 지역에서 지상 참조를 위한 효율적이고 비용 효율적인 대체 방법을 제공한다는 것을 나타낸다.